THÈSE

En vue de l'obtention du

DOCTORAT DE L'UNIVERSITÉ DE TOULOUSE

Délivré par
Université Toulouse III – Paul Sabatier
Discipline ou spécialité :
Chimie Macromoléculaire et Supramoléculaire

Présentée et soutenue par
Julie Massaad
Le : vendredi 23 novembre 2012

Titre :
Photo-modulations *vs* gated phtochromism in a dithienylethene dye

---

JURY

Prof. Elena Ishow, Université de Nantes, rapporteur
Prof. Cyril Ruckebusch, Université Lille 1, rapporteur
Prof. Alain Vigroux, Université Paul Sabatier, examinateur
Prof. Gonzalo Guirado Lopez, Universitat Autonoma de Barcelona, examinateur

---

Ecole doctorale :
Sciences de la matière (SDM)
Unité de recherche :
Laboratoire IMRCP UMR 5623
Directeur(s) de Thèse :
Dr. Christophe Coudret

“This thesis is dedicated to my parents, my brothers and Florian”

Acknowledgements

At the end of my thesis at the IMRCP, I would like to thank all those people who made this thesis possible and an unforgettable experience for me.

First of all, I would like to thank Monique Mauzac, director of the IMRCP for welcoming me in her laboratory. My gratitude also goes to my supervisor Christophe Coudret and to Jean-Claude Micheau who offered their continuous advice and encouragement throughout the course of this thesis. I thank them for the systematic guidance and great effort they put into training me in the scientific field. It was a great pleasure to work with both of them.

I would also like to thank Myrtil L. Kahn from the LCC laboratory, Fabienne Gauffre from the University of Rennes 1, Stéphanie Delbaere from the University of Lille 2 and Michel Sliwa from the University of Lille 1 for being part of this project.

I thank Prof. Elena Ishow from the University of Nantes and Prof. Cyril Ruckebusch from the University of Lille 1 for examining this work. My thanks also go to Prof. Gonzalo Guirado Lopez from *Universitat Autonoma de Barcelona* for his interest towards my research and being part of the jury. Last not but least I would like to thank Prof. Alain Vigroux for accepting to be the president of the jury.

During the last three years, I met very special people with whom I had a great time and made my stay in Toulouse a moment of happiness and friendliness: Jacques Al Kai, Elie Khoury, Walid Hankache, Adele Karam, Géo Hankache, Phélomène Makhraz, Youssef El Rayess, Sandy Rahmé, Layale Saab, Georges Khalil, Bendy Tanios, Antoine Halabi, Youssef Bou Issa, Rajaa Akoury, Rawad Tadmouri, Wael moukarzel and Dimitri Matioszek. Thank you for all the wonderful moments. My appreciation also extends to Florence Frechou and Charles Louis Serpentini for their kindness, encouragement and support. I would like to thank all the members of the laboratory and all the students: Virginie Rahal, Ophélie Riou, Arnaud Lemelle, Joris Ivroas, Marion Martignac, Samia Affoulous, Marie-Anne Carpene, Jad Chemali, Anass Dazzazi….

Finally, I take this opportunity to express the deepest gratitude to my beloved parents, brothers and Florian for their love and continuous support.

Abreviations

^{1}H NMR: proton nuclear magnetic resonance spectroscopy

Abs: Absorbance

ACN: Acetonitrile

CH_2Cl_2: cloroform

CH_3CN: Acetonitrile

$Cu(OTf)_2$: Copper(II) triflate

DOSY: Diffusion Ordered Spectroscopy

DTE: Dithienylethene

$DTE(COOH)_2$: 1,2-bis(5-carboxy-2-methylthien-3-yl) cyclopentene

E°: standard electrode potentiel

ECE: Electrochemical, Chemical, Electrochemical

EPR: Electron Paramagnetic Resonance

ESR: Electron Spin Resonance

ET: Electron Transfer

eV: electron Volt

FRET: Forster Resonance Energy Transfer

HDA: hexadecylamine

HOMO: Highest Occupied Molecular Orbital

J: overlap integral

K: equilibrium constant

LUMO: lowest Unoccupied Molecular Orbital

NBD: norbornadiene

nm: nanometer

NMR: Nuclear magnetic resonance

NOE/SY: Nuclear Ovenhauser Effect/Spectroscopy

NP: Nanoparticle

ns: nanosecond

pKa: acid dissociation constant

ppm: parts per million

PSS: Photo Stationary State

Pt: Platine

QD: Quantum Dot

R_0: Forster radius

r_{DA}: donor-acceptor distance

RET: Resonance Energy Transfer

SCE: Saturated Calomel Electrode

$\tau_{1/2}$: half-time

$TBAPF_6$: tetrabutylammonium hexafluorophosphate

TEM: Transmission electronic microscopy

THF: Tetrahydrofuran

TLC: Thin layer chromatography

UV-Vis: Ultraviolet-Visible spectroscopy

$ZnCy_2$: Dicyclohexyl zinc $Zn(C_6H_{11})_2$

δ (NMR): chemical shift

ΔG: Gibbs free energy

ε: molar extinction coefficient

λ: wavelength

τ: lifetime of transient species

Φ: quantum yield

Table of contents

TABLE OF CONTENTS

Chapter I: Introduction

Chapter I - Introduction

In this chapter, the relationship between light and chemical reaction will be presented through different examples found in nature and everyday life. Then, the different families of photochromic switches will be presented and classified according to the photochemical processes taking place during the photoiomerization. Particular attention will be focused to the dithienylethene derivatives due to their thermal stability and fatigue resistance. Photoswitchable sophisticated DTEs derivatives will be presented as well as their successful interaction with chemical processes to form systems where light controls reactivity and where reactivity controls photochromism. Finally, chemical dynamic analysis methodology will be introduced as a powerful tool to study interacting networks of chemical and photochemical processes.

I.1. Light and chemical reaction's relationship

Photochemistry is a sub-discipline of chemistry that studies the relationship between light and chemical reactions. In photochemical reactions, light acts as a "catalyst" or as a "reagent". It acts as a "reagent" when photons are absorbed by a reactant molecule, and as a "catalyst" when photons are absorbed then emitted. Actually the absorption of a photon of light provides the activation energy required for the proceeding of the chemical reaction[1]. Or it changes the molecule's electronic configuration, enabling an otherwise thermally inaccessible reaction path[2]. Furthermore, if the absorbed photons don't activate a chemical reaction, photons are released as radiation energy or transferred to another molecule.

However, light is a powerful tool used to activate chemical reaction and it is an essential element in many technical and industrial processes. In nature, photochemical reactions are of fundamental importance for the origin and maintenance of life. One of the famous examples is the photosynthesis, in which solar energy is used to convert carbon dioxide and water into glucose disposing of oxygen as a side-product. Another example of natural photochemical system includes the formation of stratospheric ozone which protects us from solar radiation. Photochemical processes are found also in visual perception through the rhodopsin which is a photosensitive protein in the retina. Nowadays, photochemical processes are used in different applications such as photolithography[3], drug delivery[4] as well as photodynamic therapy where light is used to destroy tumors[5] by the action of singlet oxygen.

On the other side of the relationship between chemical reaction and light, chemical events can be used to control the photochemistry of a photosensitive molecule. In this case, a chemical event such as a supramolecular interaction or a reaction provides changes in the molecular structure of the photosensitive entity and in the electronic wave function. Those changes may inhibit or allow photo activity of the molecule during its exposure to light.

In this thesis, we are interested in *Photochromic* compounds which have been studied since the 19th century. Upon irradiation, the color and physico-chemical properties of photochromic molecules can be reversibly switched. One of the best known reversible photochromic applications is color changing lenses of sunglasses depending on lighting.

I.2. Photochromic switches

They are molecules whose physico-chemical properties can be reversibly switched using light. Such behavior forms the basis of what is called *Photochromism* which is a reversible transformation of a chemical species induced in one or both directions by absorption of electromagnetic radiation between two forms, X and Y, having different absorption spectra.

$$\mathbf{X} \underset{h\nu_2 / \Delta}{\overset{h\nu_1}{\rightleftharpoons}} \mathbf{Y}$$

Scheme (I.1): photochromism as a reversible transformation between two forms.

The thermodynamically stable form X is transformed by irradiation into form Y. The back reaction can occur thermally (*Photochromism of type T*) or photochemically (*Photochromism of type P*).

Isomers X and Y present different fluorescence signals[6], refractive indices[7], conductance[8], geometrical structure[9] or redox potentials[10].

I.2.1 Photochromism Characterization

I.2.1.1 PhotoStationnary State (PSS)

Upon irradiation at a defined wavelength, both isomers X and Y absorb light in the same region where the photochemical transformation of X is promoted. Therefore, a photochemical equilibrium is established limiting the conversion of isomer X to isomer Y. Therefore, the two photochemical processes compete with each other.

The composition of the system is termed “PhotoStationnary State” (PSS) which describes the percentage of the molecular switch that undergoes photoisomerization at a defined wavelength. Thus, we write:

$$PSS = 100 * \left(\frac{\text{Number of isomerized molecules}}{\text{Total number of molecules}}\right)$$

For future applications and in order to compare between the properties of photochromic molecules, it is necessary to quantify the efficiency of the reaction and to evaluate the resistance of these systems over a period of time and after a long irradiation. For this reason, the concepts of quantum yield and fatigue resistance are introduced.

I.2.1.2 Quantum Yield

It determines the efficiency of the photochromic change while considering the amount of the absorbed light.

$$\Phi_{AB} = \frac{\text{Number of formed molecules Y}}{\text{Number of absorbed photons by X}}$$

I.2.1.3 Fatigue Resistance

The loss of photochromism performance over the time, due to chemical degradation of a material, is called “fatigue”. Usually, the major cause of damage for photochromic substances is oxidation[11].

To quantify the concept of fatigue resistance, the determination of the number of cycles which a system can undergo, is an important experimental parameter. In a cycle, an isomer X is transformed (photochemically) into isomer Y which returns to isomer X (thermally or photochemically).

I.2.2 Classes of Organic Photochromic Switches

Photochromic molecules are divided into several important classes; the most important are salicylidene-anilines, azo derivatives, spiropyrans, spirooxazines, fulgides and diarylethenes. They can also be classified on the basis of their transformations induced by light. These photochemical transformations can be tautomerizations, *E-Z* isomerizations and electrocyclic ring closure/opening.

I.2.2.1 Salicylidene-Anilines

They undergo photochromic tautomerism (hydrogen transfer) after irradiation with UV light: a prototropic rearrangement from the enol-form to the keto-form occurs **(Scheme (I.2)).** The enol-form is pale yellow and after irradiation, the keto-form appears which is reddish or brown. This quinoidketo tautomer appears and it exists in two forms: an intramolecular hydrogen bonded *cis*-keto form and a rotated *trans*-keto form. The *cis*-keto form is not thermally stable and can go back to the enol form[12]:

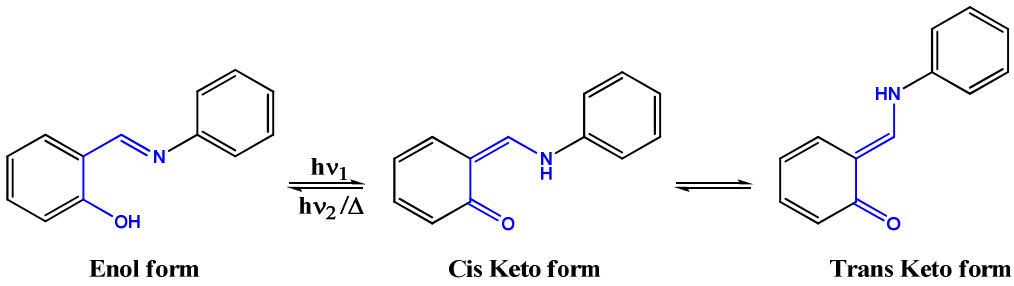

Scheme (I.2): light-induced hydrogen transfer tautomerization

I.2.2.2 Azo derivatives

Azo derivatives[13] undergo *E*-*Z* isomerization of the double bond $N = N$ under UV or visible light **(Scheme (I.3))**. They are T-type photochroms where the photogenerated *Z* state can also return thermally to the *E* state

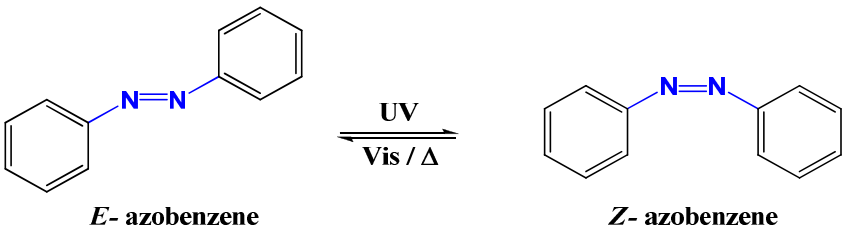

Scheme (I.3): E-Z isomerization of azobenzene

I.2.2.3 Spiropyrans

Spiropyran compounds[14] undergo a photochemical 6π electron ring-closure reaction leading to the colorless closed spirostructure from the colored open merocyanine structure **(Scheme (I.4))**. It is the ring-opening of the spiropyran which causes chromism by increasing the conjugation. As a T-type photochromic dyes, spiropyrans have several drawbacks such as low thermal stability of the merocyanine form[15], photooxidation[16] as a side reaction and thermochromic behavior.

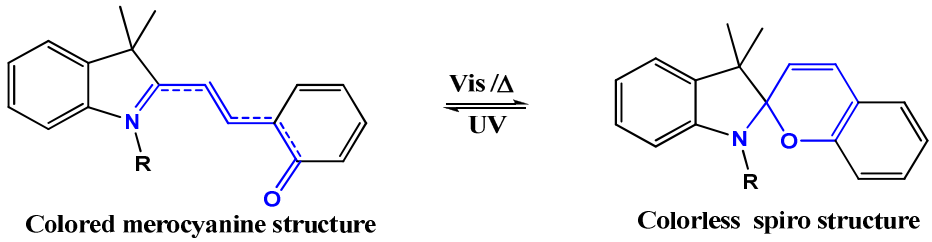

Scheme (I.4): photo isomerization of a spiropyran derivative

I.2.2.4 Fulgides

Fulgides[17] are another class of photochromic molecules that undergo a photochemical 6π electrocyclization. Upon irradiation with UV light, the colorless isomer (E-form) changes into a deeply colored isomer or it can also undergo *cis-trans* isomerization to the Z-form **(Scheme (I.5))**. The closed form is thermally not stable. However, the system becomes thermally irreversible[18] when:

- the phenyl group is replaced by a furyl group.
- a methyl group is introduced at the ring-forming carbon atom (R_2 or R_3) of the aromatic ring.

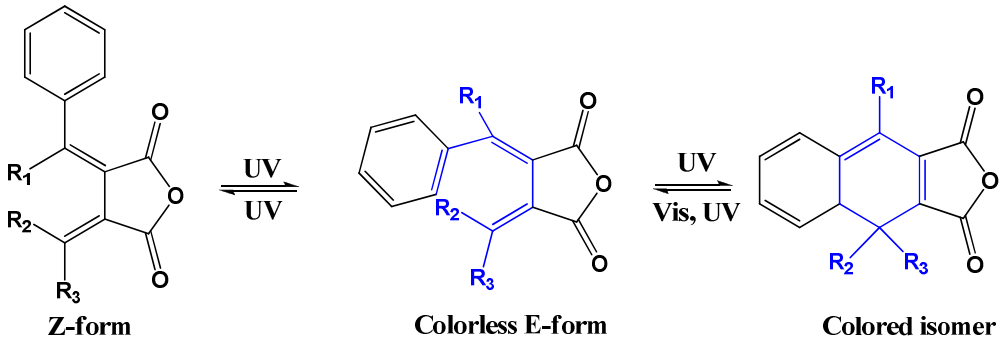

Scheme (I.5): photochemical transformations of fulgides

I.2.2.5 Diarylethenes

Diarylethenes[19] (DAE) compounds are P-type photochromic dyes. They are derivatives of stilbene. Upon irradiation, *cis*-stilbene leads to the formation of dihydrophenanthrene (a DAE closed form) which is thermally not stable **(Scheme (I.6))**. In the presence of dioxygen, the latter compound is converted to phenanthrene by rapid hydrogen elimination. In the absence of dioxygen, fast thermal cycloreversion to stilbene occurs. To prevent oxidation of dihydrophenanthrene to a phenanthrene in the presence of air or other oxidants, hydrogen atoms should be replaced by methyl groups in the 2 and 6'positions (**Scheme (I.6)):**

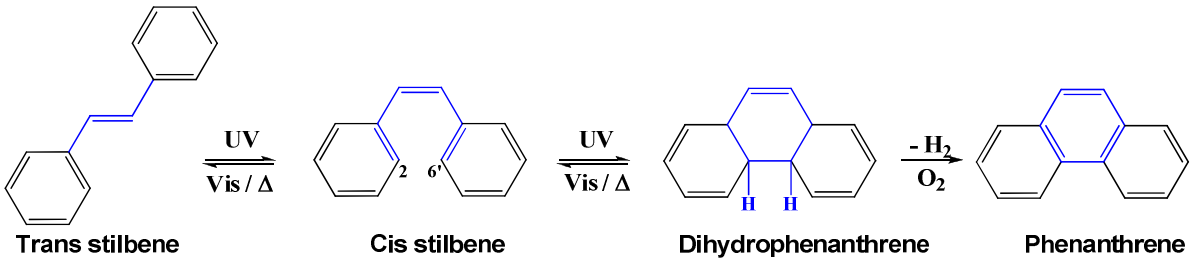

Scheme (I.6): photochemical and elimination reactions involving stilbenes

The resulting cyclized molecule is still thermally unstable[20]. To solve the problem of the thermal back reaction, diarylethenes with various aryl groups have been investigated in order to prepare a P-type chromophore. The successful switches are the ones based on five membered heterocycles instead of phenyl groups. A study by Kellogg *et al*[21] showed that replacement of the phenyl groups with thienyl rings (X=S) **(Scheme (I.7))** increases strongly the thermal stability of the closed-ring structure.

Z-E isomerization around the central double bond connection can generate a reduction in the efficiency of the electrocyclization reaction. In order to improve this point, it is possible to block the double bond connection in the Z position by adding a five-membered cycle as maleic anhydride[20], cyclopentene[22], perfluorocyclopentene[23] cycles.

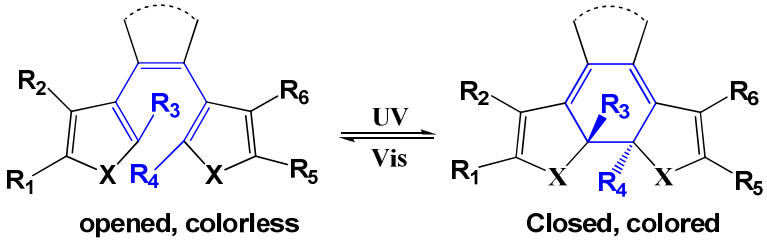

Scheme (I.7): switching cycle of diarylethenes

Applications of photochromic switches require thermally forbidden transfomations, fatigue resistance, rapid response, high sensitivity, nondestructive readout capability, and reactivity in solid state. In this context, molecular switches based on Dithienylethene (DTE) architecture[19] having high switching sensitivity (high quantum yield) and rapid response[24], satisfy these requirements.

I.3. Dithienylethene (DTE) derivatives

They undergo reversible electrocyclic reactions upon alternate photo or electrochemically transformations. These transformations allow the interconversion between their thermally stable open and closed states (**Scheme (I.8)**).

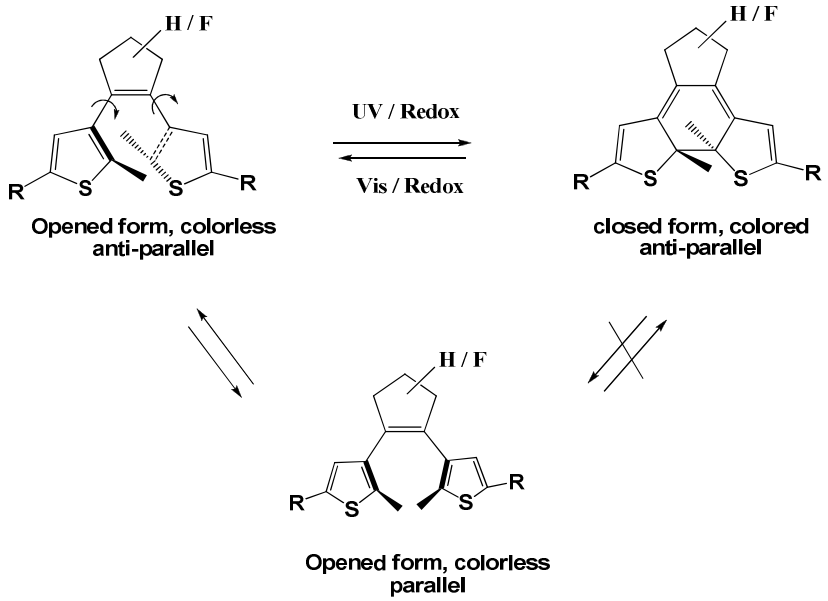

Scheme (I.8): photo and electrochemical switching of "parallel" and "anti parallel conformations of DTEs open-ring isomer.

In general, the open ring isomer (1,3,5-hexatriene) of DTE derivatives, absorbs in the UV region of the spectrum and their solutions are therefore colorless under the condition that no other absorption occurs at loner wavelengths. Upon irradiation with UV light, new absorption bands appear in the visible region of the spectrum. Thus, they are ascribed to the formation of the closed ring isomer form (1,3-cyclohexadiene). Upon irradiation with visible light, the system returns to the ring open form. The main difference between the photoisomers' properties is due to the HOMO-LUMO gap change and the extent of π system conjugation which is responsible for the coloring of the closed form. The most important properties of these compounds are the thermal stability of the closed form and the high fatigue resistance.

I.3.1 DTEs photochemical ring closure reaction

The open form of the DTEs derivatives has two different conformations: the parallel and the anti-parallel conformations which have the two rings in mirror symmetry and in C_2 symmetry respectively **(Scheme I.8)**. According to the Woodward-Hoffmann[2] rule, based on π orbital

symmetries for 1,3,5-hexatriene, the cyclization reaction is allowed in the conrotatory mode by a photochemical process and a disrotatory mode by thermal transformation. In the case of DTE, only the photochemical process is effective because the thermal process cannot take place due to the hindrance of the center methyl groups and the closed form has higher ground state energy than the open form. Only the anti-parallel conformation gives rise to the photocyclization reaction by a conrotatory mechanism. The parallel form is inactive.

The ratio between the parallel and the anti-parallel conformations is approximately $1:1$. As a consequence, the cyclization quantum yield for these molecules cannot exceed 0.5. Based on these considerations, the anti-parallel conformation and therefore the quantum yield are increased by introducing bulky substituents into the thiophene rings of DTE. Another approach is by incorporating DTE in a confined space (such a crystalline phase)[25,26], in a polymer matrix[27], or in a cyclodextrin[28,29] .

The dynamics of photocyclization and photocycloreversion reactions of DTEs has been studied by means of pico and femtosecond laser photolysis experiments[30]. These experiments revealed an extremely fast kinetics for these processes with average times of $1\,ps$ (photocyclization) and $2\,ps \sim 3\,ps$ (photocycloreversion).

The two forms can sometimes be distinguished by ^{1}H NMR at room temperature[31] . However, in other cases, separate signals are only observable at sufficiently low temperatures[32].

I.3.2 DTEs electrochromic behavior

The cyclization and cycloreversion reactions of DTEs are induced by photoirradiation. Also, in some cases, they are induced by electrochemical reduction[33] or oxidation[34] **(Scheme I.9)**. DTE chromophore is seen as the association of two basic components: aromatic thienyl groups and a hexatriene subunit. Because of the two thiophene heterocycles, the ring-open isomers tend to undergo irreversible oxidation at relatively high potentials (greater than 1 V) with accompanying electropolymerization (classic process for thiophenes derivatives) while the bridging cyclopentene group is redox-inactive.

Due to the creation of the linearly conjugated π-system upon photochemical cyclization, closed isomers are oxidized at lower potentials than their open counterparts. This is due to the fact that the Highest Occupied Molecular Orbital (HOMO) increases in energy from an open

form to the closed form. Similarly, the reduction potentials for the ring-closed isomers are less negative than their ring-open counterparts.

Koshido *et al.* described the first example that underwent cycloreversion upon oxidation of the closed-form molecule[35] **(Scheme I.9)**: opened form isomer undergoes the typical cyclization reaction when irradiated with UV light (365 nm). The reverse reaction is triggered either by exposing a solution of the closed form isomer to visible light (> 450 nm) or by applying a positive potential (+ 900 mV) that oxidizes the ring-closed isomer to its unstable radical cation. Then, the radical cation ring opens spontaneously to generate the radical cation of the opened form, which undergoes electron transfer in a catalytic process.

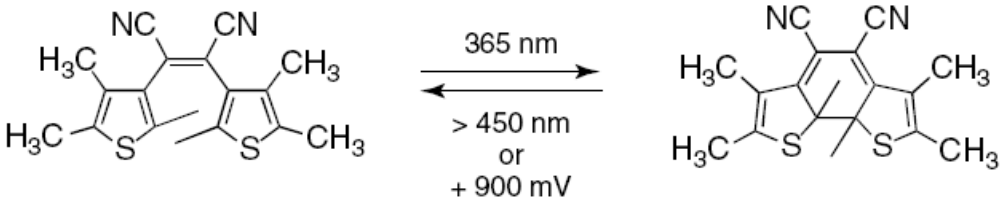

Scheme (I.9)[37]: ring-closing and opening of a DTE derivative with UV/ Vis light or electricity

Since then, it is shown that most of DTE derivatives can undergo ring-opening and only some of them undergo ring-closure reaction when an appropriate voltage is applied. Thus, DTE derivatives are oxidized or reduced. Several studies are done to know the mechanism behind the oxidative cyclization/cycloreversion process[36,37,33].

It is found that the direction of the reaction depends on the relative stability of the cationic species. If the open-form cation is lower in energy than the cation of the cyclized molecule, electrochemical ring-opening occurs. However, if the cation of the cyclized species is lower in energy, oxidative cyclization is observed.

By introducing proper thiophenes substituents and through the nature of electron-withdrawing perfluoro or electron-donating perhydro cyclopentene, the stability of the cations is influenced and the direction of the reaction is reversed:

1- Perfluorocyclopentene derivatives show spectral shifts to longer wavelengths and higher oxidation potentials in comparaison with their perhydrocyclopentene homologues. This is due to the electron withdrawing character of fluorines atoms[37]. As a result, for the hexahydrocyclopentene based compounds, oxidative ring closure of the ring-open form is observed. However, for the hexafluorocyclopentene based compounds, oxidative ring opening of the ring-closed form is observed.

2- In DTEs where the 'external' thiophenes substituents are electron donors, the radical cation is stabilized by a π-system that brings both donors into conjugation and closed isomer is favored. When the 'external' thiophenes substituents are acceptors, the less-destabilized open isomer is preferred.

As a result of their relevant properties, DTEs are promising materials for optical data storage, where destructive read out should be avoided[19] by using redox reactions. DTEs allow erasing of the information controlled by electrochemical transformations.

I.4. DTEs derivatives and chemical reactivity

Several researches have been carried out toward the engineering of multiple responsive switching systems based on the photomodulation of DTEs for practical applications. It is found that DTEs compounds are well suited to modulate chemical reactivity because the distinct geometric and the electronic properties of their isomers:

1- Geometric differences between photoisomers are due to the fact that ring open forms are relatively flexible while the closed forms are more rigid due to the presence of a tricyclic structure. Thus, in open forms, flexibility allows the interconversion between parallel and anti-parallel conformations.

2- Electronic differences between photoisomers are explained by the fact that in open isomers, the two thienyl groups are electronically isolated from each other. However, in the closed ones, a linearly π conjugated pathway is generated through the entire DTE backbone connecting electronically the external groups on the thiophene rings, allowing them to sense each other's nature.

So, the relationship between chemical reactivity and photoresponsive DTEs can be studied in two ways:

1- Light is used to modulate chemical reaction: DTE photoisomers, acting as catalysts or reagents, influence chemical events due to the difference in their electronic and geometric structure.
2- Chemical events are used to control photoactivity: a chemical event between molecules into medium allows or prevents the photoisomerization of the DTEs.

These two concepts are related to the so-called *photomodulation* and *gated-photochromism.* In both cases, the changes in the optical properties of the photochromic DTEs should be considered as readout signals identifying which isomer is present.

Several works show the advantage of the electronic and geometric changes occurring upon isomerization of DTEs to get unique chemical reactivity to each form of the photoswitches. Moreover, various strategies are available for the modulation of the DTEs photochromic properties, using changes in supramolecular interactions or the occurrence of chemical reactions which modify their photochromic behavior. Conventional approaches include: changing the acid strength[38,39,40] , tuning the intramolecular proton transfer[41], regulating substrate binding affinities[42,43], complexing with metal cation ions and anion ions[44], the stereochemical outcome of a catalytic reaction[45,46], and modulating in a binary response the fluorescence of pendant emissive dyes[47].

I.4.1 Photomodulation of DTEs reactivities

Electronic and geometric differences between open and closed isomers are used to determine their function and their properties. Also, they are used to dictate how the molecular isomers behave as catalysts, reagents, and components in supramolecular systems.

I.4.1.1 Geometric and steric differences modulation

Takeshita *et al*[48] was the first to create a system where the controlling of supramolecular events is accomplished by the use of steric and geometric changes of DTEs. A photoswitchable saccharide receptor **Scheme (I.10)** containing boronic acid groups, that show good affinity for various sugars, was synthesized. The open form showed more affinity for glucose than the closed form. This is due to the free rotation of the 2 binding sites allowing them to face each other (like tweezers) and to form a 1:1 complex with saccharides. In contrast, this complex is not formed in the closed isomer because the boronic acid groups are separated from each other.

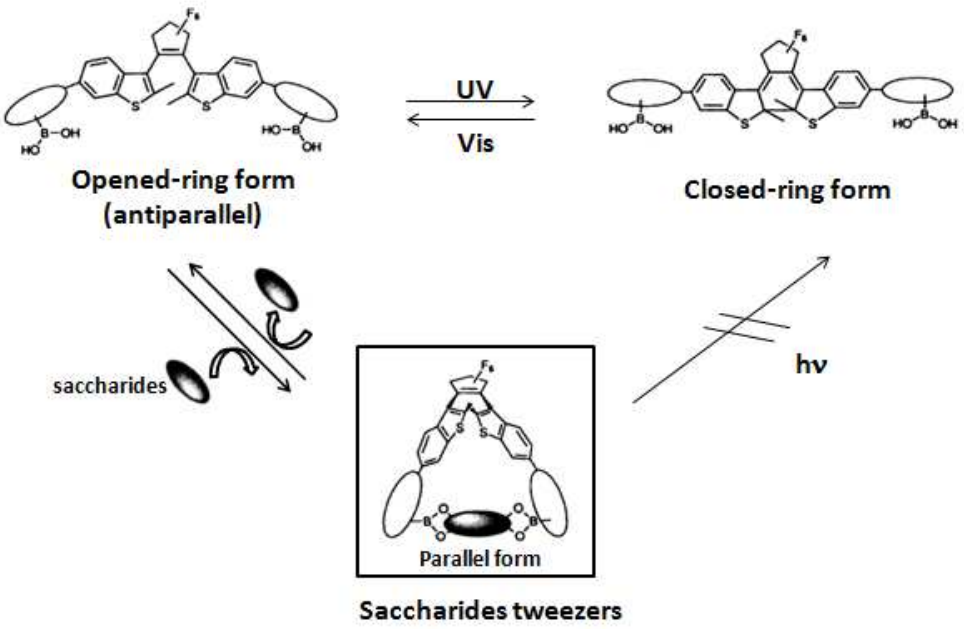

Scheme (I.10)[48]: photoswitchable molecular tweezers showing a photomodulation of a binding affinity.

The same concept has been applied to photoswitch tethered cyclodextrine dimers[43] where the difference in binding ability allows the photo controlled release and uptake of a tetrakis-sulfonatophenyl porphyrin in water.

These geometric and steric differences are used to photomodulate metal catalysed reaction. Sud *et al*[45] reported the first catalytic system regulated by light. A DTE derivative containing chiral oxazolines at the internal positions of the thiophenes rings was synthesized (**Scheme (I.11)).** The copper (I) catalyzed cyclopropanation of styrene with ethyl diazoacetate coordinated to the DTE backbone can sense the geometric differences between the two photoisomers and regulate the metal catalysed reaction. Thus, the stereoselectivity of the cyclopropanation of styrene depends on which photoisomer is present: the ring open isomer provides a chiral environnement to perform asymmetric catalysis. This is not the case of the closed isomer because its architecture is more rigid.

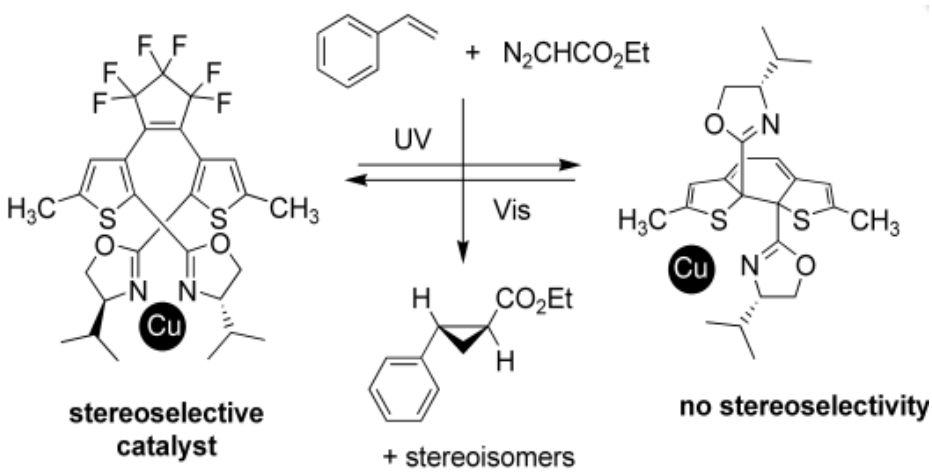

Scheme (I.11)[45]: photochemical interconversion of chiral DTE ligand.

I.4.1.2 Electronic differences modulation

After the photoinduced ring closure reaction, photoisomer's changes in π conjugation occur. The groups at the external positions on the thienyl rings can sense each other's electronic nature. This approach has been shown to be an effective strategy for the modulation of chemical reactivity in DTE based photoresponsive systems. Samachetty *et al*[49] reported a reversible photocyclization of a DTE derivative which modulates the ability of the pyridine to act as a coordinating ligand (**Scheme (I.12)).** The alkylation rate of the pyridine in both forms of the DTE is shown to be different. In the open form, the nucleophilic pyridine does not sense the electron withdrawing character of the pyridinium group. However, the ring closure reaction enables the free pyridine to feel the electron withdrawing pyridinium and it reduces its nucleophilic strength. Based on these results, the mono alkylated bis pyridine DTE derivative is used for the photoregulation of chemical processes requiring a nucleophilic catalyst. Preliminary studies have shown that the open form of the molecule is better at catalyzing the coupling of dimethylacetylene dicarboxylate to 3 nitrobenzaldehyde.

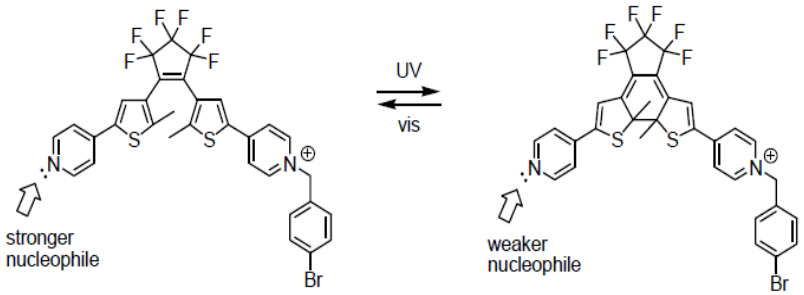

Scheme (I.12)[49]: reversible photocyclization modulating the nucleophilicity of a free pyridine, in a photoresponsive DTE derivative

I.4.1.3 Fluorescence modulation

Fluorescent molecular switches based on photochromic compounds can be classified into two main groups depending on their structure:

1- Intrinsic fluorescent switches

2- Multicomponent fluorescent switches

Intrinsic fluorescent switches are constituted by switchable fluorophores which can be photoresponsive dithienylethene[50], spiropyran[51] or fulgide[52] derivatives. They interconvert reversibly between two states: fluorescent and non-fluorescent states. Reversible interconversion between these states consists on, cyclization, *Z-E* isomerization or tautomerism.

Multicomponent fluorescent molecular switches incorporate luminescent components (such as organic compounds or inorganic nanoparticles) and photochromic switches. The changes in absorbance and/or redox potentials associated with the reversible interconversion of the two states of a photochromic DTE compound are exploited to modulate the emission of a fluorescent partner[53] based on electron and energy transfer processes. The emission intensity is reversibly switched between high and low values under the influence of optical stimulations.

Folling *et al*[54] reported a system in which multiple fluorophore photochromic DTE dyads are covalently attached to a silica nanoparticle based on amide bonds. Each dyad incorporates a rhodamine fluorophore and a DTE derivative (**Scheme (I.13))**.

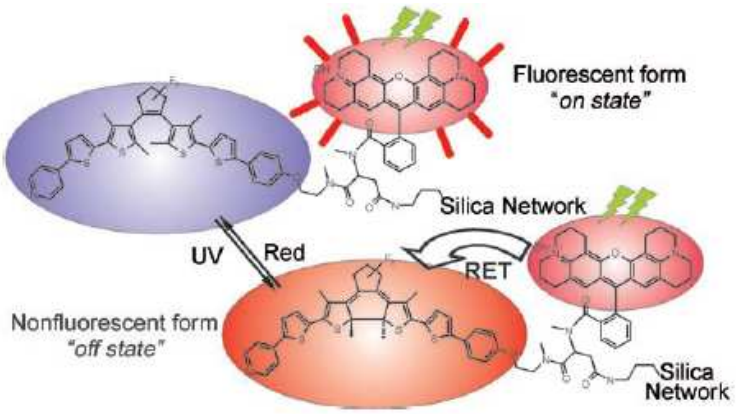

Scheme (I.13)[54]: photochromic reaction responsible for the fluorescence modulation

The selective excitation of the fluorescent component results in the appearance of an intense band at 610 nm in the emission spectrum. Upon UV irradiation, DTE switches to its ring-closed isomer which absorbs in the same range of wavelengths where the fluorophore emits. As a result, the excitation energy of the fluorophore can be transferred to the DTE with a concomitant decrease (94 %) in emission intensity. This change is reversed by irradiating the nanostructured construct with visible light and the original emission intensity is restored. Thus, the fluorescence of this particular construct is repeatedly switched between high and low values by alternating UV and visible irradiation based respectively on the activation and the suppression of an intercomponent energy transfer process.

I.4.2 Gated photochromism of DTEs

In gated-photochromism, one or both forms of the photochromic system are transformed (chemically or electrochemically) reversibly into a none photochromic form. The photoisomerization reactivity is made sensitive to some external stimuli such as another photon, reactive chemicals, an electrical field, oxido-reduction and solvation.

I.4.2.1 Sterically gated photochromism

One of the first attempts to observe gated-photochromism is reported by Irie et al[55, 56]. The effect is based on the inhibition of the photochromic reactivity of a diarylethene when the molecule adopts a parallel conformation. This conformation is stabilized by the presence of suitably disposed interlocking arms. The molecule regains photoactivity when the intramolecular lock is released by different ways:

1- The addition of hydrogen bond breaking **(Scheme (I.14))** by adding a competitive hydrogen-bonding solvent such as ethanol or propylamine or by heating the system above 100°C in decalin.

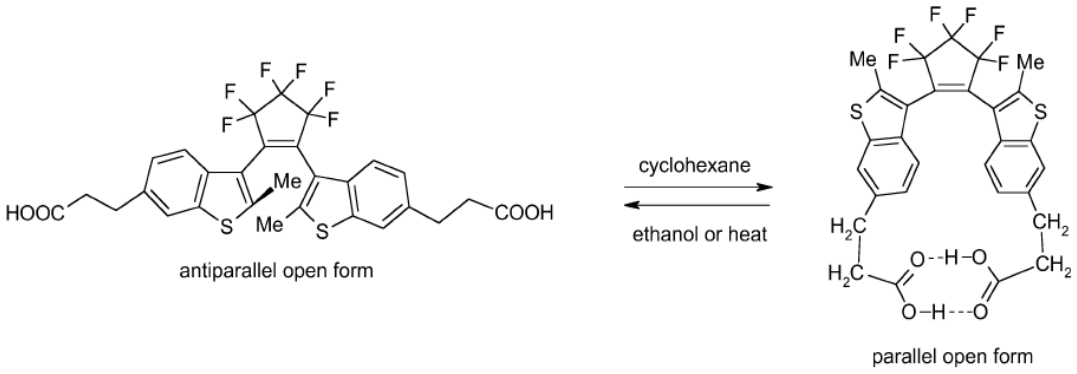

Scheme (I.14)[55]: DTE derivative with intralocking arms, formed by hydrogen bonds

2- The addition of reducing agents: the intramolecular disulfide bond holding the two arms together **(Scheme (I.15))** is reduced by tris (*n*-butyl) phosphine which allows free rotation and photochemical ring-closing.

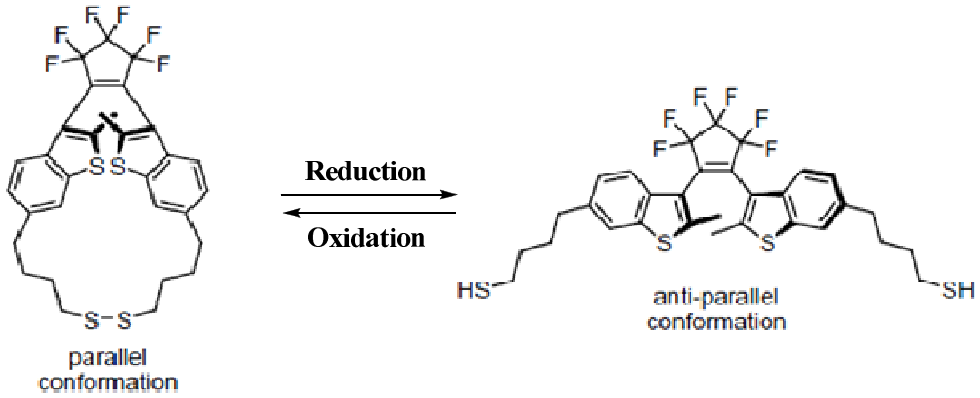

Scheme (I.15)[56]: DTE derivative with intralocking arms, formed by disulfide bond

I.4.2.2 Electrochemically gated-photochromism

Kawai *et al*[38] reported a system for which the electrochemistry has 'gated' the photochemistry of the DTE backbone. A bis phenol open isomer undergoes UV-induced cyclization to generate the closed form and ring-opening is triggered by exposing the system to visible light. Cyclic voltammetry was performed to study the electrochemical behavior of the DTE by using a standard three-electrode configuration with a glassy carbon (3 mm diameter disk)

working electrode, a platinum wire counter electrode and a Saturated Calomel Electrode (SCE) equipped with a double fritted sheild as the reference electrode. The electrolyrte used was nBu_4NBF_4. The ring-open isomer is inert to oxidation within the -1 to +1 V domain. However, the ring-closed one is reversibly oxidized at 735 mV in acetonitrile. Quinone is the obtained product. It is photochemically inactive because it does not have the cyclohexadiene required for photochemical ring-opening. The ring-opening photoreaction can be restored only after quinone has been reduced back to the bis phenol **Scheme (I.16)**.

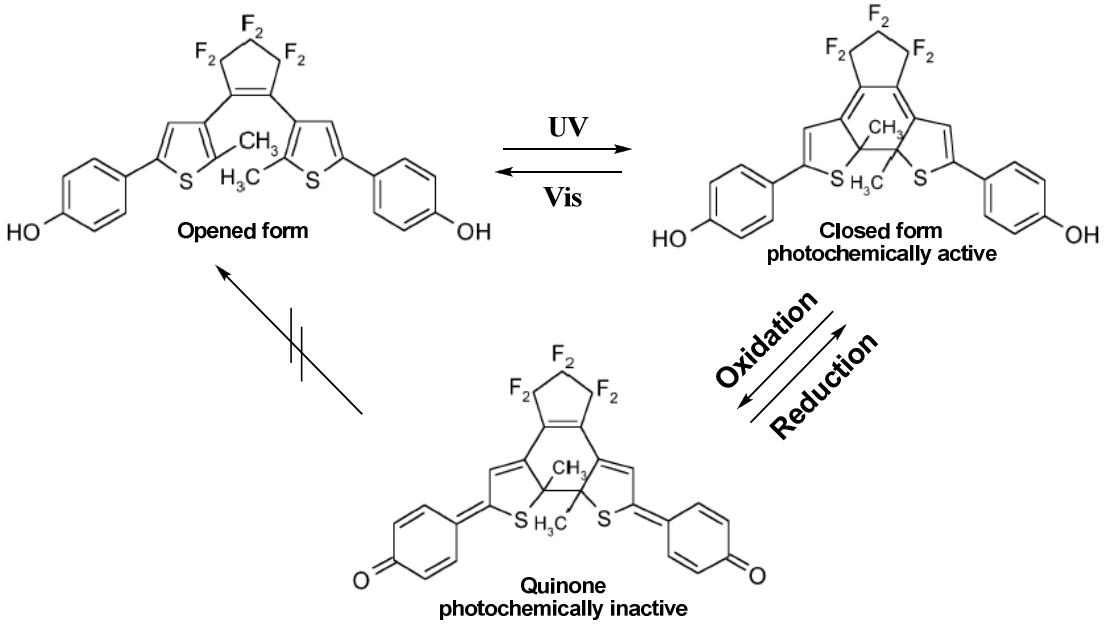

Scheme (I.16)[38]: oxidation of the ring-closed isomer prevents photochromism retrocyclization process

I.4.2.3 Gated photochromism by complexation

Qin *et al*[57] reported a system which improves the photochromic properties of the photoswitch. The presence of Zn^{2+} in a solution of a bis pyridine DTE increases the photocyclisation quantum yield **(Scheme (I.17))**. The photoactive anti parallel conformer is favored by the formation of a crablike complex of the open isomer and two Zn^{2+} cations.

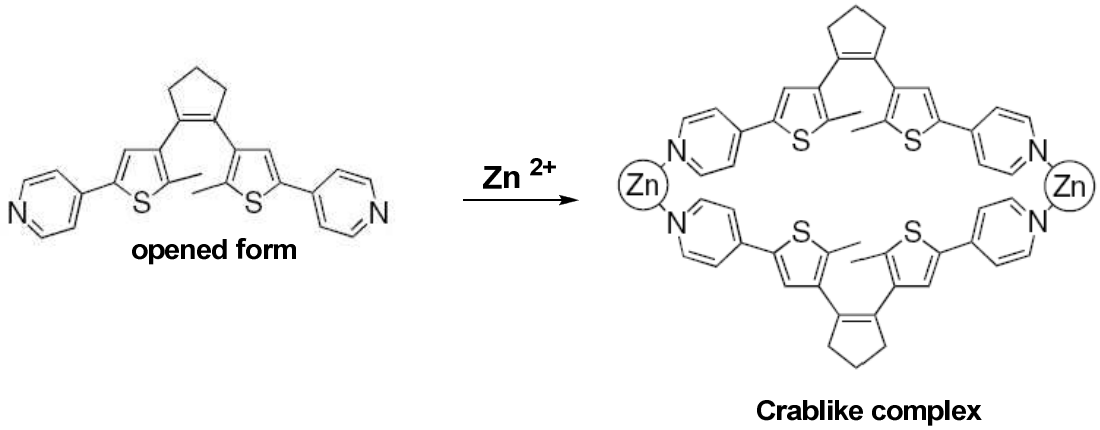

Scheme (I.17)[57]: crablike complex formed by two open isomers and two Zn^{2+}

I.4.2.4 pH gated photochromism

Kawai *et al*[58] developed a photochromic system where the photoactivity of the closed isomer is reduced upon deprotonation. The ring closing photoreaction is totally prevented by deprotonation of the open form **(Scheme (I.18)).** This phenomenon is explained by a through space effect whereby an ionic interaction between the phenolate and pyridinium groups locks the molecule in the photoinactive parallel conformation.

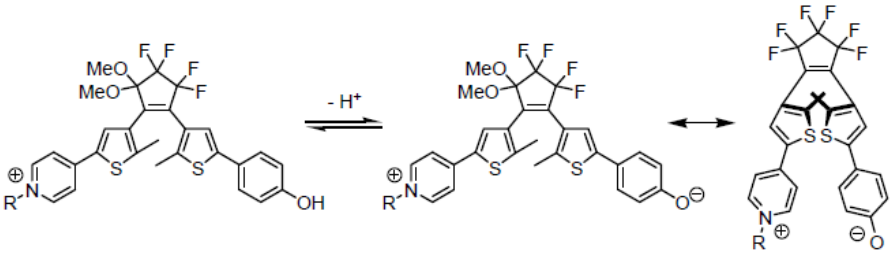

Scheme (I.18)[58]: photochemical pKa-modulation of a DTE derivative

I.4.2.5 Gated photochromism by intramolecular proton transfer

Ohsumi *et al*[41] developped a system in which the excited state of the open form is quenched by an intramolecular proton transfer from a phenol group to a carbonyl group **(Scheme (I.19))**. In this form, the DTE molecule is photoinactive and protection of the phenolic unit by esterification inhibits the proton transfer. Therefore, the molecule becomes photoswitchable. When the closed isomer is deprotected by hydrolysis, the phenolic unit is restored and the photoinduced ring opening reaction is not inhibited. Moreover, the open isomer will be photoinactive

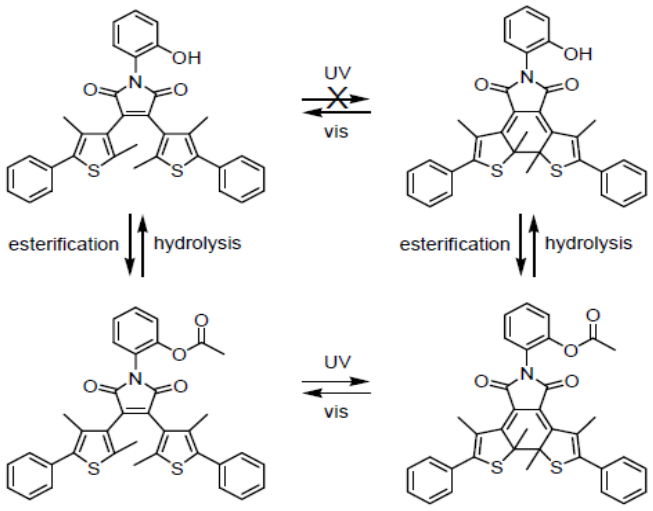

Scheme (I.19)[41]: chemical control of the photochromic reactivity of a DTE derivative.

I.4.2.6 Protons gated from P- to T- photochromism

Kobatake *et al*[59] developed a P-type photochromic diarylethenes having a diethylamino group **(Scheme (I.20))** which can switch to T-type photochromic system by the addition of trifluoromethanesulfonic acid as an external stimulus. This behavior allows for controlling the thermal ring opening reaction of the molecular switch using light or chemicals.

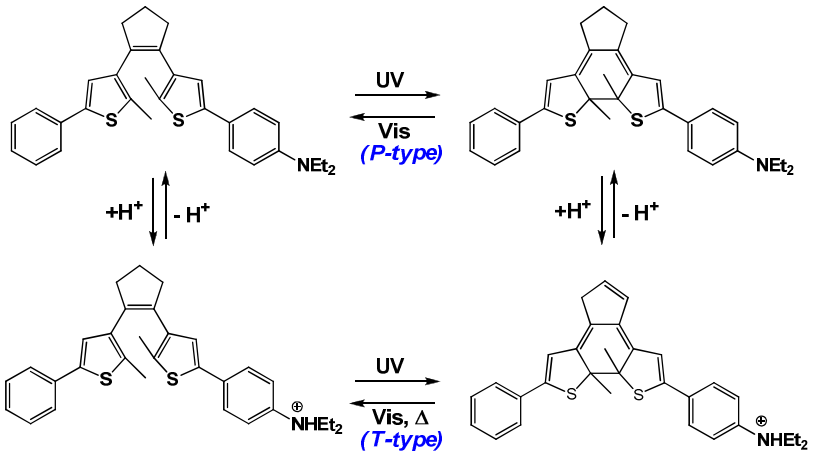

Scheme (I.20)[59]: acid-induced photochromic system switching of a DTE derivative between P- and T-types

All examples presented above, show two possible behaviors for DTEs derivatives: they act as an actuator (in reactivity photomodulation) or as a sensor (in gated photochromism). Examples show also that photomodulation and gated photochromism originate from the coupling between the photochemical isomerization of DTEs derivative and the thermal process involving one or both of the photoisomers.

I.4.3 The combination of photomodulation and gated photochromism

The relationships between photomodulation and gated photochromism, can be presented by an interacting kinetic network of chemical and photochemical reactions. Photochemical and chemical processes construct a square network **(Figure (I.1))** in the particular case of a complexation of the photochromic molecule with another chemical entity (it is represented by the red circle in **figure (I.1)**. This entity can be a metal-ion[60] or a proton[40]

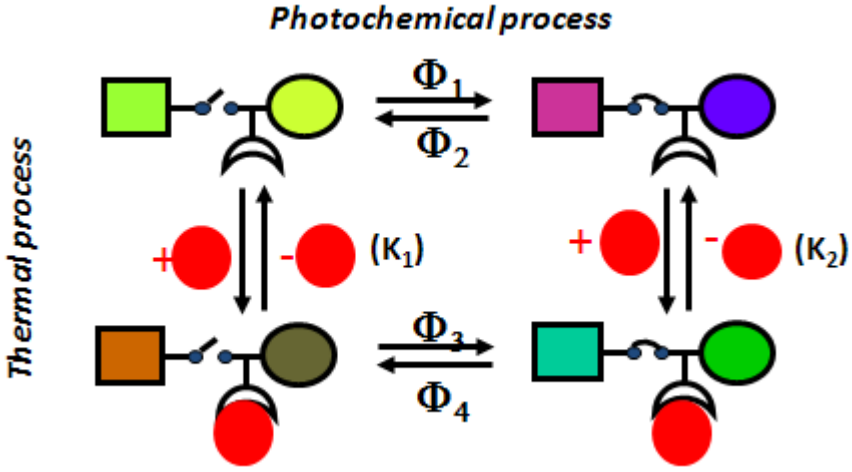

Figure (I.1): The relationships between photomodulation and gated photochromism

The two horizontal processes are related to the photochemical transformation between the photoisomers, open and closed forms. These processes lead to the "gating" of the photochromic property (coloration or discoloration) as the photochemical transformation process is made sensitive to complexation process (thermal process). The two vertical processes involve thermal processes and compare the two isomer's affinity for the chemical entity. Therefore, the complexation constant can change with light leading to the "photomodulation" of the complexation equilibrium.

Photomodulation and Gated photochromism are generally claimed to be strictly on/off reactions[61]. Unfortunately this situation is not always achieved, and observed results cannot be reduced to the simple commutation between two ideal situations. Usually, the two photoisomers coexist at the photostationnary state and respond simultaneously to the thermal reaction leading to a complex interacting chemical system. In such a complex system, mechanisms are often made up of many steps, interconnected by the presence of several common species. In this case, the analysis of such a system and the determination of

parameters such as quantum yields, multiple-equilibria stability constants or kinetic rate constants will be more difficult. Hence, the interest for using dynamic analysis methodology in which all the interacting chemical and photochemical processes are considered.

I.4.3.1 Dynamic Modeling methodology

Dynamic modeling[69] is a powerful tool for the understanding of complex reacting systems. It takes into account all the interactions and all the processes inside the system.

Kinetic studies of the temporal evolution of complex systems allow us to establish a representative model of the mechanism. This model is constructed from a description of the different steps by using differential equations.

Given the complexity of the mechanism in such systems, only numerical methods can be used to integrate differential equations. Once integrated, these equations give the simulated curves of the species evolution. Then the simulated curves are fitted to the experimental curves in order to adjust the model parameters. Using this fitting method it is possible to reject some mechanistic assumptions and to extract the numerical values of physico-chemical parameters such as rate constants or molar extinction coefficients.

This method of dynamic modeling allows to test the validity of complex reaction mechanisms and to extract the parameters values from the starting experimental data. Once the model is validated and parameterized, it allows to envisage certain effects and to imagine other experiments permitting to check its predictive character.

Chemical dynamic modeling established in this thesis, were carried out by using the local software named (SA), Simulation and Adjustment. It allows simulating and adjusting a dynamic model which leads to optimize its parameters. It is built by independent blocks which are easily accessible **Figure (I.2):**

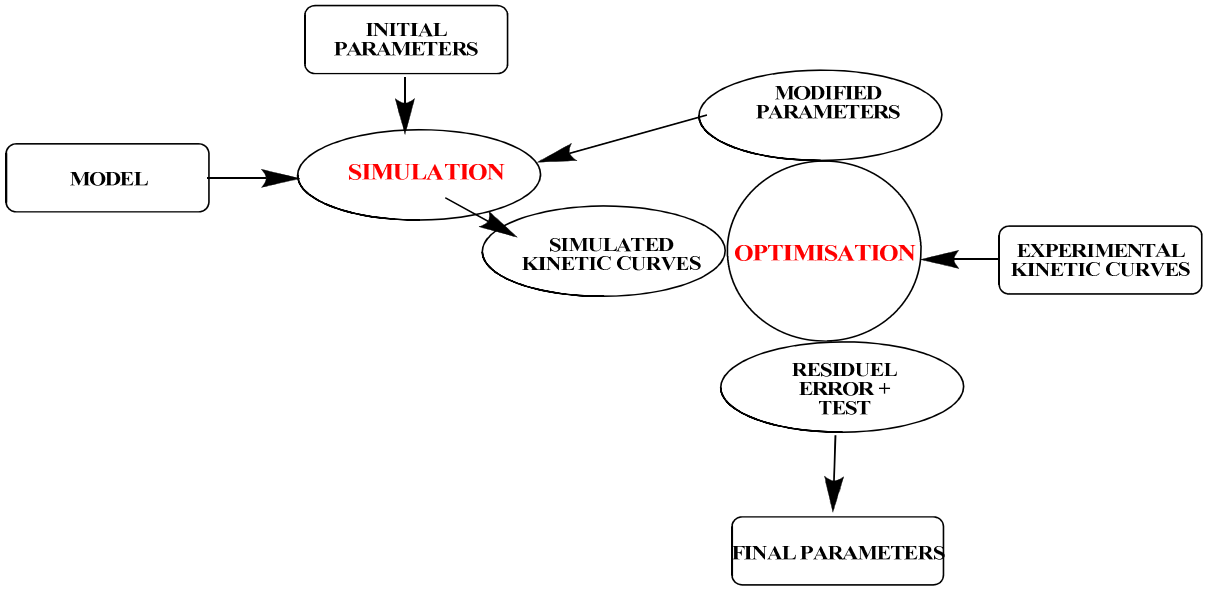

Figure (I.2): diagram of the method of simulation and adjustment

Starting from a proposed model, the corresponding differential equations are written and numerically integrated. To start the integration, the known values of the experimental constraints (initial concentrations) and the realistic initial values of the various unknown parameters (constants rate, quantum yields, molar absorption coefficient, equilibrium constants….) should be introduced. The simulated curve obtained by integration is compared with the experimental data by calculating an error function *F* based on the method of the least square:

$$F = \sum i \sum m \left\{ \frac{\left[Y_{exp}(m) - Y_{calc}(m) \right]^2}{i\, m} \right\}$$

where *i* represents the number of the simultaneous fitted plots and *m* represents the number of measurement's points in each plot. The terms Y_{exp} and Y_{calc} represent the experimental and the calculated values respectively.

In an optimization process, the preceding function is considered as a function of all the parameters to adjust. The estimation of these values is made in an iterative way. In other words, after a first evaluation of F, the optimizer seeks a new handset of parameters. These new parameters are reinserted, by successive iterations, in a simulation to give a minimum value of *F*. Thus, the optimized values of the parameters are extracted.

I.5. Summary

In this introductory chapter, the relationship between photochemical and chemical processes was investigated through the integration of photochromism and chemical reactivity in defined systems. The combination of photochromism and chemical reactivity can be applied in different scientific domains; it can be useful for the regulation of the drug delivery or in chemical detection systems. For this purpose, photoswitchable sophisticated DTEs derivatives were presented as well as their successful interaction with chemical processes to form systems where light controls reactivity and where reactivity controls photochromism. Finally, chemical dynamic analysis methodology was introduced as a powerful tool to study interacting networks of chemical and photochemical processes.

I.6. Thesis Overview

The aim of this thesis is the study of reactivity photo-modulation and gated photochromism behaviors of a mini-sized diacid DTE derivative in different guest systems:

In chapter 2, a complete quantitative investigation of the diacid DTE derivative is carried out in the presence of base. This quantitative study is established according to the chemical dynamics methodology. It allows the determination of the main photochromic, spectral and thermodynamic parameters of this base sensitive DTE. Photoisomerization between open and closed isomers is investigated by UV-visible and ^{1}H NMR spectroscopy. Despite its very simple structure, this compound shows a rich variety of behaviors, based on “gated photochromism “and “photomodulation”.

In chapter 3, the isomerization between the diacid DTE photoisomers, open and closed form were studied in the presence of copper (II). The effect of Copper (II) was investigated in two cases: in the photo-coloration process and in the redox-bleaching process: In the case of photo-coloration, the presence of copper (II) in the medium leads to a delay in the coloration process. In the redox-bleaching process, the copper oxidizes the diacid DTE closed isomer leading to the formation of the colorless opened isomer. When the diacid closed isomer is partially deprotonated, copper reactivity is inhibited and the bleaching doesn’t take place.

In chapter 4, the same diacid DTE was investigated in presence ZnO nanoparticles. Each one of the two isomers (open and closed) is exploited to modulate the emission of the fluorescent ZnO quantum dot. The extinction of the emission intensity by electron and energy transfer processes was suggested. The emission intensity can reversibly be switched between high and low values under the influence of optical stimulations.

Chapter II:
Acidity photomodulation and gated photocromism of diacid DTE derivative

Chapter II - Acidity photomodulation and gated photochromism of a diacid DTE derivative

The aim of this chapter is to present a quantitative study of gated photochromism and the acidity photomodulation properties of a diacid dithienylethene compound, DTE(COOH)$_2$. Chemical dynamic modelling methodology will be applied to establish main photochromic (quantum yields of photocyclization and cycloreversion processes), spectral (molar extinction coefficients) and thermodynamic (equilibria constants) parameters of the diacid DTE(COOH)$_2$ in the presence of a base, the tetrabutylammonium hydroxide. The photochromism of the diacid DTE(COOH)$_2$ will be investigated firstly in pure acetonitrile, then in the presence of various amounts of base,, in acetonitrile/water mixtures. From the whole set of these quantitative experiments gated photochromism and photomodulation effects will be determined.

II.1. Introduction

A developing area of photochromic compound studies is devoted to the examination of the dye as an "actuator" or a "sensor". Such a property, originates in the coupling between the photochemical isomerization and an associated thermal process involving one or both of the photoisomers. The interplay between the two reactions can be depicted from two points of view:

- From the photochromic reaction, one can define the *gated photochromis*: this corresponds to a special form of photochromism which one or both forms of a photochromic system are chemically and reversibly transformed into a non-photochromic form[62]. In these conditions, the photochromic dye acts as a "sensor", since the photochromic efficiency depends on the presence of the other reagents.

- From the thermal process side, *photomodulation* refers to the light-induced difference in the physico-chemical properties between the two photochromic isomers such as the ability to alter metal-ion[60] or proton-binding constants[40]. In some cases, the interacting dark process is a sophisticated catalytic cascade: the efficiency of the catalyst being modulated by light[63]. In this second point of view, the dye acts as a photoactive "actuator", triggering a chemical process in the medium.

Chapter II - Acidity photomodulation and gated photochromism of a diacid DTE derivative

Among the various photochromic compounds that have been submitted to *gated photochromism* and *photomodulation* studies, dithienylethenes (DTE) exhibit some advantageous photochromic properties, such as thermal irreversibility and fatigue resistance[19]. *Gated-photochromism* and *photomodulation* effects in DTE's have been extensively studied for controlling various chemical and physical properties from light stimulations[64].

Most of these effects are based on changes in the extension of π-conjugation upon the ring closure and ring opening photochromic reaction. For this purpose, the DTE moiety is inserted between a reactive group which is the locus of the aforementioned thermal process and a substituent with a strong electronic impact. After the DTE ring closure, a push-pull polyene connexion appears between the two ends of the molecule, thus modifying the reactivity of the functional site.

II.2. Acidity photo-modulation and gated photochromism of base sensitive DTEs derivatives

Lehn and co-workers reported a photomodulation of the pK_a in a DTE compound bearing at each end of the dithienylethene π-conjugated chain, a phenol group as a proton donor and a pyridinium group as an acceptor[58] (compound (1) in **scheme (II.1)**.

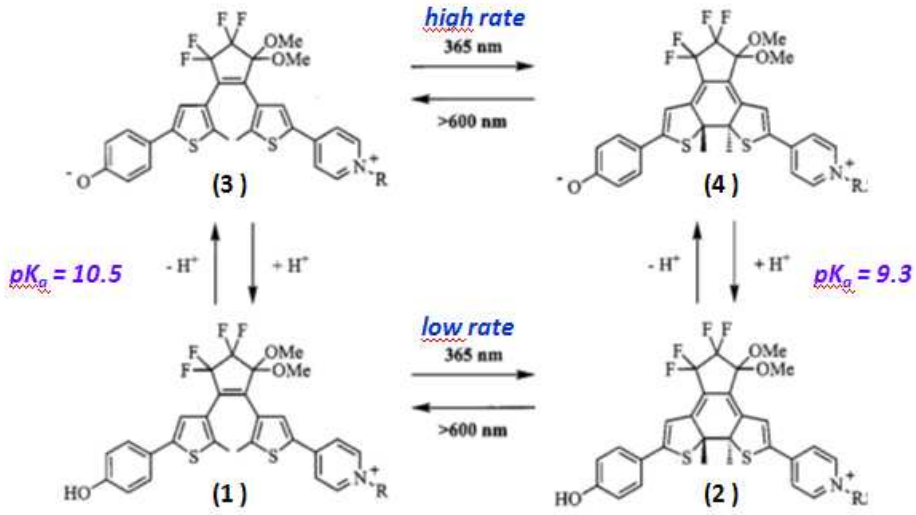

Scheme (II.1)[58]: photomodulation of the pK_a and gated-photochromism in a DTE derivative

A decrease of more than one pK unit was observed when the dithienylethene is closed. Moreover, at high and low pH values, the relative rates of photocyclization were found to be 1 and 0.003, respectively. The provided interpretation of this *gated-photochromism* effect is that once deprotonated, an ionic interaction between the phenolate and pyridinium groups locks the molecule in a parallel conformation where it cannot undergo photocyclization. This effect is matched with a *photomodulation* of the pK_a, because once the DTE is closed, the phenol and the pyridinium groups become conjugated.

Since the pioneering work of Lehn and co-workers, many systems have been scrutinized. Odo *et al*[39] have investigated dithienyletethene derivatives containing a 2,5-diaryl-3-thienyl group. The DTE derivatives contain also a phenol group as a proton source and a pyridinium group as an acceptor unit (**scheme (II.2)**).

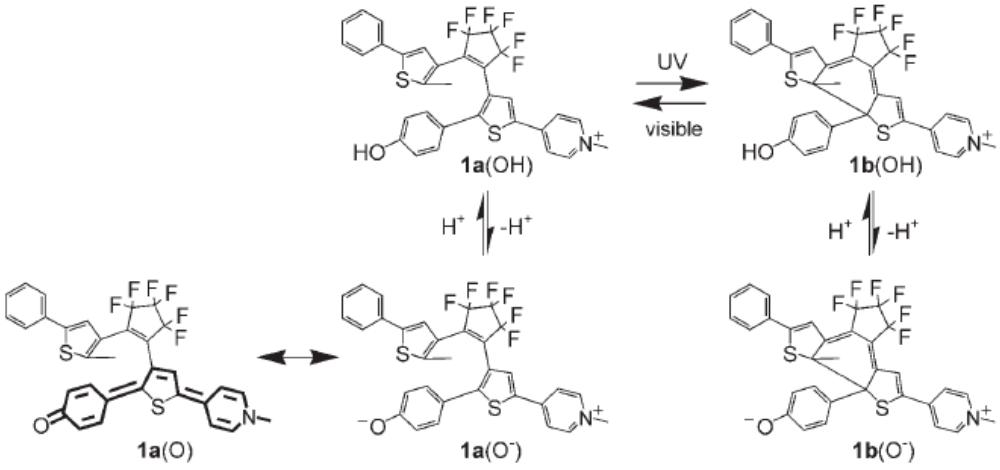

Scheme (II.2): pk_a photomodulation in the case of a base sensitive DTE derivative

The photochemical transformation between the two isomers was affected by the addition of base; the photocyclization reaction was inhibited under high-pH conditions (compound 1a(O^-) in scheme (II.2)). Spectral shifts of open form and PSS mixture upon KOH addition have also been recorded. A pK_a decrease upon cyclization was also witnessed.

Other works have been carried-out to study different base sensitive DTEs derivatives. Chen and co-workers[65] studied the photochromic property of diarylperfluorocyclopentenes bearing pyridinium benzimidazole (betaine) groups. The investigated DTE can be switched by

alternative addition of acids and alkalis. It has been found that these compounds gave typical photochromic reaction, but after the addition of alkalis, the quantum yields of ring closure vanished. Upon acid addition, the photochromism was recovered. Lewis acidity can also be photomodulated [66]. The binding constant of the closed isomer with pyridine has been determined at around $(7.0\pm0.4)x10^{3}$ M^{-1}. Although not accurately measured, the corresponding binding constant with the open form has been assumed to be very small. It was also found that the photobleaching rates decreased in presence of pyridine.

All the cited examples above show that reactivity photomodulation and gated photochromism are inseparable phenomena. Therefore the two behaviours aforementioned are investigated simultaneously in the case of a base sensitive DTE derivative.

The relationships between photomodulation and gated photochromism in the case of a base sensitive DTE derivative are presented by a square network. This network involves five species (X, Y, H, XH and YH) and eight processes [67]**(scheme II.3)**. From the chemical dynamics point of view, gated-photochromism and photomodulation can be described as elements in this network.

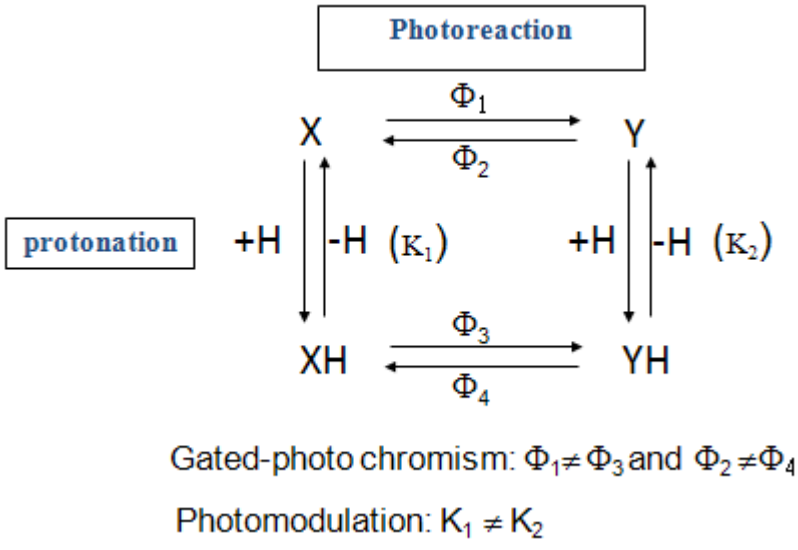

Scheme (II.3): interacting network of photochemical (photoreaction) and chemical (protonation) processes.

Quantitative investigation of such a network requires the determination of a lot of parameters, among them are: the forward and reverse quantum yields of the free and associated photochroms (Φ_1, Φ_2, Φ_3 and Φ_4), the association acid-base constants (K_1 and K_2) of the open and closed photoisomers (X and Y) and their respective absorption spectra. For this purpose, chemical dynamic modelling is used as a tool to determine simultaneously several parameters of the set of coupled chemical and photochemical reactions. It allows considering all species and all processes simultaneously under realistic conditions.

In our work, we wish to extend the gated photochromism and photomodulation concepts from the complete analysis of the **scheme (II.3)** using a very simple molecule, the diacid dithienylethene DTE$(COOH)_2$.

II.3. Acidity photo-modulation and gated photochromism of a diacid dithienylethene

II.3.1 Presentation of the diacid DTE dye, DTE$(COOH)_2$

The 1,2-bis(5-carboxy-2-methylthien-3-yl) cyclopentene hereafter **(scheme (II.4))** labelled diacid DTE **1** can exist either as its ring-opened ($\mathbf{AH_2}$) or ring-closed form ($\mathbf{BH_2}$).

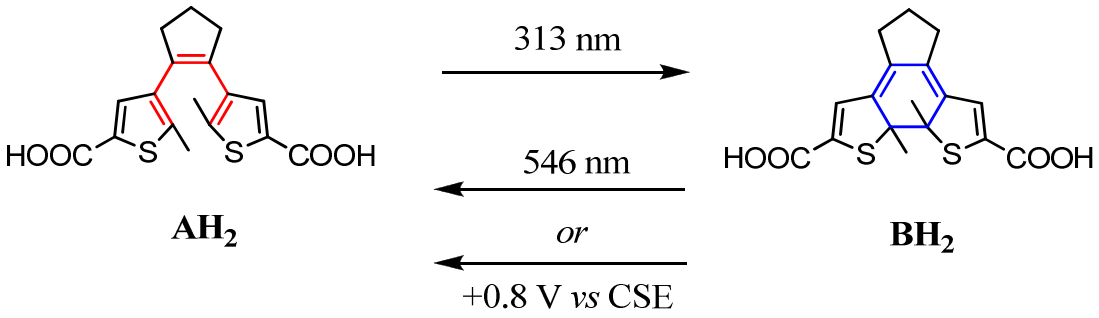

Scheme (II.4): Photochemical and electrochemical[37] interconversion processes between the ring open AH_2 and the ring closed BH_2 isomers of the dicarboxylic acid DTE 1

The CO_2H functionalities are directly grafted on the photoactive core. Noticeably there are neither electronically active groups nor fluorinated substituents that can be conjugated to the CO_2H moiety in any of the isomers. This compound has been used as an intermediate in the synthesis of more complex molecules[68] or has been studied for its electrochemical properties: the ring closed isomer $\mathbf{BH_2}$ can be indeed ring opened back to the open $\mathbf{AH_2}$ one by constant

potential electrolysis at 0.8V (*vs* SCE) in acetonitrile[37]. After photoisomerization, the only qualitative modification due to the change of conjugation is a shift from a thiophenecarboxylic acid (close to benzoic acid) to a substituted acrylic acid **(scheme II.4)**. Therefore, any photomodulation of the acido-basic properties should be attributed solely to the change of the photochromic structure and any gated photochromism effect can be attributed to some deprotonation induced conformational and charge distribution changes. No extensive assay of the behavior of this molecule has been reported so far.

The photochromism of the diacid DTE **1** is investigated firstly in pure acetonitrile, then in the presence of various amount of base, tetrabutylammonium hydroxide, in acetonitrile/water mixtures. From the whole set of these quantitative experiments recorded either in the dark or under 313 and 365 nm irradiation, gated photochromism and photomodulation effects have been determined.

II.3.2 Determination of the quantum yield in neutral acetonitrile

II.3.2.1 Photokinetic analysis

Irradiation with UV light (313 nm) of an acetonitrile solution of the open form ($\mathbf{AH_2}$) of diacid DTE **1** triggered the photocyclization reaction and generated the ring-closed isomer $\mathbf{BH_2}$ (**Figure (II.1)**). The change in color of the solution from colorless to blue was due to the formation of the extended π-conjugated backbone created in the ring-closed isomer. As expected, the corresponding UV-Vis absorption spectra showed the typical signature of ring closing reactions of DTE's **(figure II.1)**. The absorption maximum of the closed form $\mathbf{BH_2}$ appeared at 536 and 354 nm with a clear-cut isosbestic point at 315 nm. The colored solution was thermally stable and returned to the colorless one by irradiation with 365 nm light. The closed-ring isomer $\mathbf{BH_2}$ was isolated by preparative TLC ($\varepsilon(536) = 8100$ $L.mol^{-1}.cm^{-1}$), this work was carried out by *Dr.Rafael Sanchez Sanchez* at *Universitat Autònoma de Barcelona* in *Spain*. The photocyclization conversion at the photostationary state was determined by comparing the absorption spectra of isolated $\mathbf{BH_2}$ with the photostationary solution **(figure (II.3))**. Under 313 nm irradiation, the conversion in acetonitrile was close to 100%.

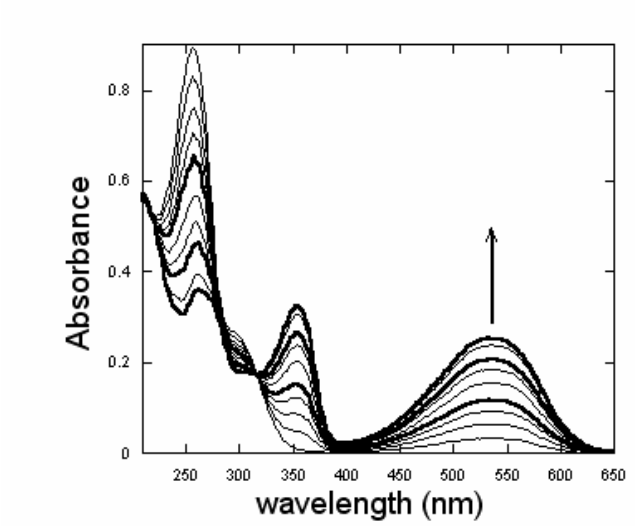

Figure (II.1): Overlay spectra of photocoloration of diacid DTE 1 under 313 nm irradiation of a $3.1x10^{-5}$M CH_3CN solution; Δt between spectra: 13 s, then 26 s, then 65 s, the photostationary state is reached after 260 s of irradiation.

The quantum yields of the cyclization ($\Phi_{AH2\rightarrow BH2}$) and cycloreversion ($\Phi_{BH2\rightarrow AH2}$) of diacid DTE **1** have been readily measured in acetonitrile solution using a photokinetic technique allowing also the determination of the full UV- visible spectrum of the closed form, from the numerical modelling of the absorbance *vs* time kinetic curves recorded under continuous monochromatic irradiation **(figure II.2)** without the need of a chemical isolation[69].

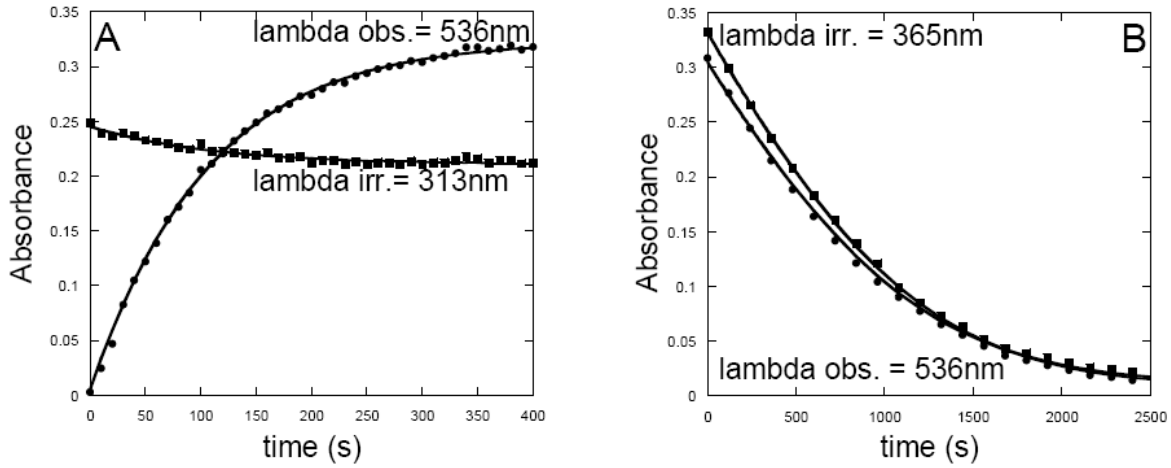

Figure (II.2): Determination of the quantum yields of photocoloration and photobleaching by the photokinetic analysis of the abs *vs* time curves under continuous monochromatic irradiation.A: photocoloration until photostationary state (PSS(313) upon 313 nm irradiation. B: photobleaching until photostationary state (PSS(365) upon 365 nm irradiation

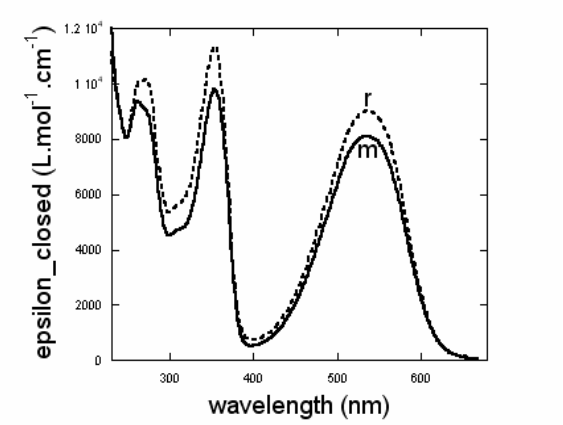

Figure (II.3): Quantitative comparison of the UV-visible spectra of the closed form. m: measured after chemical isolation; r: recalculated from the model

Table (II.1) shows the determined photochromic parameters: quantum yields of cyclization ($\Phi_{AH2\rightarrow BH2}$) and cycloereversion ($\Phi_{BH2\rightarrow AH2}$), molar absorption coefficient of pure BH_2 and at photostationnary state. The molar absorption coefficients are determined at 536 nm and 354 nm.

$\Phi_{AH2\rightarrow BH2}$	$\Phi_{BH2\rightarrow AH2}$	$\varepsilon_{(BH2;\ 536\ nm)}$	$\varepsilon_{(BH2;354\ nm)}$	ε (pure BH2; 536 nm)	ε (pure BH2; 354 nm)
0.9 ± .09	0.025 ± .005	11300 ± 500	9000± 500	8100 ± 300	9800 ± 300

Table (II.1): Photochromic quantum yields and molar absorption coefficients (in $L.M^{-1}.cm^{-1}$) of the closed isomer BH_2 in acetonitrile

The most remarkable result is the very high quantum yield of the photocyclization ($\Phi_{AH2\rightarrow BH2}$ > 0.9). Such a value is relatively unusual among the DTE's which generally show photocyclization quantum yields lower than 0.5. In DTEs derivatives, the cyclization takes place only if the two thienyl groups are arranged in a C2 symmetric conformation having the smallest distance between the two reactive carbon. This conformation is usually called "anti-parallel". However, due to the DTE structure, a thermal equilibrium exists between the photochemically reactive (anti-parallel) conformer and the unreactive (parallel) one. Theoretical studies[70] have shown that cyclization is a very efficient process since the excited state's potential energy surface leads invariably to the *ad hoc* conical intersection. As a

consequence, the ring closure efficiency seems to be limited only by the population of the reactive anti-parallel conformer.

After examination in the literature, to the structures that give high quantum yields[71], we found that bulky substituents on the thiophenic ring increase the photocyclization quantum yields. Many examples are shown in **table (II.2)**

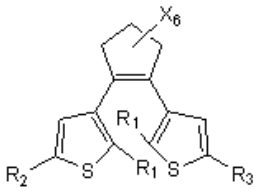

X	R_1	R_2	R_3	$\Phi_{cyclization}$	Solvent	reference
F	C_2H_5	H	C_6H_5	0.52	Hexane	71 l
F	CH_3	CH_3	*p*-CN-C_6H_5	0.54	Hexane	71 b
F	CH_3	C_6H_5	C_6H_5	0.59	Hexane	71 j; 71 i
F	CH_3	CH_3	*o*-F-C_6H_5	0.63	Hexane	71 d
F	CH_3	CH_3	*p*-Cl-C_6H_5	0.68	Hexane	71 g
F	CH_3	CH_3	*o*-OMe-C_6H_5	0.68	Hexane	71a
F	CH_3	C_6H_5	*p*-NEt_2-C_6H_5	0.70	Acetonitrile	71 c
F	CH_3	$NMePyr^+$	$NMePyr^+$	0.71	Methanol	71 k
F	CH_3	C_6H_5	*m*-Cl-C_6H_5	0.72	Hexane	71 f
F	CH_3	*p*-Cl-C_6H_5	*p*-Cl-C_6H_5	0.77	Hexane	71 h
F	CH_3	*p*-C_2H-C_6H_5	*p*- C_2H -C_6H_5	0.92	Acetonitrile	71 e

Table (II.2): Structures of dithienylethenes with higher than 0.5 photocyclization quantum yields. $NMePyr^+$ = N-methylpyridinium; C_2H = ethynyl. References refer to the main text. Even higher ring-closure quantum yields (0.98) are exhibited by some structurally slightly different DTE[72].

II.3.2.2 NMR investigations for the opened form isomer

High quantum yield values originate certainly from a restriction of the thienyl moieties rotation. In order to test if this hypothesis could be extended to the diacid DTE **1**, a variable temperature ^{1}H NMR study has been carried-out in THF. This work was realized in collaboration with *Pr.Stéphanie Delbaere* at *Université Lille 2.*

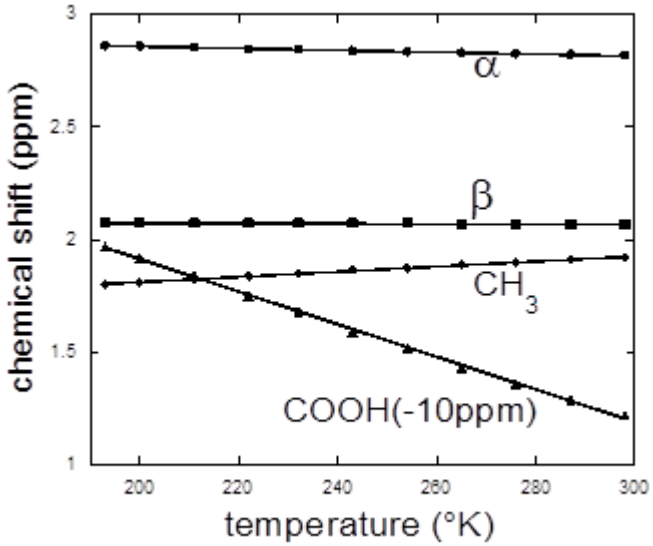

Figure (II.4): Linear variation of the chemical shifts of the various protons on the diacid DTE 1. Refer to the formula for the attributions in scheme II.5.

As expected for a molecule of such a size, the interconversion rate between the parallel and anti-parallel conformations is fast on the NMR time scale. Therefore the temperature effect leads only to a roughly linear drift of the chemical shifts **figure (II.4)** in the variable temperature NMR analysis of the diacid DTE 1 open form.

However, a NMR study on a simple "inverse" dithienylethene (*i.e.* deriving from the 1,2-bis-(thien-2-yl)-ethene core instead of a thien-3-yl)[73] can be used to interpret the temperature decrease shielding effect. For instance, as shown on **scheme (II.5)**, the methyl groups are in the shielding cones of the thienyl aromatic rings in the anti-parallel conformation $\mathbf{AH_2}$, but not in the parallel conformation $\mathbf{aH_2}$. The apparent shielding of the methyl group signal **(figure II.4)**, when the temperature decreases, shows that the anti-parallel conformation is more stable than the parallel one.

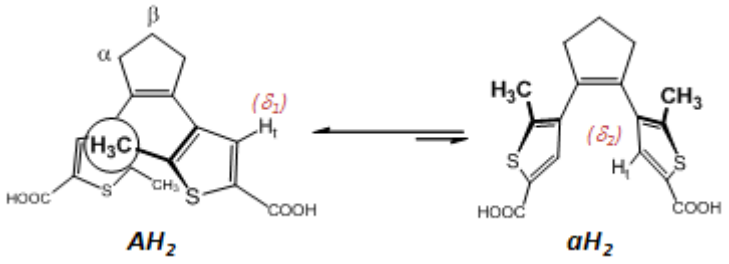

Scheme (II.5): parallel and anti-parallel conformations of the diacid DTE(COOH)$_2$

For the estimation of the parallel *vs* anti-parallel ratio: It is assumed that the parallel and anti-parallel conformers are in rapid equilibrium: $A \leftrightarrow a$

AH_2 is the anti-parallel conformer and aH_2 is the parallel conformer. Each conformer exhibits its own chemical shift, therefore the average observable chemical shift is given by:

$$\delta = \delta_1\alpha + (1-\alpha)\delta_2 = (\delta_1 - \delta_2)\alpha + \delta_2 \qquad \textbf{(1)}$$

Where α is the molar fraction of the anti-parallel conformer AH_2, δ_1 its chemical shift, δ_2 being the chemical shift of the parallel conformer aH_2.

The equilibrium constant:

$$\boldsymbol{K = \frac{[aH_2]}{[AH_2]} = \frac{(1-\alpha)}{\alpha}}, \qquad \textbf{(2)}$$

then :

$$\alpha = \frac{1}{K+1} \qquad \textbf{(3)}$$

$K < 1$ and $\Delta G^0 > 0$

$$`\delta = \frac{\delta_1 - \delta_2}{1 + \exp(\frac{-\Delta G^0}{RT})} + \delta_2 \qquad \textbf{(4)}$$

Most of the regarded protons behave linearly with the temperature. In these conditions, it is not possible to estimate the equilibrium position between the parallel and anti-parallel conformers because this linear relationship imposes that if $T \to \infty$, $\delta \to \pm\infty$.

However, careful examination of the thiophenic proton Ht profile shows that it exhibits a slight curvature **(figure II.5)** which can be fitted using equation **(4)** allowing a rough estimation of the equilibrium constant.

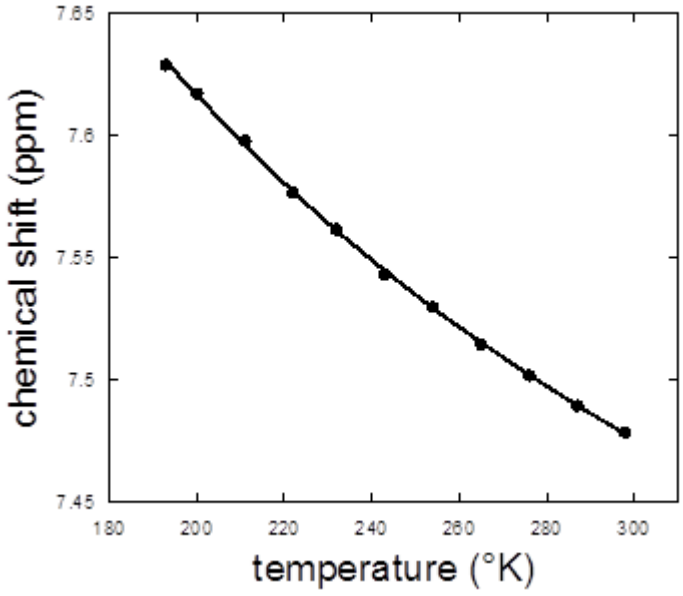

Figure (II.5): decrease of the chemical shifts the thiophenic proton H_t on the diacid DTE 1 with temperature.The variation of the chemical shift of the thiophenic proton H_t allows the estimation of the $\Delta G^0 / R$ parameter at about 280 ± 80 *K* with δ_1 = 7.8 ppm and δ_2 = 6.3 ppm. Note the increase of the shielded parallel conformation with temperature. K ≈ 0.4 ± 0.1 at 300 K *i.e.* α ≈ 80 ± 5 % of the anti-parallel conformer. Such a value is not incompatible with our quantum yield results.

Therefore, the quasi-linear variations of the chemical shifts precluded an accurate measurement of the ΔG^0 of the parallel *vs* anti-parallel equilibrium. However, a rough estimation of $\Delta G^0 \approx 0.6 Kcal / mol$ can be given from the analysis of the shifts of the thiophenic proton H_t signal which exhibit a slight parabolic shape with temperature.

From this value, it was calculated that at room temperature around 80% of the open isomer should exist under the **AH_2** anti-parallel photochemically reactive conformer. Such a value is

in agreement with our quantum yield determination. This remarkable result cannot be accounted in terms of steric hindrance, since the thiophene ring substituents (CH_3 *vs* COOH) are of apparent similar size. A possible explanation may come from electrostatic considerations: the local dipole moments born by each thiophene rings being mutually compensated in the anti-parallel conformation or from the fact that the methyl group lying above the thiophene ring, a CH-π hydrogen bond may exist[74].

On the other hand, the ring opening quantum yield ($\Phi_{BH2\rightarrow AH2}$ = 0.025) remains rather low when compared to much higher values encountered in many DTE's where the cycloreversion quantum yields can exceed 50%, for instance in bis(2-thienyl) perfluorocyclopentenes and in dithienylethene derivatives having a pyrazole unit[75].

II.3.3 Neutralization of the diacid DTE$(COOH)_2$ opened form

Upon addition of base, the absorption spectra of the opened form isomer's solution changed as shown in **Figure (II.6)**. The neutralization is carried out in acetonitrile by successive addition of aliquots of tetrabutylammonium hydroxide. The absorption band of the opened form at λ = 310 nm, showed a shift to shorter wavelengths.

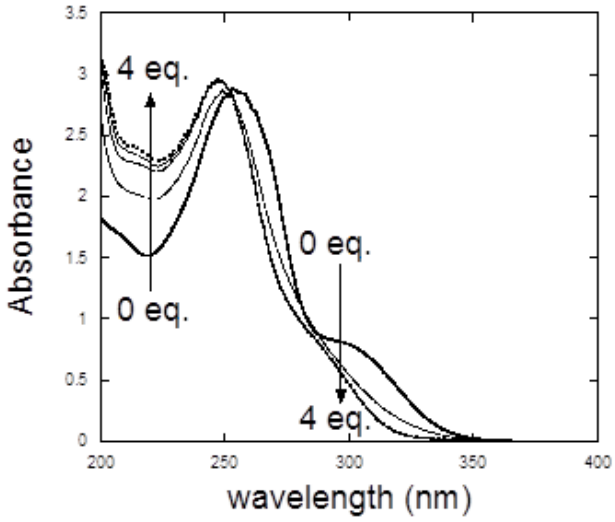

Figure (II.6): Variation of the absorption spectrum of the open form during neutralization by 0 to 4 equivalents of tetrabutyl ammonium hydroxide in acetonitrile [DTE 1]$_0$ = 10^{-4} M.

II.3.3.1 Determination of the acidity constants

The analysis of the neutralization of the open form allows the determination of the acidity constants of the diacid DTE$(CCOH)_2$**. Figure (II.7)** illustrates the titration curves obtained by measuring the absorption changes at λ = 268 and 310 nm. These two wavelengths relate to the maxima absorption differences between the dianion and diacid forms.

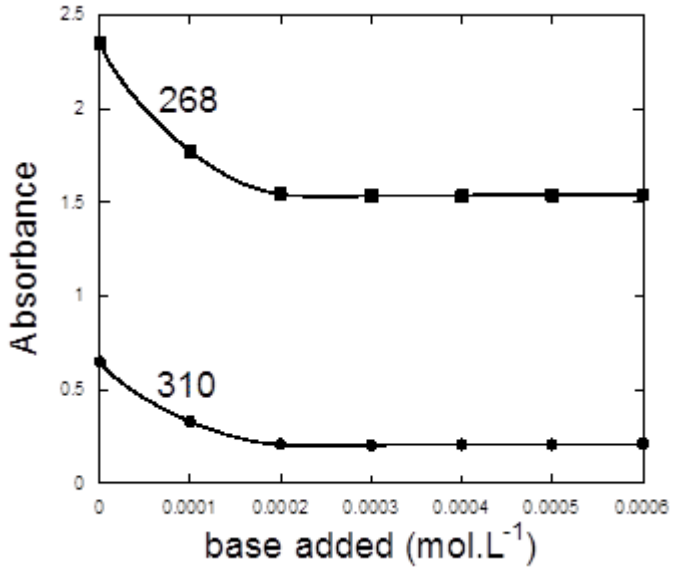

Figure (II.7): Variation of the absorbance at two selected wavelengths during the neutralization of a 10^{-4}M ACN solution of the opened form isomer. Maximum base added correspond to 6 equivalents. Data points = experimental values; solid line fitting by the model.

The following model has been assumed to extract the acidity constant by fitting the variations of the absorbance at two selected wavelengths (λ = 268 and 310 nm) during neutralization **Scheme (II.6)**:

$$AH_2 + OH^- \leftrightarrow AH^- + H_2O; \qquad \log K_1 = 1.2 \pm 0.1$$

$$AH^- + OH^- \leftrightarrow A^{2-} + H_2O; \qquad \log K_2 = 1.6 \pm 0.1$$

Scheme (II.6): neutralization model of the opened form isomer of the diacid DTE$(COOH)_2$

Numerical modeling also provides the species distribution *vs* the base added.

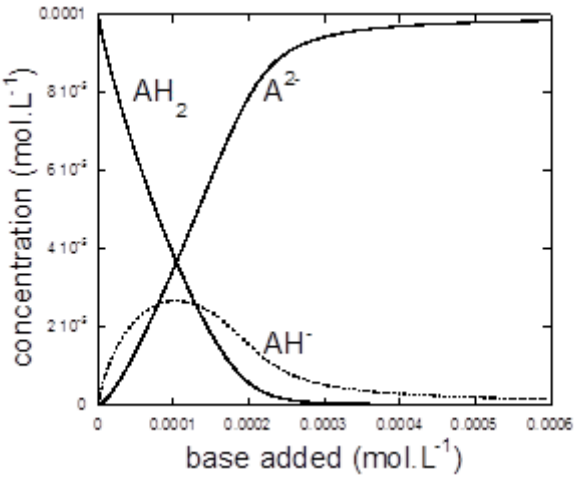

Figure (II.8): Variation of the species concentration during the neutralization of the diacid DTE 1 open form (10^{-4}M) AH_2 : diacid; AH^-: mono-acid, mono-anion; A^{2-}: di-anion

II.3.4 Neutralization of the photostationnary-state of the diacid DTE(COOH)$_2$

Upon addition of base, the absorption spectra of the photostationary-state solution changes as shown in **Figure (II.9)**.

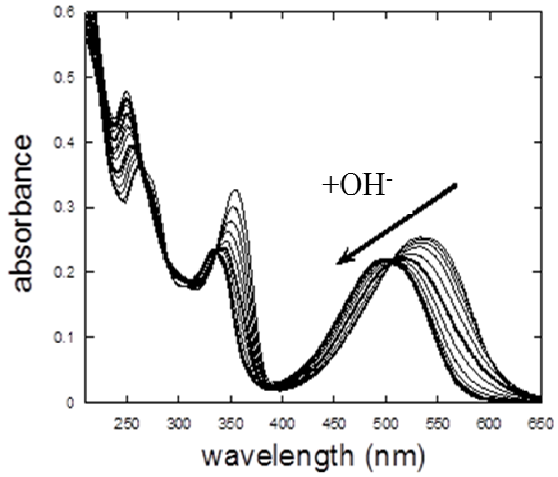

Figure (II.9): Variation of the 313 nm photocolored photo-stationary state spectrum during deprotonation by adding 3.2 equivalents of tetrabutylammonium hydroxide (bold lines are correspondingly at 2.0 and 3.2 eq. of base added). Note the hypochromic and hypsochromic shifts of the visible band of the closed form.

During base addition, the absorption band of the closed form at λ = 536 and 354 nm decreased and new bands appeared at λ = 501 and 335 nm respectively **(figure II.9).** The absorption maximum showed a blue-shift of about 35 nm. Thermal cycloreversion was not observed during the acid–base titrations at room temperature. **Figure (II.10)** illustrates the titration curves obtained by measuring the absorption changes at λ = 248 and 562 nm.

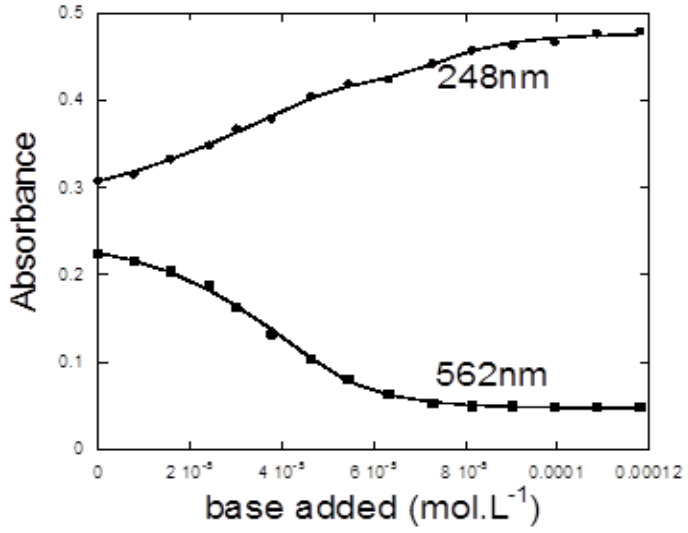

Figure (II.10): Variation of the absorbance at two selected wavelengths during the neutralization of a mixture of open and closed forms of diacid DTE 1. Data points experimental results; solid line: fitting by the model. Maximum of base added corresponds to around 3.2 equivalents.

II.3.4.1 Determination of the acidity constants of the closed ring isomers

The deprotonation equilibrium constants were determined from the numerical modelling of the absorbances *vs* the number of equivalents of base added using the model shown on **Scheme (II.7)** including the deprotonation equilibria in acetonitrile solution of both the open (**AH_2**) and closed (**BH_2**) forms :

$AH_2 + OH^- \leftrightarrow AH^- + H_2O$;	$\log K_1 = 1.2 \pm 0.1$ fixed from previous measurements
$AH^- + OH^- \leftrightarrow A^{2-} + H_2O$;	$\log K_2 = 1.6 \pm 0.1$ fixed from previous measurements
$BH_2 + OH^- \leftrightarrow BH^- + H_2O$;	$\log K_3 = 2.6 \pm 0.4$
$BH^- + OH^- \leftrightarrow B^{2-} + H_2O$;	$\log K_4 = 2.6 \pm 0.2$

Scheme (II.7): **neutralization model of the photo-stationnary state of the diacid DTE(COOH)$_2$**

The extracted equilibrium constants must be considered as only relative pK_a values as the titrations have been performed in an acetonitrile rich solvent where the base dissociation and autoprotolysis constants are not known accurately[76]. However, their ratio or differences (in log-scale) are representative of the acidity changes after photo-isomerization. The model allows also the full determination of the species distribution as a function of the amount of base added **(figure II.11)**

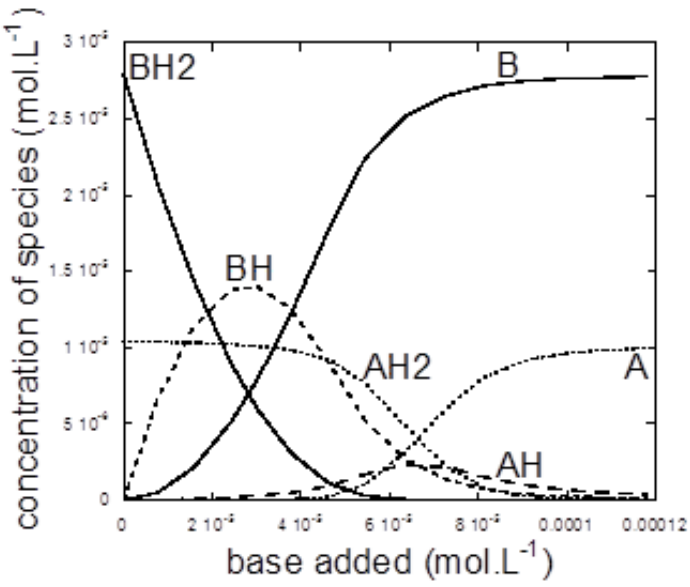

Figure (II.11): Species distribution during neutralization of a mixture 74:26 of closed (BH_2) and open (AH_2) forms. Total concentration of diacid DTE 1 is 3.8*10^{-5}M.

These results show that the acidity of the first carboxylic acid DTE **1** is decreased by about 1.4 pK_a unit upon ring closure. The effect on the second acidity is within the same order of magnitude. In both acidities, **BH_2** is more acid than **AH_2**. Such a pK_a photomodulation is

rather remarkable when compared to some previously published results. For instance, ΔpK_a = 0.8 from the reversible photoswitchable steric shielding of spirofused piperidines[77], ΔpK_a = 1.2 in diarylethene derivatives having a phenol group as a proton source and a pyridinium group as an acceptor unit at each end of the π-conjugated chain[39,58] and ΔpK_a = 1.7 in diarylethenes bearing a diethylamino group[78].

Another outcome from this numerical modelling is the recalculation of the UV-visible absorption spectra of the various deprotonated species of the open and closed forms **(figure II.12a and II.12b).**

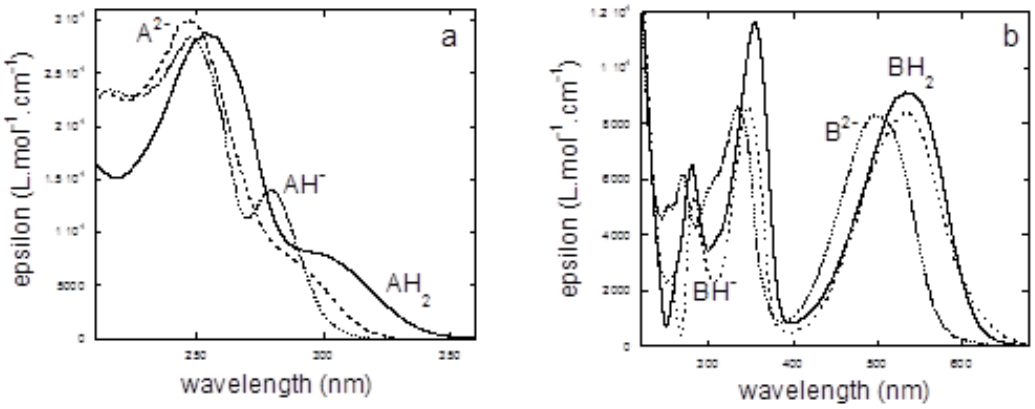

Figure (II.12): Recalculated spectra of the various deprotonated species; a: open forms; b: closed forms. AH_2 spectrum has been measured from the pure open form.

For the opened form, the recalculation of the intermediate spectra: ε_{AH-} and ε_{A2-} have been performed using:

Beer-Lambert Law which is given by: $Abs = \varepsilon_{AH_2}[AH_2] + \varepsilon_{AH^-}[AH^-] + \varepsilon_{A^{2-}}[A^{2-}]$

and mass balance equation: $[AH_2]_0 = [AH_2] + [AH^-] + [A^{2-}]$

For the Photostationnary state solution, the Beer-lambert's law becomes:

$$Abs = \varepsilon_{AH_2}[AH_2] + \varepsilon_{AH^-}[AH^-] + \varepsilon_{A^{2-}}[A^{2-}] + \varepsilon_{BH_2}[BH_2] + \varepsilon_{BH^-}[BH^-] + \varepsilon_{B^{2-}}[B^{2-}]$$

And two mass balance equations will be used:

$$[AH_2]_0 = [AH_2] + [AH^-] + [A^{2-}]$$

$$[BH_2]_0 = [BH_2] + [BH^-] + [B^{2-}]$$

The spectrum of the open form **(figure II.12a)** reveals the presence of two main bands, the higher wavelength band is occurring under the form of a shoulder in $\mathbf{AH_2}$ (300 nm) and $\mathbf{A^{2-}}$ (290 nm), but it is more resolved in the semi-protonated intermediate $\mathbf{AH^-}$ where a nice peak is clearly visible at 280 nm. A slight blue shift upon deprotonation is also visible on the lower wavelength band moving from 255 nm in $\mathbf{AH_2}$ to 247 nm for the mono and dianion. The closed form **(figure II.12b)** behaves similarly exhibiting also a significant blue shift upon depronation. This blue-shift is accompanied by a weakening of the absorption intensities in $\mathbf{BH^-}$ and $\mathbf{B^{2-}}$(hypochromic effect).

These quantitative determinations of the intermediate spectra of the deprotonated isomers must be highlighted because, looking at the literature there are no many examples of quantitative spectral results related to pK_a photomodulating photochromic compounds[58, 65,78]. The main reason of such a few numbers of quantitative findings is that the exact conversion rate at the photostationnary state (PSS) is not known accurately[79].

II.3.5 Reactivity photomodulation vs Gated photochromism

The influence of bases on the photochromic reactivity of the diacid DTE$(COOH)_2$ has been investigated by measuring the photocyclization and photocycloreversion quantum yields in the presence of various amounts of tetrabutyl ammonium hydroxide equivalents. The results are gathered on **figure (II.13).**

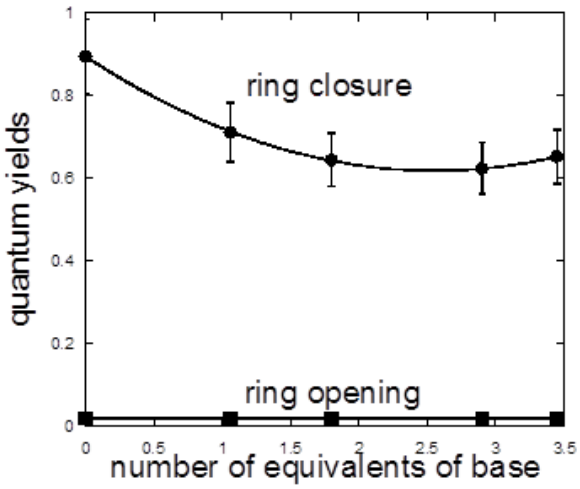

Figure (II.13): Variation of the apparent quantum yields of ring closure (photocoloration) and ring opening (photobleaching) as a function of base addition. Note that the ring opening process is not base sensitive.

Knowing the species distribution of the open form before irradiation, it is possible to estimate the photocylization quantum yields of each individual species. For the recalculation of the quantum yields of the intermediate species AH_2, AH^- and A^{2-}: It has been assumed that the observed quantum yield of photocyclization was a linear combination of the individual quantum yields of the diacid, mono-anion and dianion species.

$$\Phi_{obs} = \Phi_{AH_2}[AH_2] + \Phi_{AH^-}[AH^-] + \Phi_{A^{2-}}[A^{2-}]$$

eq. added	Φ_{obs}	$[AH_2]$	$[AH^-]$	$[A^{2-}]$
0	0.90	100	0	0
1	0.71	0.365	0.270	0.365
1.8	0.64	0.087	0.187	0.726
2.9	0.62	0.006	0.058	0.936
3.5	0.66	0.003	0.039	0.958

Table (II. 3): Variation of the quantum yield of photocyclization and calculated proportions of species distribution during the neutralization of diacid DTE$(COOH)_2$ open form.

$$\Phi_{AH_2} = 0.90\,,\ \Phi_{AH^-} = 0.50\,,\ \Phi_{A^{2-}} = 0.67\ .$$

It was found that the photocyclization quantum yield of the dianion form $\mathbf{A^{2-}}$ is around 0.67, while it is only ≈ 0.5 for the monoanion $\mathbf{AH^-}$. This result reveals that deprotonation shifts the anti-parallel *vs* parallel conformation equilibrium towards the photo-inactive parallel conformer ($\mathbf{aH^-}$). Such a result can be explained if another stabilizing interaction appears in the molecule. Indeed it is possible to create, in the monoanion form, an intramolecular hydrogen bridge[80] between the COOH and the COO^- **(Scheme II.8).**

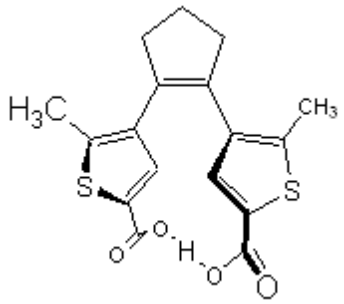

Scheme (II.8): the anti-parallel conformation of mono-anion form of the open ring isomer of DTE(COOH)$_2$

In this structure, the proton plays the role of a "lock" for the parallel conformation[81]. The hydrogen bonding effect disappears when the compound is under its dianionic form, giving rise to a further increase of the photocyclization quantum yield. Such an assumption is also in agreement with the UV visible data above-mentioned. The conformation of the molecule in the parallel geometry should strongly distort the molecule thus reducing its global conjugation: this can explain why the extracted spectrum of the $\mathbf{AH^-}$ form is more blue-shifted than the other two species $\mathbf{AH_2}$ and $\mathbf{A^{2-}}$.

Figure (II.14) summarizes the main processes and species involved in the pK_a photomodulation and gated photochromism of the diacid DTE(COOH)$_2$. pK_a photomodulation occurs because the proton release is easier when the compound is under its closed form. On the other side, gated-photochromism is related to the shift of the parallel *vs* anti-parallel equibrium under deprotonation. The two phenomena are matched because they are two aspects of the same global phenomenon: the interactions between the added bases and the various isomer and conformers of the photochromic compound.

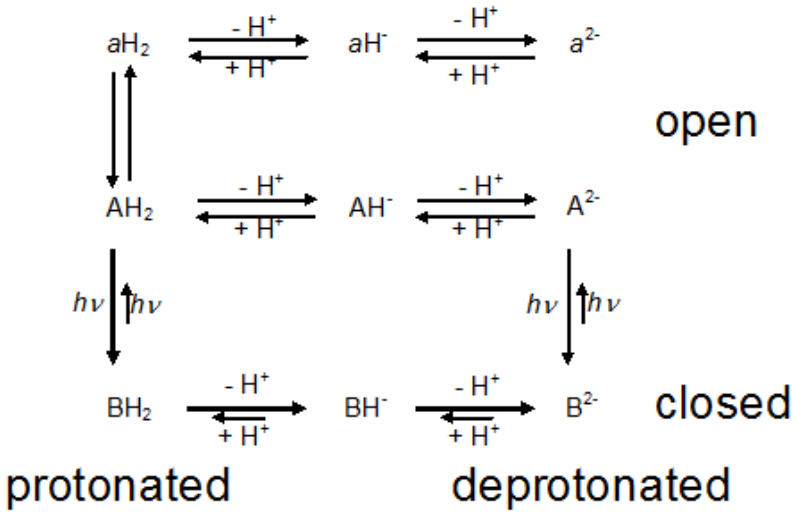

Figure (II.14): Schematic model of the pK_a photomodulation and gated photochromism of the diacid DTE 1. *a*H_2 and AH_2 represent respectively the parallel and anti-parallel conformers of the open forms of the diacid DTE 1. Bold arrows are related to fast processes, while medium and small-sized arrows symbolize medium and slow processes.

Such kinetic schemes, including multistate multifunctional systems, are important because they are also encountered in photochromic chemosensors[82] and flavylium networks[83]. As a feasible application is the creation of a photoacid generator. Numerical simulation of a schematic model of the acidity photomodulation and gated photochromism of the diacid DTE$(COOH)_2$ shows that the concentration of hydroxide ions [OH^-] can be significantly altered under 313 nm then 365 nm irradiation **(figure II.15)**.

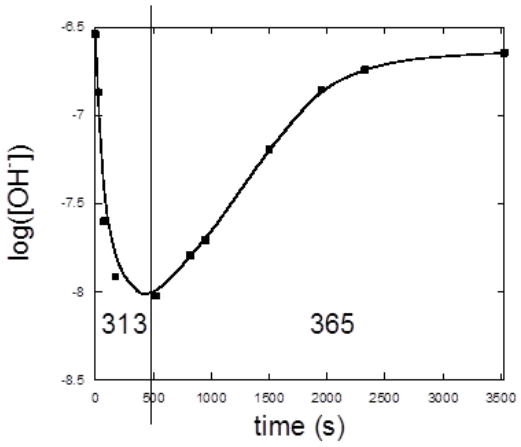

Figure (II.15): Numerical simulation of the variation of the [OH-] concentration (in log-scale) of a mixture of diacid DTE$(COOH)_2$ and hydroxide base ($3.1x10^{-5}$ and $1.5x10^{-5}$ mol.L^{-1} respectively) under 313 (photocoloration) then 365 nm (photobleaching) irradiation.

This prediction has been confirmed experimentally using a water/acetonitrile (20/80) mixture as solvent. As expected, the pH dropped-off by more than one unit after 313 nm irradiation of a partially neutralised diacid DTE$(COOH)_2$. Then, a slower pH raise of about 0.75 was recorded under 365 nm irradiation. Table (II.4) gathers all the kinetic, thermodynamic and spectroscopic parameters that characterize the gated photochromism and acidity photomodulation of the DTE diacid 1 in acetonitrile solution.

	AH_2	AH^-	A^{2-}	BH_2	BH^-	B^{2-}
$\Phi_{cyclization}$	0.9 ± 0.09	0.5 ± 0.05	0.67 ± 0.07	-	-	-
$\Phi_{cycloreversion}$	-	-	-	0.025± 0.005	0.025± 0.005	0.025± 0.005
log K	1.2 ± 0.1	1.6 ± 0.1	-	2.6 ± 0.4	2.6 ± 0.4	-
λ (nm)	255; 300	247; 280	247; 290	355; 536	346; 533	332; 498
ε ($L.mol^{-1}.cm^{-1}$)	29900; s	28200; 14000	28700; s	11600; 9100	8500; 8400	8600; 8300

Table (II.4): Measured and extracted parameters related to the gated-photochromism and acidity photo-modulation of diacid DTE 1.

II.4. Conclusion

For the first time, we have provided a complete quantitative analysis of the gated-photochromism and photomodulation properties of a photochromic diacid DTE. Photomodulation of the acidity results to a more than one pK unit difference between the open and closed forms which appear more acidic. It is likely that this effect is related to the global electronic reorganization and geometrical changes that accompany the photocyclization. In particular, the rigidity of the closed isomer puts the carboxylic substituents in a less hindered environment where the proton release ability is enhanced. On the other side, gated-photochromism effects are much more remarkable as the photocyclization quantum yield drops from the outstanding value of 0.9 to 0.5 by the removing of only one proton on the DTE$(COOH)_2$. The high photocyclization quantum yield value of the diacid open form has been confirmed from the variable temperature ^{1}H NMR analysis of the anti-parallel *vs* parallel conformational equilibrium. Lower photochromic reactivity under the mono-anionic form suggests that the conformation is fastened in parallel orientation by an intramolecular hydrogen bond between the two carboxylates. This system has been demonstrated to be a reversible photoacid generator when irradiated with 313 nm, then with 365 nm light.

Chapter III:
Study of the interaction between Cu(II)and the diacid DTE$(COOH)_2$

Chapter III: Study of the interaction between Cu(II)and the diacid DTE(COOH)2 77

The ring closure reaction of the diacid,$DTE(COOH)_2$, a P-photochrom, occurs upon UV irradiation while its ring opening reaction is triggered by a photochemical isomerization reaction. It is known that the electrochemical oxidation leads to a ring opening reaction, the closed isomer BH_2 being transformed into its opened form AH_2 by means of an ECE mechanism involving the closed isomer radical cation $BH_2^{\cdot +}$ as an intermediate.

The aim of this chapter is to investigate the chemical ring opening reaction of the diacid $DTE(COOH)_2$ closed isomer into its ring opened isomer. We choose Cu(II) as an oxidizing reagent to promote ring opening reaction of the $DTE(COOH)_2$ closed isomer because the redox couple of Cu(II) lies between those of the closed and opened form. Indeed the thermal bleaching of a PSS mixture of closed and opened isomers was observed but with complex kinetics. In order to define the possible mechanism taking place in the reaction medium, slow and fast kinetic studies were carried out.

III.1 Introduction

Two different stimuli, light or electricity, can be used to trigger interconversion's reactions of DTEs derivatives. Indeed, when substituted by electron withdrawing substituents, the closed form *BH_2* **(figure (III.1) A)** of dithienylethene yields the open form isomer *AH_2* upon oxidation, thus bypassing the photochemical ring opening reaction. In other words the P-photochrom becomes a T-photochrom under oxidative conditions.

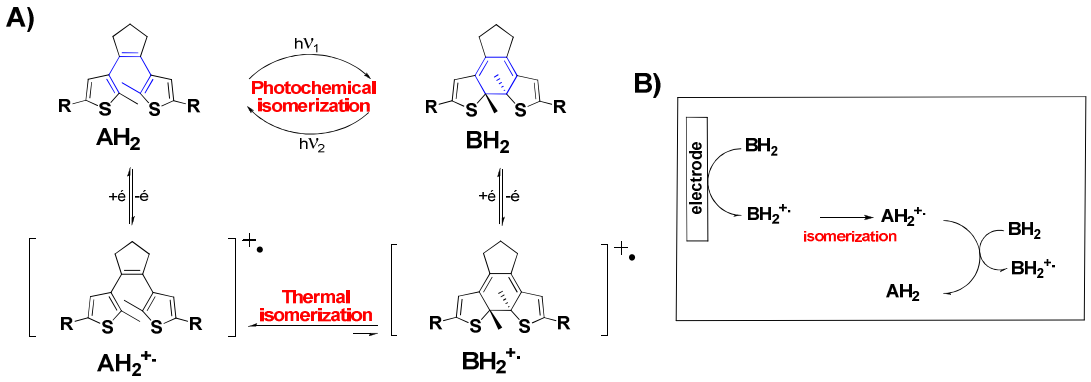

Figure (III.1): A) photochemical and electrochemical interconversions processes involved in the cyclization and cycloreversion reactions of DTEs derivatives B) mechanism of chain reaction after oxidation (BH_2)

For most of the examples described in the literature, the oxidation reaction is running electrochemically. The mechanism proposed, based on the analysis of cyclic voltammograms at various scan rates, consists of two steps: the first step is an electrochemical reaction corresponding to the heterogeneous electron transfer (oxidation of BH_2 into $BH_2^{\cdot+}$), the obtained radical evolves then thermally into its open isomer $AH_2^{\cdot+}$**.** This radical is then reduced to give the neutral open form. In term of electrochemical kinetics the mechanism is an ECE sequence. However, the redox couples are not organized in a decreasing way: in fact the redox couple E°($AH_2^{\cdot+}$/ AH_2) of the open form isomer is usually higher than the redox couple of the closed form isomer E°($BH_2^{\cdot+}$/ BH_2), (for $DTE(COOH)_2$: open form 1.4V, closed form: 0.8 V vs. SCE in acetonitrile[37] thus the product is more oxidizing than the reactant. This property can be used to envision a chain reaction **(figure (III.1) B).**

III.2 Forms of the diacid DTE $(COOH)_2$

In the previous chapter, the dicarboxylic acid dithienylethene $DTE(COOH)_2$ was regarded as a bifunctional molecule having a photochromic unit and two acidic functions. Thus introduction of the redox properties brings now a third functionality. As the studied diacid carries two electron-withdrawing groups (two COOH groups) the electrochemical process will then be the ring opening.

All transformations can be organized according to 3 directions **Figure (III.2)**:

1) Photochemical status : it corresponds to the photochromic interconversions
2) Redox status: all DTEs are able to undergo a redox process. Only the first oxidative reaction will be considered in our study
3) Protonation status: it is due to the COOH groups. 3 species per photo-isomer can be considered.

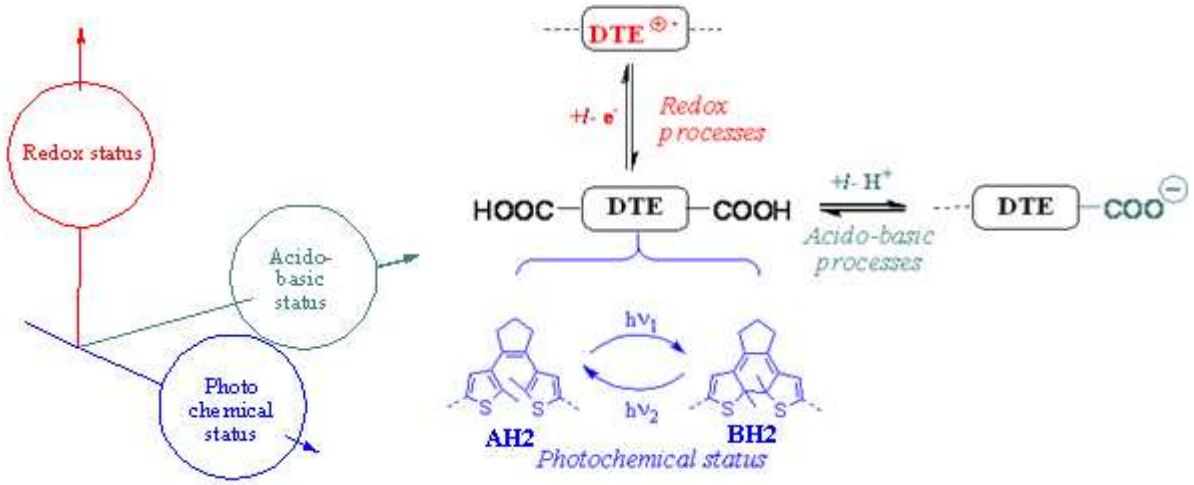

Figure (III.2): Diagram of the involved species as a function of the photochemical status, redox and protonation state.

From this point of view, the dicarboxylic acid dithienylethene is capable of generating at least 12 species. According to the two states of the diacid ; opened isomer $\boldsymbol{AH_2}$ and closed isomer $\boldsymbol{BH_2}$, two sets of diacid species are obtained. By varying the pH and redox potential, each set contains six species which differ in their protonation and redox states:

Opened form Series:

$\boldsymbol{AH_2}$, $\boldsymbol{AH^-}$, $\boldsymbol{A^{2-}}$: di protonated, mono protonated and deprotonated forms

$\boldsymbol{AH_2^{\cdot+}}$, $\boldsymbol{AH^{\cdot}}$, $\boldsymbol{A^{\cdot-}}$: di protonated, mono protonated and deprotonated radicals

Closed form Series:

$\boldsymbol{BH_2}$, $\boldsymbol{BH^-}$, $\boldsymbol{B^{2-}}$: di protonated mono protonated and deprotonated forms

$\boldsymbol{BH_2^{\cdot+}}$, $\boldsymbol{BH^{\cdot}}$,$\boldsymbol{B^{\cdot-}}$: di protonated mono protonated and deprotonated radicals

In Chapter 2, we studied the photochemical properties of the diacid $DTE(COOH)_2$ as a function of pH variation. Deprotonation constants were determined for each of the following species: for the open form ($\boldsymbol{AH_2}$, $\boldsymbol{AH^-}$, $\boldsymbol{A^{2-}}$) and the closed form ($\boldsymbol{BH_2}$, $\boldsymbol{BH^-}$, $\boldsymbol{B^{2-}}$).

To determine the redox potential of the first oxidation of each of the six species ($\boldsymbol{AH_2}$, $\boldsymbol{AH^-}$, $\boldsymbol{A^{2-}}$) and ($\boldsymbol{BH_2}$, $\boldsymbol{BH^-}$, $\boldsymbol{B^{2-}}$), cyclic voltammetry studies were carried out at *Universitat Autònoma de Barcelona* in Spain with *Professor Gonzalo Guirado Lopez*.

III.3 Cyclic voltammograms of A and B forms

The determination of the first oxidation redox couples of the variously protonated species was achieved simply by recording the cyclic voltammograms of a solution of the appropriate substance during its acido-basic titration. We have chosen to run this titration starting from the basic end by adding aliquots of perchloric acid to a neutralized solution of $DTE(COOH)_2$ by the tetrabutylammonium hydroxide ($nBu_4NOH.30H_2O$). For the colored form, the open diacid was exposed to UV light before treatment with the base.

Open form A:

The voltammograms recorded after each addition of perchloric acid to the solution of the dianion open form $2nBu4N^+.A^{2-}$ are shown in **(Figure (III.3)A).** The most remarkable feature to be noticed is that the potential of the irreversible wave increases steadily until the protonation is complete. This is expected as the molecule anionic character (electrostatic barrier) is lost and also because that electron density decreases when going from COO^- to COOH. Peaks of oxidation of the open form dianion $\boldsymbol{A^{2-}}$ and diprotonated $\boldsymbol{AH_2}$ were easily identified **(Figure (III.3)A)** while the oxidation peak of the monoprotonated open form $\boldsymbol{AH^-}$ is almost invisible. The estimation of this peak was made from the slight curvature of the wave corresponding to the addition of intermediate quantities of perchloric acid. Once the oxidation peak potential of the different species of the open form $\boldsymbol{AH_2}$, $\boldsymbol{AH^-}$, $\boldsymbol{A^{2-}}$ have been identified, the redox potential can be calculated.

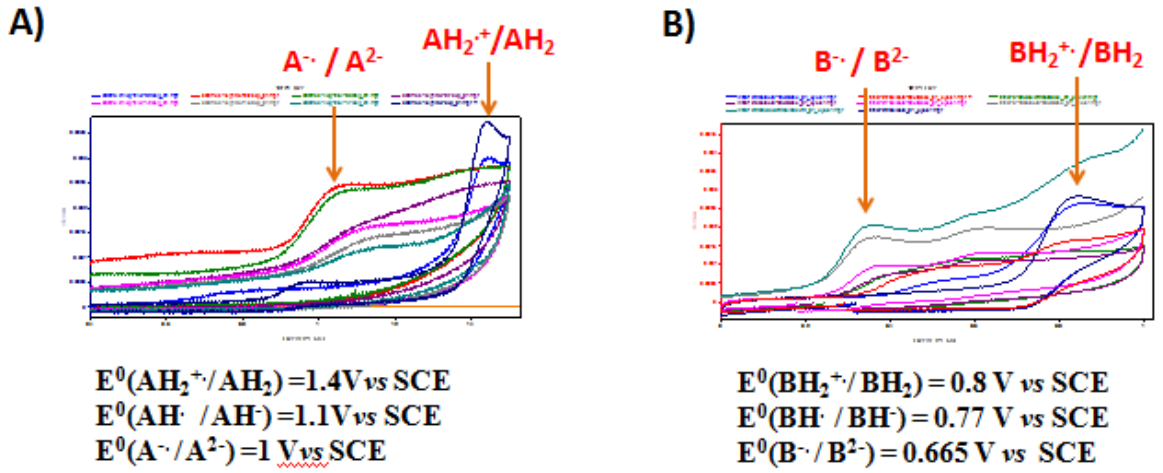

Figure (III.3): Voltammograms (0.1 M $TBAPF_6$, 0.5 Vs-1, SCE / Pt) recorded in acetonitrile and corresponding to the titration of: A) the di anion open form ($2nBu_4N^+.A^{2-}$) and B) the di anion closed form ($2nBu_4N^+.B^{2-}$).

Closed isomer:

For the closed form, the same analysis procedure of voltammograms **(Figure (III.3)B**) was used. As for the open form A, it was found that protonation increases the value of the anodic peak potential. Redox couples of the closed form are much smaller than those of the open form **(Figure (III.3)B**). This is consistent with the fact that the highest occupied molecular orbital (HOMO) energy increases from the open form to the closed form in a dithienylethene derivative. Thus, the ionization potential of the closed form of the dithienylethene is smaller than that of the open form. The second remarkable feature is that the first oxidation wave keeps its irreversible character at 0.5V/s.

III.4 Spectroelectrochemical study

It is known that the first oxidation of the closed form is related to the ring opening reaction via the above-mentioned ECE mechanism. Thus an exhaustive electrolysis at controlled potential above the B form's redox couple leads to a thermal bleaching of the solution.

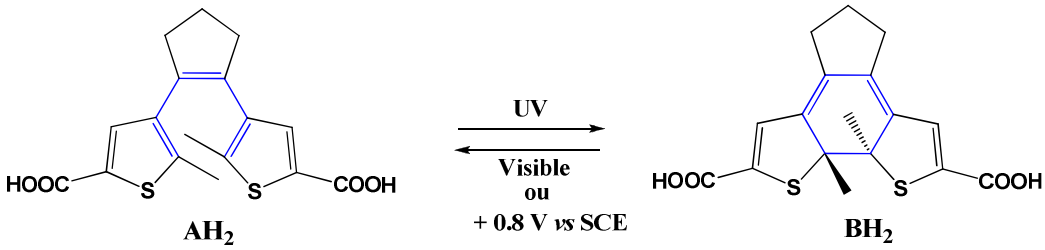

Scheme (III.1): photochemical and electrochemical interconversions between the two isomers, opened (AH_2) and closed (BH_2), of diacid DTE $(COOH)_2$

A question of importance is how the protonation affects the efficiency of the electrochemical bleaching. Thus we have studied the coulometries by spectroelectrochemistry. A controlled potential electrolysis (1V vs. SCE) of the closed form in its di protonated state $\boldsymbol{BH_2}$, or di anion state $\boldsymbol{B^{2-}}$, **(Figure (III.4))** leads to a bleaching of the solution. The progress of the reaction was followed by UV-vis spectroscopy at $\lambda = 500\ nm$ or 512 nm in order to monitor the variation of the closed isomer's absorption band in the visible domain.

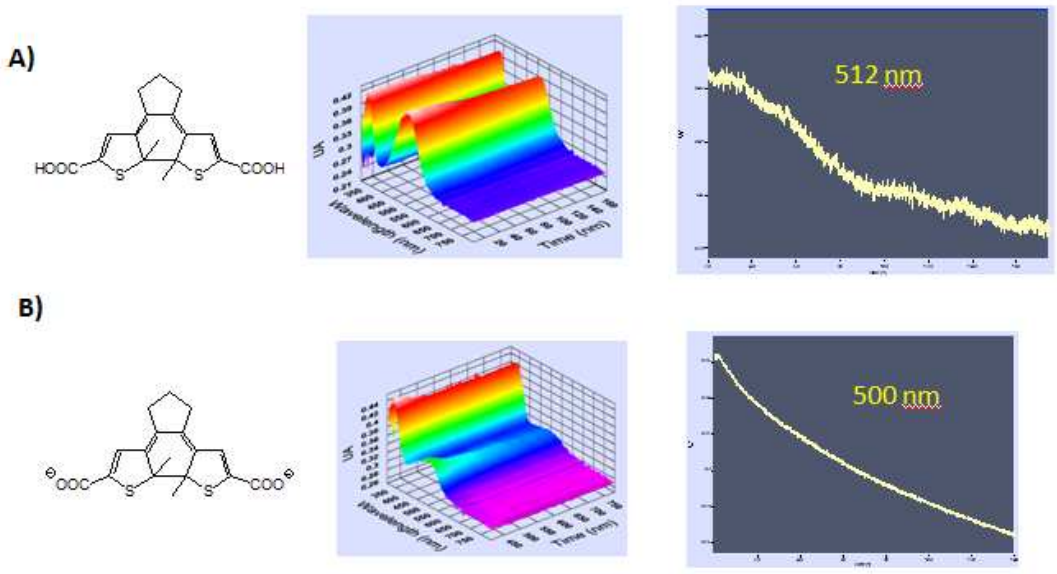

Figure (III.4): Controlled potential electrolysis at 1.00 V vs. SCE for A) di protonated closed form and B) di anion closed form.

In both cases, with the di-protonated and the di-anion closed form, we have seen the ring opening (disappearance of the absoption band in the visible domain) process upon oxidation by spectroelectrochemistry. We found also that the decay of the dianion is faster than the diacid, which means that the ring opening process is faster.

III.5 Copper (II) as an oxidizing reagent

After determining the redox potentials of diacid $DTE(COOH)_2$ isomers, open [E^0($\boldsymbol{AH_2}^{\cdot+}$ / $\boldsymbol{AH_2}$) = 1.4 V / SCE in acetonitrile] and closed form [E^0($\boldsymbol{BH_2}^{\cdot+}$/ $\boldsymbol{BH_2}$) = 0.8 V / SCE in acetonitrile], the aim of our work was to find an oxidant reagent which catalysis ring opening process of $\boldsymbol{BH_2}$ and therefore generates $\boldsymbol{AH_2}$.

The only example of a chemical oxidation of a photochromic compound[84] is the back isomerization of a quadricylane (QD) to norbornadiene NBD with tri-(parabromophenyl) aminium hexafluoro-antimonate (p-$BrC_6H_4)_3N^{\cdot+}SbCl_6^-$). As for the DTE family the NBD^+/NBD, E°(NBD^+/NBD is more anodic than the QC^+/QC. The main interest of the work is that the oxidizing agent ($Ar_3N^{\cdot+}$/Ar_3N) can be made catalytic as its redox couple lies between the two isomers'one:

$QC + Ar_3N^{\cdot+} \rightarrow QC^+ + Ar_3N$ $\quad$ $E°(QC^+/QC) = 0.91$ V *vs* SCE

$QC^+ \rightarrow NBD^+$ $\quad$ $E°(Ar_3N^{\cdot+}/Ar_3N) = 1.05$ *vs* SCE

$NBD^+ + Ar_3N \rightarrow NBD + Ar_3N^{\cdot+}$ $\quad$ $E°(NBD^+/NBD) = 1.56$ V *vs* SCE

The authors explain the propagation of the reaction by proposing that the positive charge is only carried by the amine catalyst. Thus, once oxidized, the QC^+ isomerizes to NBD^+ that reacts with the reduced catalyst, regenerating a stable compound. However, in our case this compound was found to be ineffective, and also, its deep blue colour precluded a complete analysis of the UV-visible spectrum. Other oxidizing agents[85] having better spectroscopic properties have been tested, (I_2, Br_2) but without success. However when copper(II) triflate $Cu(CF_3SO_3)_2$ was used, immediate bleaching occurred.

Copper (II) triflate in acetonitrile presents the very interesting property to be almost colorless and its absorption in the UV region is rather weak; however its redox couple was found to be difficult to define. Thus its values varies from 0.95V[86] up to 1.1V[87] vs SCE

In fact the redox chemistry of copper (II) in acetonitrile is rather complex: the high redox couple value for the Cu(II)/Cu(I) couple is due to the strong stabilization of the oxidation level +I by the solvent. On the other hand, as a Lewis acid, the cupric ion is able to bind to hard ligands such as oxygen containing molecule or halide anions. This induces a remarkable stabilization of the +II oxidation level. Therefore the best oxidizing copper reagent contains non coordinating anions such as triflate. The impact of water on the redox properties of a Cu(II) solution has been studied: for instance Irangu et al[88] have used aqueous acetonitrile to vary the driving force of the oxidation of ferrocene by $Cu(OTf)_2$ from 0.15 to 0.5eV. This change[89] in the redox potential is attributed to the formation of aquo complexes and this speciation can be assayed spectrophotochemically. **Figure (III.5)** below shows a UV spectrum of Cu(II) triflate in dry acetonitrile. We calculated epsilon of $[Cu(ACN)_4]^{2+}$ at 780 nm ≈ 22 $L.mol^{-1}cm^{-1}$, this technique allowed us to check the quality of copper solution.

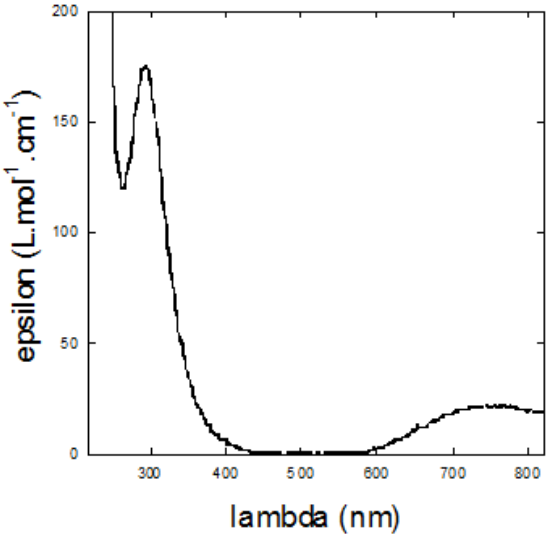

Figure (III.5): UV spectrum of Cu (II) triflate in dry CH_3CN

This is also why the E°(Cu(II)/Cu(I)) value fluctuates in the literature. E°(Cu(II)/Cu(I)) = 1.03V *vs* SCE (NEt_4BF_4 , CH_3CN, Pt)[90].

In organic chemistry, copper (II) triflate is usually used as a Lewis acid, but in some case it is used to oxidize a substrate. Thus Gopidas and co-worker[86] have reported that the reaction of aromatic amines with $Cu(ClO_4)_2.6H_2O$ in acetonitrile ($E°(Cu^{2+}/Cu^{+}$ =0.952Vvs SCE) solution gives rise to the amine radical cation.

$$Amine + Cu(II) \rightarrow Amine^{\cdot +} + Cu(I)$$

The radical cations are formed through the donation of an electron from the amines to Cu(II)[91]. The amines under investigation were N,N-dimethylaniline (DMA), N,N,N'N'-tetramethyl-p-phenylenediamine (TMPD), tris-(p-bromophenyl)amine (TBPA), N-methylphenothiazine (NMPT), 2-N,N-dimethylaminotetrahydropyrene (DMTHP) and 2-N,N-dimethylamino-7-carboethoxytetrahydropyrene (DMCTHP) and tris(4-anisyl)amine (TAA). In this latter case, an excess of Cu(II) gives rise to the formation of a di-cation[92]. Such a way to generate triarylamine radical-cations has been used *in-situ* to mediate the oxidative ring-closure[93] of polycyclic hydrocarbon from squalene-like precursors.

Cu(II) is also an active catalyst of lipid oxidation, but the mechanism of its action is not clear. It is generally agreed that copper acts as a strong pro-oxidant by catalyzing the decomposition of hydroperoxides[94]. However, there is no agreement regarding the importance of copper in the initial step in which hydroperoxides are formed. On the other hand, copper toxicity is related to its participation to Fenton-like reaction involving the participation of reactive oxygen species[95].

Before getting into the study of the interaction between Cu(II) and diacid closed form isomer $\boldsymbol{BH_2}$, a brief survey on the association of DTEs derivatives with copper (II) is established.

III.6 Copper (II) and DTEs derivatives

Literature survey shows that there are only few papers where photochromic compounds are associated with copper. They can be classified according to their application purposes.

Recently Cui *et al*[96] have synthesized a multiple responsive photochromic dithienyethene, the 1-[2,5-dimethyl-3-thienyl]-2-[2-methyl-5-(2-pyridyl)-3-thienyl] perfluoro cyclopentene with excellent fatigue resistance **Scheme (III.2)**.

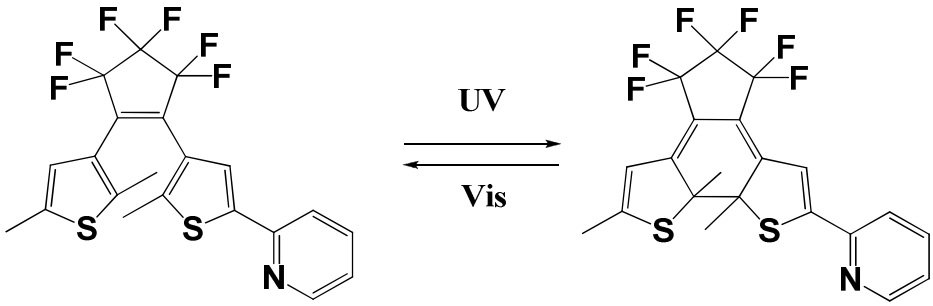

Scheme (III.2): Photochromism of 1-[2,5-dimethyl-3-thienyl]-2-[2-methyl-5-(2-pyridyl)-3-thienyl] perfluoro cyclopentene

This dithienyethene shows a special binding selectivity to Cu(II), when exposed to "$Cu(NO_3)_2$" (no hydration level was specified) in acetonitrile, allowing to envision environmental copper(II) ion sensoring and *in vivo* fluorescence imaging.

Another example at the border between analytical chemistry and magnetism is found in the photochromic dithiazolylethene series[97]. In this paper, it was found that the photochromic activity of a dithiazolylethene bridging ligand was maintained in solution only in the case of the copper binuclear complex. EPR studies revealed not only a weak magnetic coupling between the two copper ions, but also an interesting photo-controlled release and uptake of the $Cu(hfac)_2$ moiety.

Besides the analytical chemistry purposes, devices with information storage potentialities have also been developed, some of them are based on the photoswitching of magnetic properties.

A dithienylethene coordination ligand bearing a 1,10-phenanthroline ring and nitronyl nitroxide radical **Scheme (III.3)** has been described by Irie *et al.*[98]. When its $Cu(II)(hfac)_2$ complex was irradiated with UV light, a new ESR peak due to large exchange interaction appeared between those of the nitroxyl radical and Cu(II) revealing that the magnitude of the spin interaction was amplified by a factor more than 100 by photoirradiation.

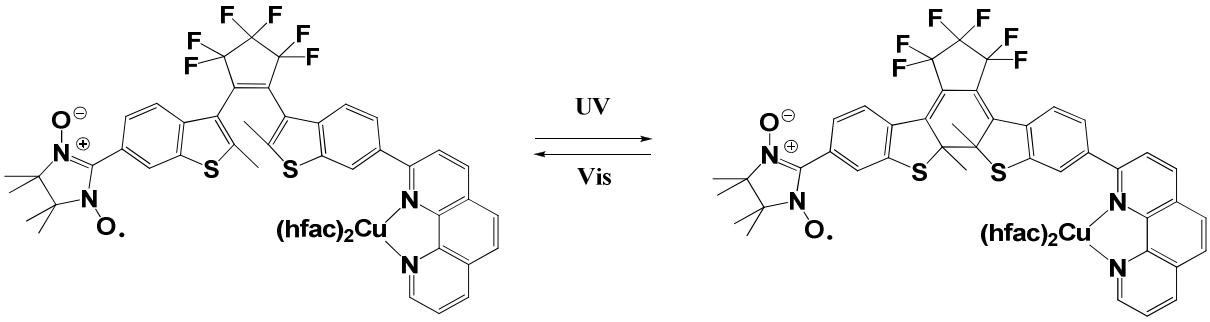

Scheme (III.3): Photochromic reactions of a dithienylethene coordination ligand bearing a 1,10-phenanthroline ring and nitronyl nitroxide radical.

DTE copper complexes have also been synthesized by Irie *et al*[99] with the purpose to develop single molecule magnets (SMM). For instance, the magnetic properties, and photochromic behaviours of copper(II)-terbium(III) SMMs linked by photochromic ligands with dithienylethene and dicarboxylate groups were investigated **Scheme (III.4)**.

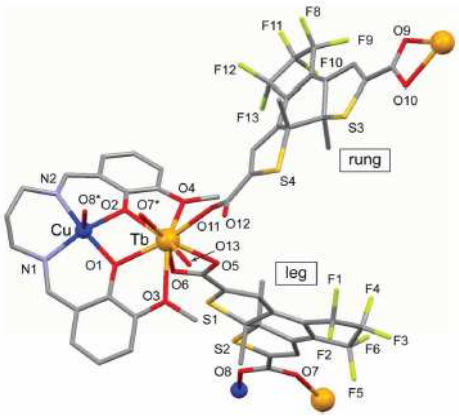

Scheme (III.4)[99]: Ball and stick plot of single-molecule magnets (SMMs) linked by photochromic ligands

Magnetic studies revealed that the displayed molecule had ferromagnetic interactions between the copper(II) and terbium(III) ions in the [Cu(II)Tb(III)(L)] unit and exhibited frequency dependence of its magnetic susceptibility due to the slow relaxation of the [CuTb] units. Upon irradiation with ultraviolet light and visible light, the photochromic reaction was associated with a distinct change of the frequency response of the magnetic susceptibility.

A new multi-state 1,8-naphthalimide-piperazine-tethered dithienylethene **Scheme (III.5)** was prepared by Zhang *et al*[100] to mimic functional electronic components, since each isomer of the photochromic compound can represent ‘0’ or ‘1’ of a digital code corresponding to ‘on’

and 'off' states stimulated by UV/Vis light. This system is based on alternative UV/Vis irradiation, protonation/deprotonation and copper (II) ion complexation/dissociation. The fluorescence and absorption spectra were used as output signals. Copper (II) ion (but without any indication of counterion) was introduced to mimic an inactive state by complexation with the two intramolecular piperazines thus locking the diarylethene open form into the photo-inactive parallel conformation.

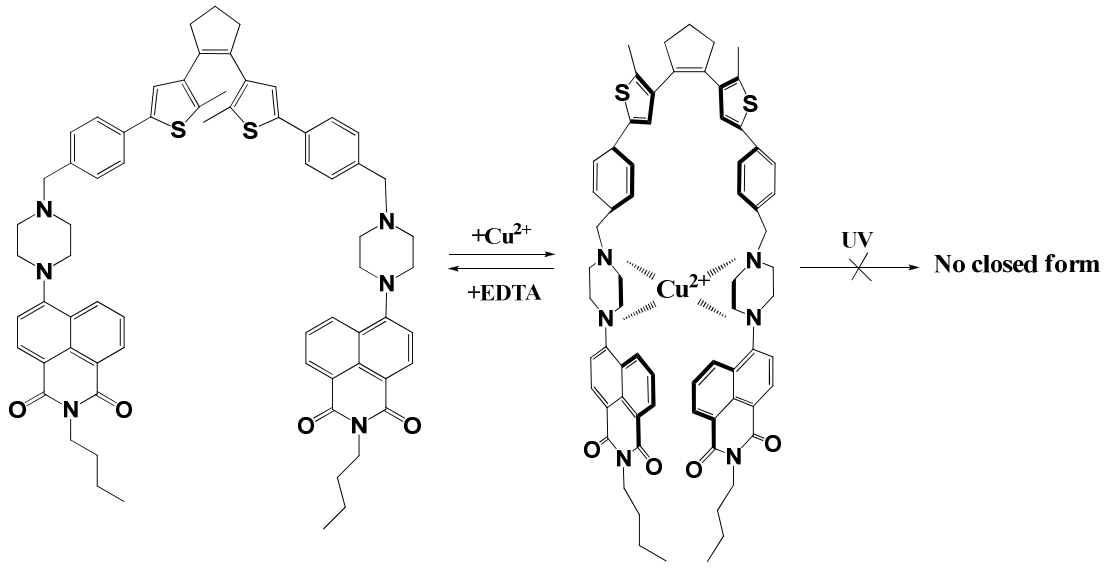

Scheme (III.5): Complexation with copper (II) ion between two piperazine moieties leads to the photo-inactive state which prohibits the photocyclization (gated-photochromism).

It can be noticed that in all the previous examples, the copper(II) ion is supposed to bind to a hard center (O and/or N atoms) thus affecting greatly its oxidizing properties. In particular the example of Irie *et al*[99] shows that copper (II) does not suppress the photoreactivity of a DTE-COO anion.

To be exhaustive on the topic, we can mention the use of a DTE ligand to modulate the catalytic properties of a copper(I) center. In 2005 Branda *et al.*[101] have described the photoswitching of the stereoselectivity of a catalytic reaction involving a copper dithienylethene complex. They prepared a chiral bis(oxazoline) photochromic dithienylethene ligand **Scheme (III.6)** which can only chelate to a metal ion when the photoswitch is in its flexible ring-open state.

Irradiation with UV light generates the corresponding ring-closed form which cannot chelate the metal because the photochemically produced rigid backbone forces the two oxazolines to exist in a divergent relative position. The copper-catalyzed cyclopropanation of styrene with ethyldiazoacetate **Scheme (III.6)** using bis (oxazolines) photochromic dithienylethene ligands was selected as a simple model reaction providing an easy to analyze product distribution.

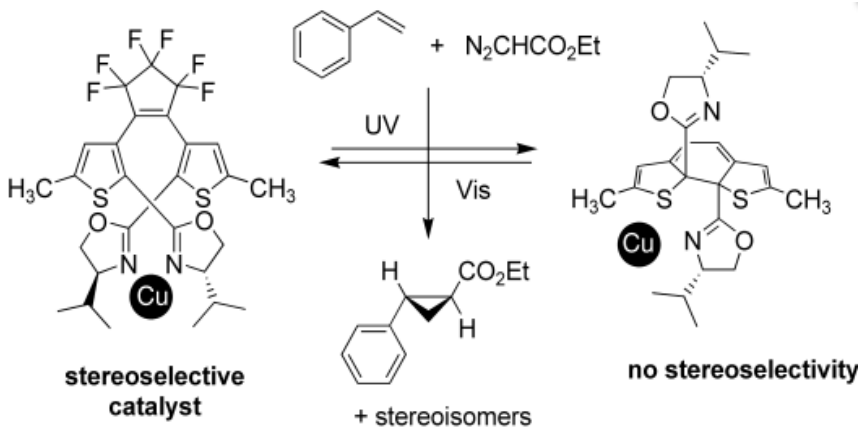

Scheme (III.6)[101]: photochemical interconversion of a chiral DTE ligand

A significant enantioselectivity was observed when the open DTE was used as a ligand and Cu(I) triflate as the metal source. When the DTE was previously irradiated with 313 nm light to form the photostationary state, the catalytic reaction appeared as less enantioselective as a result of the formation of the less chelating closed form. The enantioselectivity was shown to be turned back on by converting the ring-closed isomer back into its ring-open counterpart by irradiation with visible light. This observation was the first example of a photoswitching of a stereoselective catalytic reaction. An interesting phenomenon of gated photochromism was also observed. For instance, in CH_2Cl_2, the photoinduced ring-closing reaction was inhibited in presence of Cu(I) triflate. It was assumed that this lack of reactivity was caused by a too tight binding of the copper ion to allow the photochrom to undergo the necessary geometric changes. Adding a small amount of the more competitive coordinating solvent CH_3CN to the CH_2Cl_2 solutions allowed a recovery of the photochromism.

From these scarce examples, it can be seen that the interaction of copper with dithienylethene gives rise to a large variety of interesting behaviours. However, the use of Cu (II) as oxidizing agent to promote the ring opening on an otherwise thermally irreversible photochromic compound is yet unexplored.

III.7 Copper (II) and DTE $(COOH)_2$

III.7.1 Preliminary experiments

As mentioned previously the reaction between the $Cu(OTf)_2$ and the colored form BH_2 is fast and complete bleaching is observed within minutes when an excess of copper reagent is used. The evolution of the UV-vis spectrum of the medium after Cu(II) addition on a photostationary state mixture of closed and open form (largely closed) is relatively complex and its details are displayed on **Figure (III.6)**

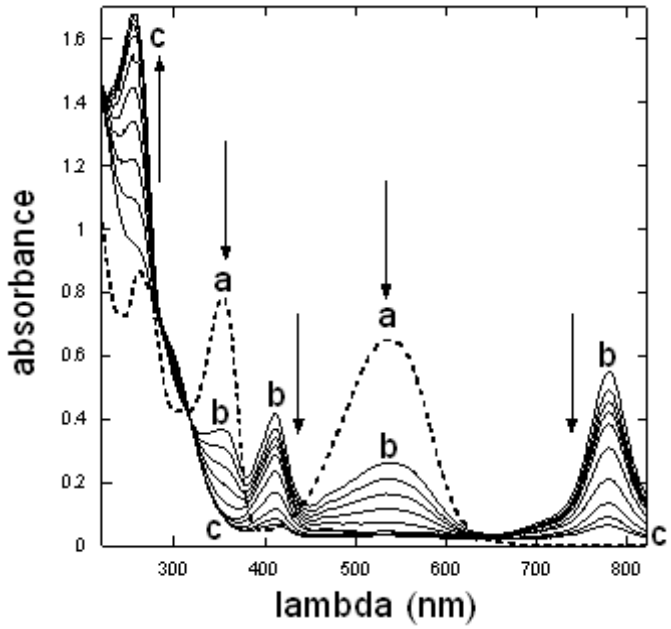

Figure (III.6): Typical spectral evolution after Cu(II) addition.

a: PSS spectrum before Cu(II) addition. $[BH_2]_0 = 6.98*10^{-5}$M; $[AH_2]_0 = 2.74*10^{-6}$M; (92.2% of closed form); b: spectrum of the mixture 3s after Cu(II) addition. $[Cu(II)]_0 = 6.21*10^{-5}$ M. Note the "instantaneous" loss at 538 nm and the corresponding increase at 780 nm and 410 nm.c: slow decay of both closed form and intermediate and open form recovery. Time interval between spectra is 5 s.

Dashed spectrum “a” displays the PSS photochromic mixture containing a large proportion of closed form before Cu(II) addition. Addition of Cu(II) triggers a fast evolution towards spectrum “b” showing a partly depleted closed form and the appearance of two new bands at 410 and 780 nm. These new bands were attributed to an intermediate as they are no longer stable; they slowly decay from the spectrum “b” to the completely bleached spectrum “c”. This last spectrum is reminiscent of the AH_2 open form. The evolution between spectra “a” and ”b” is too fast to be monitored with a conventional UV-visible spectrophotometer. On the contrary, the evolution from “b” to “c” is slower. Therefore, the preliminary investigations were limited to the analysis of the amplitude gap variations between spectra “a” and “b” upon Cu(II) addition.

Transient absorption spectra from 700 to 850 nm reveal the possible presence of radical-cations generated by electron transfer from DTE to Cu(II)[102]. However such spectroscopic feature was not observed during the coulometric electrolysis. It is thus very likely that the transient species is associated to a copper (410 nm). A similar blue intermediate **Scheme (III.7)** is formed during the Cu(II) mediated oxidative transformation of a vic-dioxime to the corresponding furoxans. On the basis of the spectroscopic evidence and the nature of the final products, the intermediate is proposed to be a mononuclear copper(II) complex ligated by a vicdioxime and a dinitrosoalkene[103].

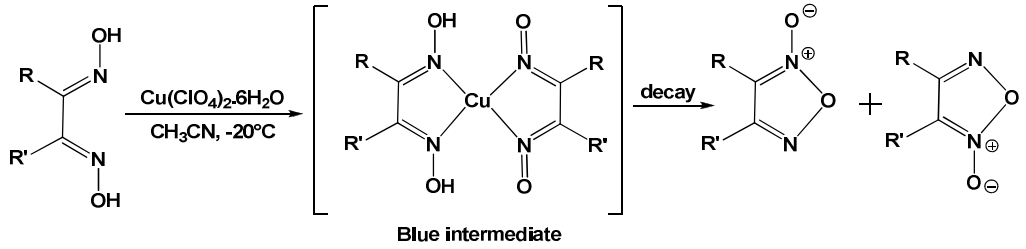

Scheme (III.7): oxidation of a vic-dioxime compound with Cu(II).

III.7.1.1 Investigations on the stoichiometry of BH_2 + Cu(II) fast reaction

The amount of closed form which has been depleted upon Cu(II) addition has been quantified from the absorbance difference between spectra “a” and “b” at 538 nm.

$$\text{BH2 promptly bleached} = \frac{(\text{Abs}_{(538\text{nm})\text{a}} - \text{Abs}_{(538\text{nm})\text{b}})}{\text{epsilon}_{\text{BH2}(538\text{nm})}}$$

This amount has been plotted versus the initial concentration of Cu(II) added in order to determine how many moles of BH_2 closed form have been destroyed per atom of Cu(II) added. Diagram shown on **Figure (III.7)** gather all the experiments (29 data points) that have been recorded whatever their initial concentrations of closed form and Cu(II). From the slope of the linear regression, ($slope \approx 0.69 \pm 0.10$), it appears that during the fast decay 1 mole Cu(II) destroys almost 0.7 mole of closed form.

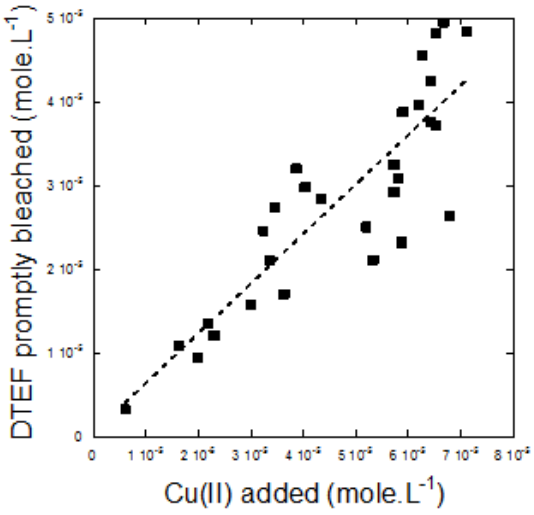

Figure (III.7): Experimental linear relationship between the amplitude of the fast bleaching of the closed form (from spectrum "a" to spectrum "b" on figure III.6) upon Cu(II) addition.

In the same way, the molar absorption coefficients of the 780 nm and 410 nm absorbing intermediate can be estimated from the rapid amplitude surge.

III.7.1.2 Estimation of the apparent epsilon at 780 nm

Estimation of the apparent epsilon at 780 nm is established from the linear correlation between the fast 538 nm-decrease and simultaneous 780 nm-increase, after Cu(II) addition (**Figure (III.8).**

Although the concentration of the 780 nm absorbing intermediate was rapidly evolving, it is possible to establish a linear correlation between the rises at 780 nm and the amplitude variation gaps at 538 nm (closed form). From the slope which is almost 1.7±0.55, it is

assumed that epsilon at 780 nm of the intermediate is around: 1.7*epsilon $_{(538nm)}$ ≈ 15500±5000 L.mol^{-1}.cm^{-1}.

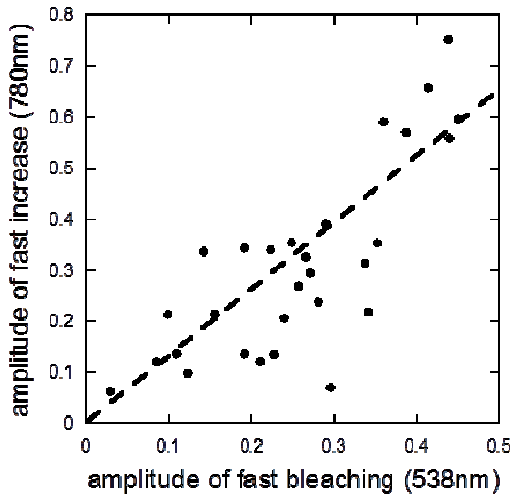

Figure (III.8): Linear relationship between the amplitude variation rise at 780 and the prompt bleaching at 538 nm.

This determination has been refined by considering that epsilon at 780 nm is around: the maximum of the amplitude of fast increase at 780 nm / $[Cu(II)]_0$ = 0.8/8e^{-5} ≈ 10000. Finally, a value of epsilon $_{(780nm)}$ =11500 L.mol^{-1}.cm^{-1} has been used in the subsequent analysis.

III.7.1.3 Estimation of the intermediate's epsilon at 410 nm

Estimation of epsilon at 410 nm of the intermediate is established from an absorbance vs absorbance plot (**Figure (III.9)**. Upon Cu(II) addition, the increase of the second intense band at 410 nm has been also monitored. Plotting 780 nm *vs* 410 nm shows a beautiful linear correlation demonstrating that the 410 nm band can be used to monitor the evolution of the 780 nm absorbing intermediate and that the evolutions of the BH_2 closed form can be independently monitored at 538 nm. Epsilon at 410 nm of the intermediate has been estimated from the slope: Epsilon$_{(410nm)}$ of the intermediate ≈ 11500/1.3 ≈ 8850 L.mol^{-1}.cm^{-1}. (See **Figure (III.9)**)

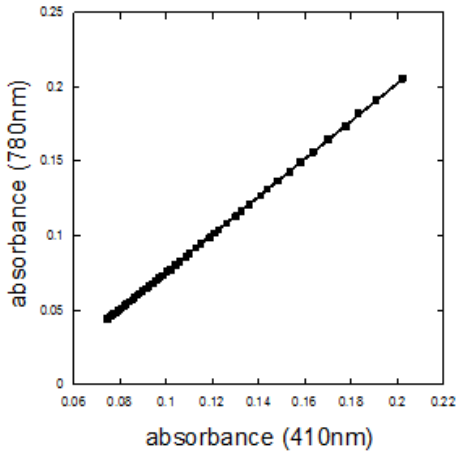

Figure (III.9): Absorbance *vs* absorbance diagram showing that during the slow evolution of the reaction, the 780 and 410nm bands provide the same kinetic information; ($[BH_2]_0$ = 6.98*10^{-5} mol.L^{-1}, $[AH_2]_0$ = 2.74*10^{-6} mol.L^{-1}, $[Cu(II)]_0$ = 6.21*10^{-5} mol.L^{-1} (0.9eq.)

III.7.2 Stopped Flow experiments

A first series of stopped flow experiments have been designed in order to monitor the rapid surge of the 780 and 410 nm absorbing intermediate species after addition of Cu(II) on the BH_2 closed form. **Figure (III.10)** shows that the rise was very fast as more than half of the maximum amplitude was reached within the mixing-time of the apparatus. Maximum was attained in less than 0.1s, while the total duration of the slow decay was more than 10s (see below).

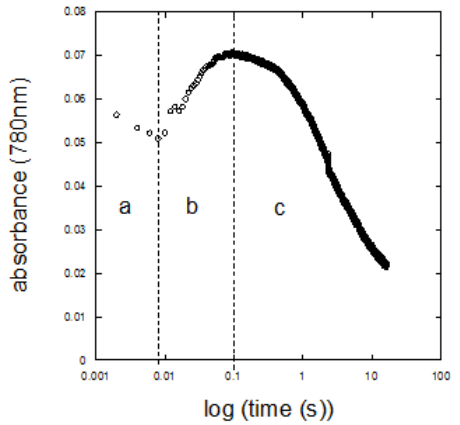

Figure (III.10): Fast rise (b) and slow decay (c) of the 780 nm absorbance during a typical stopped-flow experiment: Syringe A: $[BH_2]_0$ = 4.89*10^{-5} M at 4.69mL/s; Syringe B: $[Cu(II)]_0$ = 9.18*10^{-4}M at 0.31 mL/s; (1.25 eq.), dead volume 37µL, mixing time (a) ≈ 7ms, optical path: 0.15cm. Note the time log-scale.

Such a result is in accordance with the impossibility to monitor the fast rise during a slow kinetic experiments where the spectra were recorded several seconds after the Cu(II) mixing.

Several fast rise at 780 nm have been recorded on Cu(II) mixing with the closed form in order to estimate the initial slope. The purpose of this series of experiment was to try to estimate the apparent kinetic order of the Cu(II) on the formation of the 780 nm absorbing intermediate and to check the estimation of the epsilon at 780 nm of the absorbing intermediate.

Figure (III.11) shows how the initial slope has been estimated. Due to the mixing time effect the zero-time is hard to define. Therefore, it was arbitrarily chosen at the earlier time where the evolution is not noisy and sufficiently regular. It is clear that, in these conditions, the initial absorbance is not at zero, but the evolution is suitably linear to allow an accurate determination of its slope.

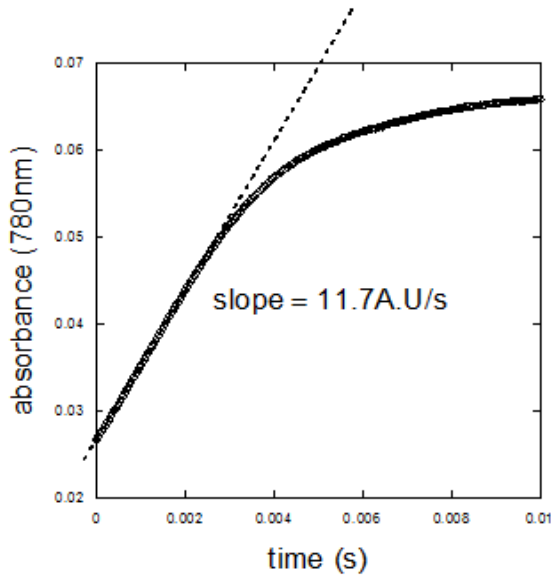

Figure (III.11): Determination of the linear slope of the intermediate evolution recorded at 780 nm during a stop flow experiment ([BH_2] = 10^{-5}M with 9.4eq. Cu(II))

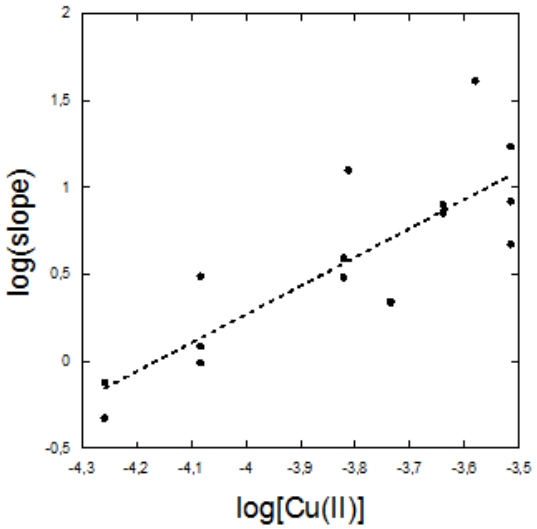

Figure (III.12): Linear relationship between log(slope) versus log($[Cu(II)]_0$) allowing a determination of a Cu(II) partial order between 1.65 and 2.4.

The kinetic order (**Figure (III.12))** of the [Cu(II)] for the formation of the 780 nm absorbing intermediate is around 2 ± 0.4. Such a value is a strong indication that more than one Cu(II) ion are involved into the mechanism of this intermediate's formation at 780 nm. Moreover, these preliminary stopped flow experiments allow also an independent estimation of the molar absorption coefficient of the 780 nm absorbing intermediate.

By assuming that the stoichiometry of the absorbing transient was 1:1, the molar absorption coefficient was calculated from the concentration of the minor reactant from the following formula:

$$Epsilon_{(780nm)} = \frac{Absorbance_{(780nm)max}}{[X]} ,$$

Where X is the minor reactant.

Table (III.1) gathers the initial conditions of the various experiments that have been performed and the corresponding re-calculated values of molar absorption coefficient of the intermediate.

Equivalent of Cu(II)	$[BH_2]$ ($mol.L^{-1}$)	[Cu(II)] ($mol.L^{-1}$)	minor reactant	Abs(780)max	$Eps(max)/n_X$ ($L.mol.cm^{-1}$)
1.20	$4.59e^{-5}$	$5.51e^{-5}$	closed form	0.07	10200
1.86	$4.44e^{-5}$	$8.26e^{-5}$	closed form	0.082	12300
3.56	$4.33e^{-5}$	$1.51e^{-4}$	closed form	0.0727	11200
4.71	$3.91e^{-5}$	$1.84e^{-4}$	closed form	0.0762	13000
6.27	$3.67e^{-5}$	$2.30e^{-4}$	closed form	0.076	13800
9.39	$3.26e^{-5}$	$3.06e^{-4}$	closed form	0.0665	13600
0.38	$4.07e^{-4}$	$1.54e^{-4}$	Cu	0.27	11700
0.75	$3.49e^{-4}$	$2.63e^{-4}$	Cu	0.46	11700
0.94	$3.26e^{-4}$	$3.06e^{-4}$	Cu	0.55	12000

Table (III.1): Estimation of the epsilon at 780 nm of the absorbing transient from the preliminary stopped flow experiments recorded in various conditions.

The obtained values are the same whatever the minor reactant Cu(II) or BH_2. This result confirms that the stoichiometry of Cu(II) and BH_2 is 1:1. The estimated value of epsilon at 780 nm is : 12200 ± 1200 $L.mol.cm^{-1}$; it is similar to the previous value (11500 $L.mol.cm^{-1}$) estimated from the absorption gap variations. Such a result is a strong check of the reliability of all the kinetic measurements that have been carried-out.

Simultaneous monitoring of the fast bleaching of the closed form and fast rise of the intermediate has been carried-out. Therefore, in order to limit the size of the spectral range, the intermediate has been monitored at 410 nm instead at 780 nm.

Using, $Epsilon_{(410nm)}$ of the intermediate ≈ 11500/1.3 ≈ 8850 $L.mol^{-1}.cm^{-1}$, the absorbance *vs* time data from stopped-flow experiments have been converted into concentration [c] vs time kinetics (see **Figure (III.13))**.

Figure (III.13) displays the early evolution of the reaction. Within this time range, the intermediate species (int) accumulates at the expense of the BH_2 closed form, a global mass balance $[BH_2]$ + [int] = constant is roughly respected.

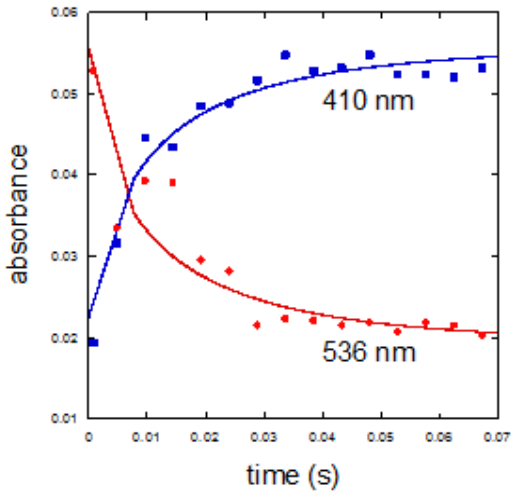

Figure (III.13): Two wavelengths monitoring of a stopped-flow experiment involving 2.3 equivalent of Cu(II) (dots). $[DTE]_0 = 3.1*10^{-5}M$; $[Cu(II)]_0 = 7.1*10^{-5}M$. Continuous lines: fitting using the "stopped-flow" model.

III.7.2.1 Establishment of a kinetic model

Result from **figure (III.7)** shows that 1 Cu(II) destroys 0.7 mole of closed form i.e. more than 1 ion of Cu(II) are involved in the mechanism of bleaching of the closed form. This result is in agreement with the apparent values of the partial order of the Cu(II) which is almost 2. Moreover, recalculation of the concentrations using the estimated epsilon values from figures (III.8) and (III.9) shows that the mass balance is more or less respected between the closed form (from the 538 nm decay) and the intermediate (form the 410 nm rise) **(figure (III.13))**. The simplest kinetic scheme involves the successive participation of two Cu(II) ions.

BH_2 + Cu(II) ← → C (reversible activation of the closed form by Cu(II))

C + Cu(II) ← → int + Cu(I) (reversible electron transfer)

Where C is a [1:1 closed form Cu(II) complex], it is assumed that an activation is occurring, but not yet an electron transfer. "int" is the absorbing intermediate (at 780 nm and 410 nm) where electron transfer is effective with the formation of reduced copper Cu(I). Within this time scale (70 ms), the transient "int" accumulates and no decay is detectable. Therefore, no consumption process has been considered in this model.

The first step is reminiscent to the possible chelation of a single copper ion by a dicarboxylate ligand[104]. The second step corresponds to a reversible electron transfer within the encounter complex with the generation of the closed form radical cation[105]. In the framework of this hypothesis, "int" would be a Cu(II) complex with a radical cation ligand. It is assumed that the transition-state of the electron transfer is a carboxylate dicopper complex[106]. Reversibility is related to the small difference between the oxido-reduction potential of the two couples: Cu(II) and the C complex on one side and Cu(I) and the "int" intermediate on the other side[107].

III.7.2.2 Estimation of the kinetic parameters of the model

Figure (III.13) shows that an acceptable reproduction of the concentration [c] *vs* time traces in a stopped flow experiment can be obtained with the proposed mechanistic model using the parameters gathered in **Table (III.2)**.

process	rate constant	unit	equilibrium constant
BH_2 + Cu(II) → C	$k_0 > 10^7$	$M^{-1}.s^{-1}$	$K_1 = [C]/([BH_2][Cu(II)])$
C → BH_2 + Cu(II)	k_1 (rapid)	s^{-1}	$K_1 \approx 1.3*10^{+3}$
C + Cu(II) → int + Cu(I)	$k_2 = 1.5*10^7$	$M^{-1}.s^{-1}$	$K_2 = [int][Cu(I)] / [C][Cu(II)]$
int + Cu(I) → C + Cu(II)	$k_3 = 9*10^4$	$M^{-1}.s^{-1}$	$K_2 \approx 1.7*10^{+2}$

Table (III.2): Extracted parameters from the fittings displayed on Figure (III.13).

Note that the first process of complexation is too fast to allow the accurate determination of the individual kinetic parameters, only their ratio (i.e. the equilibrium constant K_1 can be reached). In this case, C plays the role of an activated complex where the electron transfer does not occur but where the BH_2 closed form is activated i.e. its oxidation potential is more favourable. On the contrary, the reversible electron transfer is slower and fully determined within the framework of the model. Moreover, these parameters insure that the concentration of the complex [C] remains always at a level less than 5% of the overall concentration of the initial closed form. Such a low value is in full agreement with the hypothesis of a mass balance between the closed form BH_2 and the absorbing intermediate "int".

A similar situation with the successive involvement of two Cu(II) ions has been described by Habermeyer *et al*[108] in their investigations of the closure dynamics of zinc bis-porphyrin tweezers with Cu(II) ions and electron transfer. It was shown that electron transfer was preceded by a coordination of Cu(II) to bis-Zn porphyrin. Electron transfer from [bis-Zn porphyrin/Cu] complex to $Cu(OTf)_2$ occurred with a rate constant of $5.3x10^4$ $M^{-1}s^{-1}$ to afford the corresponding radical cations. Another example is provided by the Cu(II / I) self-exchange rate[88] of electron transfer with dimethyl ferrocene lying around 10^4 $M^{-1}s^{-1}$ in pure acetonitrile. These literature data support our mechanistic model involving the successive participation of two Cu(II) ions.

III.7.2.1 Properties of the model

In order to check the validity of this model, it is interesting to verify if it is able to reproduce some features of the reaction between Cu(II) and the closed form. The first test was a reproduction of the stoichiometry of the Cu(II) + closed form reaction. From **Figure (III.7)**, it was found that 1 mole of Cu(II) destroys around 0.7 mole of closed form. On the other hand, the results of two numerical simulations of the model are shown on **Table (III.3)**.

[Cu(II)] ($mol.L^{-1}$)	[BH_2] ($mol.L^{-1}$)	eq.	consumed closed form ($mol.L^{-1}$)	closed consumed / Cu(II)
$4*10^{-5}$	$4*10^{-5}$	1	$1.6*10^{-5}$	0.4
$2*10^{-5}$	$4*10^{-5}$	0.5	$8*10^{-6}$	0.4

Table (III.3): Calculation of the ratio: Cu(II) / consumed closed form, from the model.

Results show a lower value than expected (0.4 < 0.7). This is an indication that the model is not complete and that some processes where the reacting power of the Cu(II) is enhanced are occurring. It is liable that they may happen mainly in the slower part of the reaction.

The second test is related to the reproduction of the initial partial order of the Cu(II). Results of four numerical simulations of the model are shown in the **Table (III.4):**

[Cu(II)] ($mol.L^{-1}$)	[BH_2] ($mol.L^{-1}$)	eq.	Abs(780)/s	log(slope)	log(Cu(II))
$8*10^{-5}$	$4*10^{-5}$	2	$3.48e^{-3}$	-2.46	-4.10
$6*10^{-5}$	$4*10^{-5}$	1.5	$2.08e^{-3}$	-2.68	-4.22
$4*10^{-5}$	$4*10^{-5}$	1	$9.86e^{-4}$	-3.01	-4.40
$2*10^{-5}$	$4*10^{-5}$	0.5	$2.62e^{-4}$	-3.58	-4.70

Table (III.4): Determination of the Cu(II) kinetic order from four numerical simulations of the model. Initial slope was measured from the surge of the intermediate at 780 nm.

Plot of log(slope) vs log(Cu(II)) gives rise to a straight line whose slope is 1.87. This value is in good agreement with the experimental determination of the Cu(II) kinetic order from **figure (III.12)** giving a value around 2 ± 0.4.

This simple model reproduces the main features of the early part of the reaction. The shapes of closed form decay and the absorbing intermediate rise at 780 nm are fitted accurately. The kinetic order of the Cu(II) is reproduced. On the other hand, the stoichiometric ratio of Cu(II) added vs closed form bleached is higher than expected. This is an indication that Cu(II) or the intermediate are involved in some reactive process where its bleaching power is enhanced. Within this model the structure of the absorbing intermediate at 780 nm is possibly a 1:1 complex between a Cu(II) atom and a cation–radical of the closed form. However due to its short life time this structure cannot be fully confirmed from EPR spectroscopy. The main idea of this model is that the electron transfer does not occur from the simple contact between Cu(II) and closed form; on the contrary electron transfer needs some "activation" to occur, such activation is provided by a pre-complexation between closed form and Cu(II), this is a second Cu(II) which is responsible from the electron transfer. Other models involving the formation of dimers or the presence of more intermediates does not fit the data with realistic parameters.

In order to shed light on the various processes occurring during the slower part of the reaction an analysis of the slow evolution has been carried-out.

III.7.3 Analysis of the slow evolution after Cu(II) addition

Table (III.5) gathers the initial conditions of the kinetic experiments. They have been monitored by UV-visible spectroscopy using a stirred and thermostated DAD apparatus. The starting point of these experiments is a photosteady state (PSS) solution containing 70% < BH_2 closed form < 97% . Then variable amounts of Cu(II) were added in order to explore the ratios from 0.46 to 1.32 equivalents (eq.). Immediately after addition, the mixture was rapidly shaken and monitored.

N°	$[BH_2]_0$ ($mol.L^{-1}$)	$[AH_2]_0$ ($mol.L^{-1}$)	%@PSS	[Cu(II)] ($mol.L^{-1}$)	eq.	T° (°C)	shape	%r
46	$4.74*10^{-5}$	$1.70*10^{-5}$	73.5	$2.18*10^{-5}$	0.46	20	m	
53	$6.46*10^{-5}$	$2.58*10^{-6}$	96.2	$3.36*10^{-5}$	0.53	20	s	
72	$5.38*10^{-5}$	$1.45*10^{-5}$	78.8	$3.87*10^{-5}$	0.72	20	s	
75	$4.63*10^{-5}$	$1.37*10^{-5}$	77.2	$3.45*10^{-5}$	0.75	20	s	79
82	$5.29*10^{-5}$	$1.66*10^{-5}$	76.1	$4.34*10^{-5}$	0.82	20	m	
84	$6.82*10^{-5}$	$5.63*10^{-6}$	92.4	$5.73*10^{-5}$	0.84	20	m	
85	$6.12*10^{-5}$	$0.45*10^{-5}$	93.2	$5.20*10^{-5}$	0.85	20	m	
91	$6.98*10^{-5}$	$2.74*10^{-6}$	96.4	$6.21*10^{-5}$	0.91	20	m	
92	$6.98*10^{-5}$	$2.57*10^{-6}$	96.4	$6.42*10^{-5}$	0.92	20	s	
119	$5.26*10^{-5}$	$1.58*10^{-5}$	82.6	$6.26*10^{-5}$	1.19	20	s	83
132	$5.38*10^{-5}$	$1.21*10^{-5}$	81.5	$7.10*10^{-5}$	1.32	20	s	

Table (III.5): List of kinetic basic experiments. m: monotonous evolution (rate decreases); s: sigmoïdal evolution (there is a period during which the rate increases); % r: percentage of the initial dithienylethene that has been recovered after Cu(II) induced ring opening.

Previous multi-wavelength analysis has shown that two monitoring wavelengths at 780 and 538 nm were sufficient to record the whole reaction process. A rather rich kinetic behaviour has been witnessed, especially on the evolution of the intermediate species: a monotonous evolution (i.e. the rate is maximum at the starting point and is continuously decreasing) and a sigmoïdal evolution (i.e. there is an induction period and the rate goes though a maximum).

Whatever the detailed shape of the "int" evolution, there was always a monotonous bleaching of the closed form. This bleaching was either partial or complete.

In order to try to precise the nature of the main processes occurring during the slow evolution a kinetic modelling has been carried-out.

III.7.4 Kinetic modelling of the partial bleaching of the closed form upon Cu(II) addition

For this purpose, the stopped-flow model has been improved by adding several radical and termination reactions. It is well known that acetonitrile cannot be considered as a really inert solvent. For instance, triplet benzophenone (^3K) abstracts a hydrogen atom from acetonitrile with a rate constant[109] higher than $100 M^{-1}s^{-1}$. According to this result, the occurrence of a radical reaction between the absorbing intermediate "int" at 780 nm and the solvent acetonitrile "RH" has been assumed.

$int + RH \rightarrow RH^{\cdot +} + Cu(II) + AH_2$ electron transfer from the solvent and ring opening

$RH^{\cdot +} \rightarrow R^{\cdot} + H^+$ proton release

$R^{\cdot} + R^{\cdot} \rightarrow RR$ radical termination

$R^{\cdot} + AH_2 \rightarrow \rightarrow T$ DTE degradation

The first process is probably the result of several pseudo elementary reactions such as:

$int \leftarrow \rightarrow BH_2^{\cdot +} + Cu(II)$ reversible dissociation of the intermediate

$BH_2^{\cdot +} \rightarrow AH_2^{\cdot +}$ cation radical ring opening

$AH_2^{\cdot +} + RH \rightarrow RH^{\cdot +} + AH_2$ electron transfer from the solvent

Termination and degradation reactions have also been taken into account in order to interpret that more than 15% of the initial AH_2 open form cannot be recovered after Cu(II) bleaching. Moreover, it is expected that they give rise to an acidification of the reaction.

A model called "monotonous and delayed evolution" (**Figure (III.14))** has been built on the basis of these hypotheses. A typical feature of this model is that it is an improvement of the

stopped-flow model as it is using the same kinetic parameters values for the early part of the reaction. In these conditions, by adjusting the newly considered kinetic parameters, it is able to reproduce both the decay of the intermediate and the partial bleaching after Cu(II) addition, to reproduce both the decay of the intermediate and the partial bleaching after Cu(II) addition, and the delayed photocoloration if the Cu(II) is mixed with the AH_2 open form prior to UV irradiation.

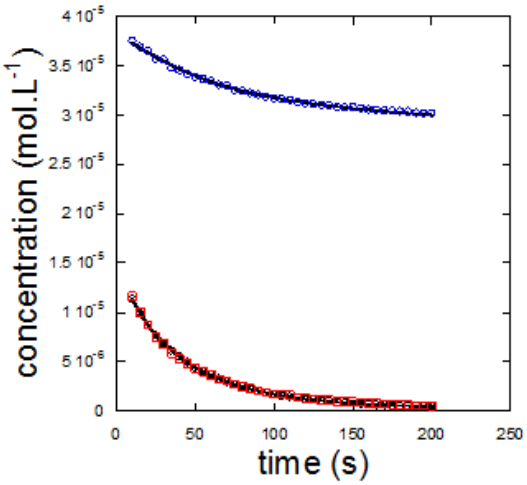

Figure (III.14): Typical monotonous "int" (red) and BH_2 closed form (blue) decay after Cu(II) addition. $[BH_2]_0 = 6.12*10^{-5}$ M; $[AH_2]_0 = 6.12*10^{-6}$ M; $[Cu(II)]_0 = 5.20*10^{-5}$M; (0.85eq); T= 20°C (open : 9%). Note that the recording starts 10s after the mixing. Data points: experiment; continuous line: fitting by the "monotonous and delayed evolution" model.

Table (III.6) gathers the values of the slower kinetic parameters that have been extracted from the fitting procedure.

process	apparent rate constant ($M^{-1}.s^{-1}$)
int + RH → $RH^{\cdot+}$ + Cu(II) + AH_2	$1.7*10^{-3}$
$RH^{\cdot+}$ → $R^{\cdot}$ + H^+	1 to $2*10^{+9}$
$R^{\cdot}$ + $R^{\cdot}$ → RR	10^{+9}
$R^{\cdot}$ + AH_2 → → T	1 to $4*10^{+9}$

Table (III.6): extracted kinetic parameters from the fitting procedure

At the end of the fast reaction most of the Cu is stored into the intermediate, then, during the slow evolution it is regenerated, partly under Cu(II) (36%), partly under Cu(I) (64%) forms. DTE degradation is estimated at 15%.

III.7.5 Delayed photocoloration experiments

Instead of adding Cu(II) upon previously photo-generated closed form (i.e. open form + hv → closed form, then closed form + Cu(II) → evolution), a different approach has been explored. The idea is to irradiate a mixture of open form and Cu(II) (open form + Cu(II) + hv → new evolution). Preliminary studies have shown that in the dark, there is no recordable reaction between Cu(II) and open form. On the contrary, upon UV irradiation, photocoloration is occurring but in a delayed way. **Figure (III.15)** shows the evolution at 536 nm of the closed form under 313 nm UV irradiation.

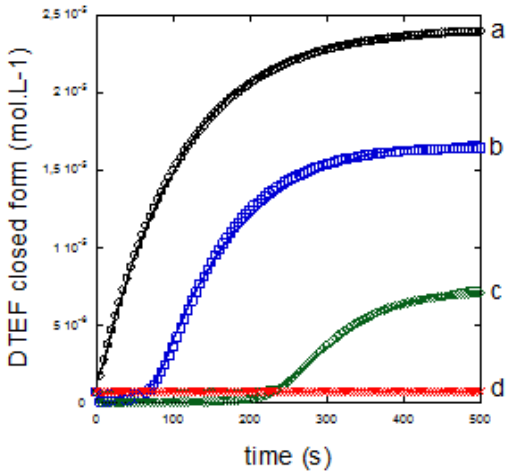

Figure (III.15): Evolution under 313nm UV irradiation of a mixture of open form ($[AH_2]_0$ = 2.5*10^{-5} M) and Cu(II). a: $[Cu(II)]_0$ = 0; b: $[Cu(II)]_0$ = 2.5*10^{-5}M(1eq.); c: $[Cu(II)]_0$ = 5*10^{-5}M(2eq.); d: $[Cu(II)]_0$ = 9*10^{-5}M (3.6eq.); Data points: experimental results; continuous lines: fitting by the "monotonous and delayed evolution" model.

Taking into account that the 4 solutions have received the same irradiation flux, it appears that curve b starts at a time (t_b = 65s) where the expected concentration of closed (calculated from curve a) is around 1.2*10^{-5}M. The presence of this delay can be interpreted by the destruction of 0.48 mole (1.2*10^{-5}/2.5*10^{-5}) of closed form by 1 mole of Cu(II) added. Same calculation from the second induction time (tc = 205 s) gives rise to the destruction of 0.44 mole of closed form by 1 mole of Cu(II) added. Finally the lack of coloration in experiment "d" is

interpreted from the total destruction of the expected $2.5*10^{-5}$ mole of closed form. From curve b and c, it appears that about 0.46 ± 0.03 mole of closed form is destroyed per mole of Cu(II) added. This value is in relatively good agreement with a previous result obtained from the fast bleaching of the closed form upon Cu(II) where it was found that 1 mole of Cu(II) was able to destroy 0.69 ± 0.14 mole of BH_2 closed form. It is also in accordance with the results gathered on **Table (III-3)** (1 mole of Cu(II) destroys 0.4 mole of closed form).

These results show the importance of the radical reactions occurring during the slower part of the evolution. The model "monotonous and delayed evolution" is able to reproduce the stopped-flow experiments, the slow monotonous evolution and the delayed photocoloration, however, it fails to simulate some other kinetic behaviours that have been recorded.

III.7.6 Study of Other kinetic behaviours

III.7.6.1 Analysis of the sigmoïdal kinetics

After adding Cu(II) to a solution of BH_2, a particularly interesting kinetic behaviour was also observed. It was a sigmoïdal evolution as displayed on **Figure (III.16)**.

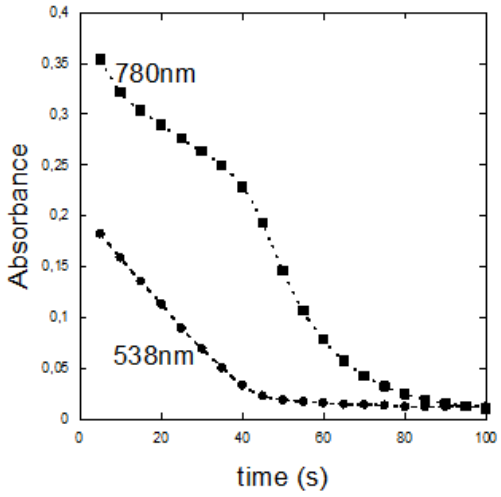

Figure (III.16): Typical sigmoïdal 780 nm-evolution and 0^{th}order–like 538 nm decay. $[BH_2]_0$ = $4.63*10^{-5}$ M; $[AH_2]_0$ = $1.37*10^{-5}$ M; $[Cu(II)]_0$ = $3.45*10^{-5}$M; (0.75eq); none degazed solutions. T= 20°C (initial open form: 23%). Note that the recording starts 5 s after the mixing.

Such non monotonous behaviour is relatively scarce in classical kinetics. It is reminiscent of an autocatalytic reaction. In that case, the evolutions are faster and more complete than in the monotonous case.

In order to precise the nature of the sigmoïdal kinetics processes which were responsible for this non-monotonous behaviour, a careful analysis has been performed. A comparison of the various rate constants (measured either at 780 or 538 nm) for sigmoïdal and monotonous kinetics has been carried-out. The following diagram has been established where it can be seen that the observed rate constants are always higher when the evolution is sigmoïdal than monotonous (**Figure (III.17)**.

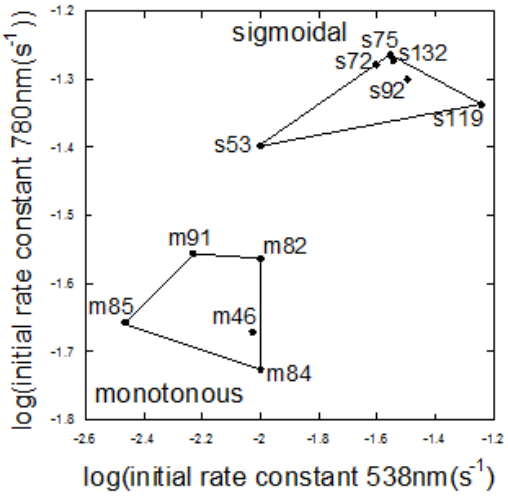

Figure (III.17): Diagram showing the higher reactivity of the kinetic sigmoïdal vs monotonous behaviours. Numbering refers to table (III.5).

This result is an indication that the sigmoïdal kinetic curves are related to an autocatalytic behaviour. The nature of the autocalysis is not known. A possible assumption is the participation of generated protons.

III.7.6.2 Acceleration of the bleaching by acidification of the medium

Figure (III.18) shows the acceleration of the bleaching of the BH_2 closed form (monitored at 536 nm) after the addition of small amounts of triflic (CF_3SO_3H) acid.

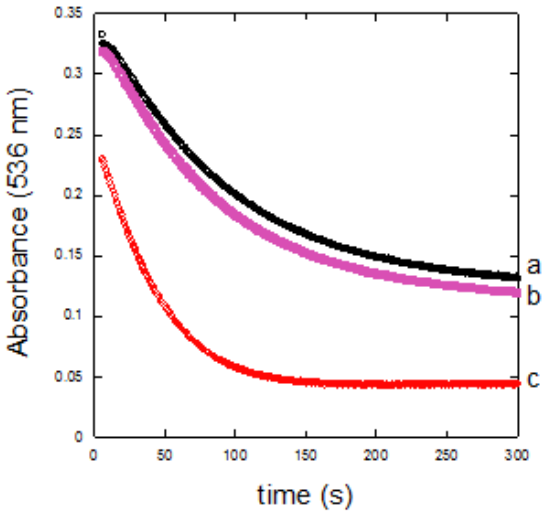

Figure (III.18): Bleaching of the BH_2 closed form after Cu(II) addition in presence of various amounts of triflic acid. a: 0; b: 0.03eq.; c: 0.11eq. $[AH_2]_0 = 1.84*10^{-5}$M; $[BH_2]_0 = 6.90*10^{-5}$M; $[Cu(II)]_0 = 7.45*10^{-5}$ M (1.08eq.).

The initial kinetic order of the triflic acid has been estimated from the initial slopes at around 0.5. This value is a clear-cut indication that the reaction is sensitive to acid catalysis. This result has been confirmed by the observation of a significant slowing-down after addition of small amount of tetrabutyl ammonium hydroxide base.

In these conditions, a possible explanation of the autocatalytic behaviour is the involvement of the protons generated during the solvent oxidation reactions. It is well known that many, if not most, redox reactions are coupled to proton transfers[110]. In our case, it is probable that the reactivities of the intermediates “int” and radicals are sensitive to their protonation states.

III.7.7 The coupling of propagation, protonation and termination processes

The participation of a propagation reaction involving spin exchanges between closed form, open form and solvent cation radical has been considered. This hypothesis is supported by several papers [111,37] indicating that in DTE series the closed form is generally more oxidable than the opened one. The propagation process can be written as:

$$BH_2^{\cdot+} \rightarrow AH_2^{\cdot+}$$

$$AH_2^{\cdot+} + RH \rightarrow RH^{\cdot+} + AH_2$$

$$RH^{\cdot+} + BH_2 \rightarrow BH_2^{\cdot+} + RH$$

The net effect of such cycle is to open the closed form without any participation of copper atom. Its involvement increases the number of bleached closed forms BH_2 per atoms of copper added. This consideration is in agreement with the results of table (III.3). When the propagation is not considered (as in the "stopped-flow" model) the amount of bleached closed form is less than expected.

Another important point to understand the autocatalytic effect is the consideration of the termination reactions, their consequence is to inhibit competitively the propagation cycle by removing some active radicals from the cycle. It is expected that the efficiency of a typical termination reaction like $R^{\cdot} + R^{\cdot} \rightarrow RR$ is modulated by the radical protonation state ($RH^{\cdot+} \leftrightarrow R^{\cdot} + H^{+}$).

Therefore, the autocatalysis can be understood in the following manner. During the evolution of the reaction there is a proton release leading to an acidification of the medium. Radical species are more or less protonated depending on the proton concentration, the proportion of protonated species increase with time. The propagation cycle is in competition with terminations. The efficiency of termination decreases with protonation. The bleaching process is more efficient in acidic medium.

All the considerations relative to the investigations on the mechanism of the thermal bleaching of the BH_2 closed form in presence of Cu(II) lead to the following list of pseudo-elementary reactions (**Table (III.7))**

	Processes	Description	Comments
1	BH_2 + Cu(II) ↔ C	(reversible activation of the closed form by Cu(II))	may be sensitive to the protonation state
2	C + Cu(II) ↔ int + Cu(I)	(reversible electron transfer)	several "int" according to the protonation state
3	int+RH→$RH^{\cdot+}$+Cu(II)+AH_2	electron transfer from the solvent	irreversible ring opening and solvent oxidation
	$RH^{\cdot+}$ ← → $R^{\cdot}$ + H^+	radical protonation / proton release	may concern all radicals (acidification)
4	$R^{\cdot}$ + $R^{\cdot}$ → RR	termination	oxidation products
5	$R^{\cdot}$ + AH_2 → → T	degradation	react also on BH_2
6	int ↔ $BH_2^{\cdot+}$ + Cu(II)	reversible dissociation of the intermediate	initiate the propagation cycle
7	$BH_2^{\cdot+}$ → $AH_2^{\cdot+}$	cation radical ring opening	may be sensitive to the protonation state
8	$AH_2^{\cdot+}$ + RH → $RH^{\cdot+}$ + AH_2	electron transfer from the solvent	also in the case of $BH_2^{\cdot+}$
9	$RH^{\cdot+}$ + BH_2 → $BH_2^{\cdot+}$ + RH	propagation	chain reaction

Table (III.7): List of processes to describe the mechanism of the thermal bleaching of the BH_2 closed form in presence of Cu(II). Processes 1 and 2 are sufficient to describe the stopped experiments. Improvements by adding processes 4 to 5 have been investigated to simulate the monotonous and delayed evolution. Taking into account the various protonation states and their relative reactivities together with processes 6 to 9 are assumed to be needed to simulate the sigmoïdal kinetic behaviour.

III.8 Conclusion

The thermally irreversible (P-photochrom) DTE can be turned into a thermally partially reversible T-photochrom by Cu(II) oxidation of the photogenerated photosteady state (PSS) containing a large proportion of the BH_2 closed form.

The reaction of ring opening occurs through the transient formation of a 780 and 410 nm copper containing intermediate. The building-up of this intermediate is very fast and cannot be recorded using conventional kinetic methods. Stopped flow experiments have allowed to show that the stoichiometry of this intermediate is 1/1 between the BH_2 closed form and the copper ion. Although no clear-cut evidence was provided by ESR test at various temperatures, it is reasonable that within this intermediate the BH_2 closed isomer is under a cation radical form and the copper under a cupric oxidation state. A simple model (the so-called "stopped-flow model") involving the previous formation of an activated complex between the BH_2 closed form and a Cu(II) atom following by an electron transfer involving a second copper atom has been shown to nicely reproduce the kinetic records of the evolution of both the intermediate and the closed form.

At longer monitoring times (i.e. after few seconds), the intermediate and the residual BH_2 closed form undergo a slow decay. Two typical situations have been recorded related to the evolution of the intermediate, the monotonous case and the sigmoïdal case.

During the monotonous case, there is a complete disappearance of the intermediate but only a partial consumption of the BH_2 closed form. This phenomenon has been understood by considering that the Cu(II) has been more or less completely consumed during the fast evolution and that the driving force of the slow evolution is a reduction of the intermediate by the solvent. An improved model including the previously established "stopped flow model" and the participation of the solvent radical reactions has been shown to satisfactorily reproduce the monotonous kinetics. This model, the so-called "monotonous and delayed model" has been shown to be also successful to simulate the delayed photocoloration, i.e. when Cu(II) is added to the AH_2 open form prior to photocyclization.

Fast evolution monitored by the stopped flow apparatus and classical kinetics records of the monotonous slower evolution are in agreement relatively to the partial order of the Cu(II) around 2, to the stoichiometry of the reaction (1 Cu(II) destroys about 0.5 BH_2 closed form molecule), to the determination of the molar absorption coefficient of the intermediate at the monitoring wavelengths and to the partial degradation of the DTE during the oxidation process.

The sigmoïdal evolutions are more difficult to understand. In that cases, the bleaching of the BH_2 closed form is complete. A careful model-free kinetic analysis has shown that the whole reactivity was significantly higher when the sigmoïdal evolution was present. A possible explanation is the start-up of a chain reaction involving open form, closed form and solvent radical-cation species. There are the protons released during the solvent oxidation processes which are responsible of the building-up of the autocatalytic loop. Inhibition of the competitive termination reactions by the protons allows the full activation of the propagation cycle. It is possible that the presence of some radical scavengers like dissolved oxygen or other impurities quenches the establishment of the chain with the consequence of a simple monotonous evolution. In these conditions the overall yield of bleaching will appear lower.

This chapter is a clear illustration of the rich behaviour of the photochromic DTE with its sensitive responsivity to various simultaneous stimuli: light, protons and oxidizing metal ions.

Chapitre IV: Photo-modulation de la luminescence des nanoparticles de ZnO par le diacide DTE$(COOH)_2$

Chapitre IV: Photo-modulation de la luminescence des nanoparticles de ZnO par le diacide DTE(COOH)2..... 119

Chapter IV - Photo-modulation de la luminescence des nanoparticles de ZnO par le diacide DTE(COOH)$_2$

La conversion photo-induite entre les deux isomères d'un ligand photochrome peut être exploitée pour moduler la luminescence des nanoparticules inorganiques. Ainsi les modifications structurales et électroniques accompagnant les transformations photo-induites du ligand photochrome, peuvent activer une voie de transfert d'énergie ou d'électron entre les composants et par la suite amener à l'extinction de la luminescence des nanoparticules. Dans ce chapitre, on va étudier l'association entre des nanoparticules de ZnO stabilisées par des ligands de type amine primaire et le diacide photochrome DTE(COOH)$_2$ ainsi que la photo-modulation de la luminescence de ces nanoparticules par le diacide.

IV.1 Introduction

Le photochromisme, qui est, le changement du spectre d'absorption par irradiation lumineuse, est un élément clé pour la construction des systèmes optiques moléculaires et supramoléculaires. De même, l'émission de la fluorescence constitue un signal de lecture ayant une haute sensibilité et une excellente résolution spatiale. Alors, la combinaison du photochromisme et de la fluorescence donne naissance à de nouveaux matériaux hybrides, qui combinent les effets caractéristiques et les propriétés des deux composants. En conséquence, le couplage du photochromisme et de la fluorescence constitue un grand avantage dans des domaines différents tels que le stockage optique des données[19] et l'imagerie biologique[112].

Récemment, un intérêt considérable s'est montré pour les quantum dots « QDs[113] » semiconducteurs ayant des propriétés optiques et électroniques uniques. Les QDs sont des nanoparticles[114] inorganiques ayant des propriétés d'émission ajustables par le contrôle de leur diamètre. Sous excitation dans l'UV, ils émettent des photons dans le visible avec une longueur d'onde qui varie du rouge au bleu selon leur taille. Leurs propriétés optiques remarquables ainsi que leur photo stabilité leurs permettent de remplacer les colorants organiques dans plusieurs applications telles que : le marquage, la détection et l'imagerie.

Les QDs semiconducteurs fonctionnalisés par des ligands photochromes sont abondamment étudiés[115] dans plusieurs domaines tels que la chimie organique et les sciences des matériaux. Les modifications structurales et électroniques accompagnant les transformations photo-induites du ligand photochrome, sont exploitées pour moduler l'émission du QD. Une irradiation lumineuse dans l'UV, peut induire la conversion du ligand photochrome d'un état

à un autre et par conséquent activer une voie de transfert d'énergie ou d'électron entre les composants. Chacune des deux voies peut amener à l'extinction de la luminescence (« quenching ») du QD. Cependant la régénération par voie photochimique ou thermique de l'état initial du photochrome permet de récupérer de nouveau l'émission du QD.

Le transfert d'énergie résonnant (*RET : Resonance Energy Transfer*) et le transfert d'électron (*ET: Electron Transfer*) constituent deux mécanismes possibles pour expliquer le processus de l'extinction de la luminescence. Le transfert d'énergie résonnant nécessite un recouvrement spectral entre le spectre d'absorption du donneur (QDs) et le spectre d'emission de l'accepteur (le photochrome). Alors que le transfert d'électron nécessite un changement considérable, dans les potentiels d'oxydation ou de réduction du photochrome lors de sa transformation photochimique, par rapport à celui du QDs. L'efficacité des deux mécanismes, le transfert d'énergie et le transfert d'électron dépendent de la façon d'attachement du photochrome sur les QDs et de la distance qui les sépare ainsi que des potentiels redox.

IV.2 Exemple d'un assemblage Quantum dot-photochrome

Branda *et al*[116] ont étudié la photo-modulation da la luminescence des quantum dots (QDs) de CdSe-ZnS par un dithienylethene (DTE) cationique contenant une pyridine et un groupe methyl- pyridinium **(figure (IV.1) : A)** le DTE est attaché à la surface des QDs par l'intermédiaire de la pyridine[117].

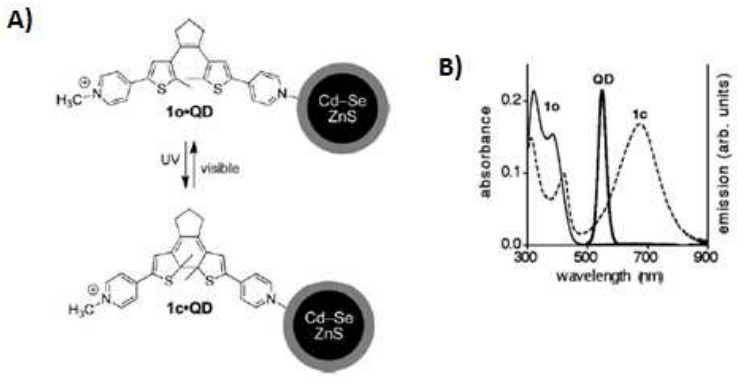

Figure (IV.1) : A) interconversion photo-induite entre l'isomère forme ouverte (1o) et l'isomère forme cyclisée (1c) d'un DTE contenant un methyl-pyridinium et une pyridine. Le contre ion de chaque espèce est le I⁻. B) spectres d'absorption UV-vis d'une solution (10^{-5} M, 20°C) de $CHCl_3$ de l'isomère forme ouverte (1o) avant (ligne continue) et après irradiation a 313 nm (pointillés).

L'intensité de la luminescence des QDs est diminuée par la présence de l'isomère cyclisé (1c) qui est fixé à la surface des QDs. La conversion de (1c), vers sa forme ouverte (1o) conduit à l'augmentation de l'intensité de la luminescence. Des analyses optiques et électrochimiques ont été menées pour pouvoir expliquer l'origine de l'extinction de la luminescence. Les mesures optiques montrent que le spectre d'absorption de la forme cyclisée (1c) **(figure (IV.1) : B)** présente dans le visible, une bande intense qui chevauche avec la bande d'émission des QDs. Le recouvrement spectral des deux bandes peut conduire à un transfert d'énergie entre les QDs et le DTE et par la suite aboutir à l'extinction de la luminescence des QDs. Les mesures de voltamétrie cyclique ont montré que l'interconversion des deux photo-isomères (1o) et (1c) produit un changement significatif dans les potentiels redox, E_{red} (1o)= -1.1 V vs SCE et E_{red} (1c)= -0.81 V vs SCE. En utilisant le potentiel d'oxydation (+1.4 V vs SCE)[118] mesuré pour des quantum dots CdSe-ZnS ayant une taille de 3 nm et l'énergie de l'émission (550 nm ou 2,25 eV), des calculs de l'énergie libre ΔG^0 du transfert d'électron vers (1o) ou (1c) après excitation des QDs ont été réalisés. La réaction est endergonique pour une valeur de ΔG^0 = 243 meV pour la forme ouverte, alors que pour la forme cyclisée (1c), elle est exergonique avec un ΔG^0 = -46,7 meV. Ces calculs montrent que l'interconversion des deux photo isomères permet un control efficace de l'extinction de la luminescence par l'intermédiaire d'un transfert d'électron. Malgré toutes les propriétés intéressantes de photomodulation présentes dans ce complexe QD-DTE, son utilisation a été limitée par sa dégradation photochimique qui se produit au bout de trois cycles de coloration et décoloration sous irradiation UV et visible.

Cependant, l'objectif principal de notre travail est de produire des quantum dots commutables par le biais d'une combinaison entre le diacide dithienylethene DTE(COOH)$_2$ et les nanoparticules d'oxyde de zinc.

IV.3 Les Nanoparticules (NPs) d'oxyde de zinc

Le ZnO est un cristal semi-conducteur ayant un large gap de 3,37 eV, une énergie de liaison excitonique de 60 meV[119] et présentant des propriétés de luminescence dans le proche ultra-violet et dans le visible. Il est utilisé dans de nombreuses applications telles que l'absorption UV, le traitement antibactérien[120], comme un catalyseur[121], photocatalyseur[122] et additif dans

l'industrie de nombreux produits cosmétiques. Ceci est dû à ses diverses propriétés optiques et électriques, ses stabilités thermique et chimique très élevées, sa non toxicité ainsi que son abondance dans la nature. Il est également utilisé dans la fabrication des cellules solaires[123], des capteurs de gaz[124] et des matériaux luminescents[125].

Suite à l'absorption d'un photon d'énergie supérieure ou égale au gap du ZnO, un électron est promu de la bande de valence à la bande de conduction. Ainsi une paire électron-trou (appelée exciton) est créée et elle correspond à un état lié entre un électron et une particule imaginaire appelée un trou d'électron. L'exciton peut être libre ou lié à une impureté ionique ou neutre du cristal, soit donneur ou accepteur. Cette impureté peut provenir des sites vacants d'atomes ou des défauts dans le réseau cristallin.

L'origine de l'émission dans l'UV des NPs de ZnO correspond à la recombinaison directe des paires électron-trou menant à l'émission dite excitonique qui se trouve près de 370 nm. L'émission excitonique est liée à des effets de confinement et dépend de la taille des NPs. Pour des tailles inférieures à 10 nm[126], l'effet de confinement peut être observé.

L'émission des NPs dans la région du visible est due aux défauts de surface et elle est fortement liée à la méthode de synthèse[127]. Ces défauts peuvent être des impuretés, des défauts de cristallinité tels des atomes interstitiels, des lacunes, ou encore des molécules adsorbées à la surface. Ces défauts présents dans la structure cristalline peuvent agir de différentes façons sur la luminescence des NPs, en fonction de leur position énergétique au sein de la bande interdite. On distingue ainsi les défauts "profonds", dont les niveaux énergétiques sont situés à quelques eV des bandes de valence et de conduction, des défauts "peu profonds" qui sont situés à quelques dizaines de meV de ces mêmes bandes.

La présence de niveaux d'énergie suffisamment profonds dans le gap induit une luminescence qui peut s'étendre du bleu au rouge selon les défauts considérés. On peut ainsi couvrir une large plage de longueurs d'onde et obtenir une lumière blanche en combinant les bons défauts[128]. Si l'on considère uniquement les défauts tels que les lacunes ou les atomes interstitiels de zinc et/ou d'oxygène, on peut obtenir des niveaux d'énergie très différents. Cependant, la structure intime des défauts participants à cette luminescence ne peut pas être identifiée[129].

Van Dijken et al[130] ont montré que les profonds pièges de trous combinés à des lacunes d'oxygène, sont responsables de l'émission jaune située au-dessus de 500 nm. Alors que l'origine de l'émission bleue (440 nm) a été attribuée aux défauts tels que le zinc[131] interstitiel, ou les groupes OH^- à la surface des particules[132].

Bien que la nature de l'émission provenant des défauts dans la structure cristalline des NPs de ZnO constitue toujours le sujet de recherche de plusieurs groupes, plusieurs études qui exploitent le transfert d'énergie à partir des états énergétiques correspondant aux défauts vers des fluorophores organiques[133] attachés à la surface des NPs peuvent être trouvées dans la littérature : nous en développons maintenant deux.

IV.3.1 Exemples d'assemblages NPs ZnO – fluorophore

Makhal *et al*.[134] ont étudié l'émission de la lumière d'un complexe formé par un assemblage entre des NPs de ZnO et l'Oxazine 1 (OX1)[135] qui est un fluorophore bien connu en tant que marqueur biologique. L'exploration du processus d'émission de la lumière de ce complexe ZnO-OX1 a été réalisée par l'étude des déclins de fluorescence transitoire picoseconde. Le complexe ZnO-OX1 a été préparé en mélangeant une solution colloïdale de ZnO avec des quantités pré calculées d'OX1 cationique et en agitant le mélange durant 3 heures dans le noir. Les mesures spectroscopiques d'émission et d'absorption UV-visible montrent qu'il existe un recouvrement spectral dans le visible **(figure (IV.2) : A)**, entre la bande d'émission des NPs de ZnO et le spectre d'absorption de l'OX1. Ainsi un transfert d'énergie, FRET (Forster Resonance Energy Transfer), peut avoir lieu du donneur (NPs ZnO) vers l'accepteur (OX1).

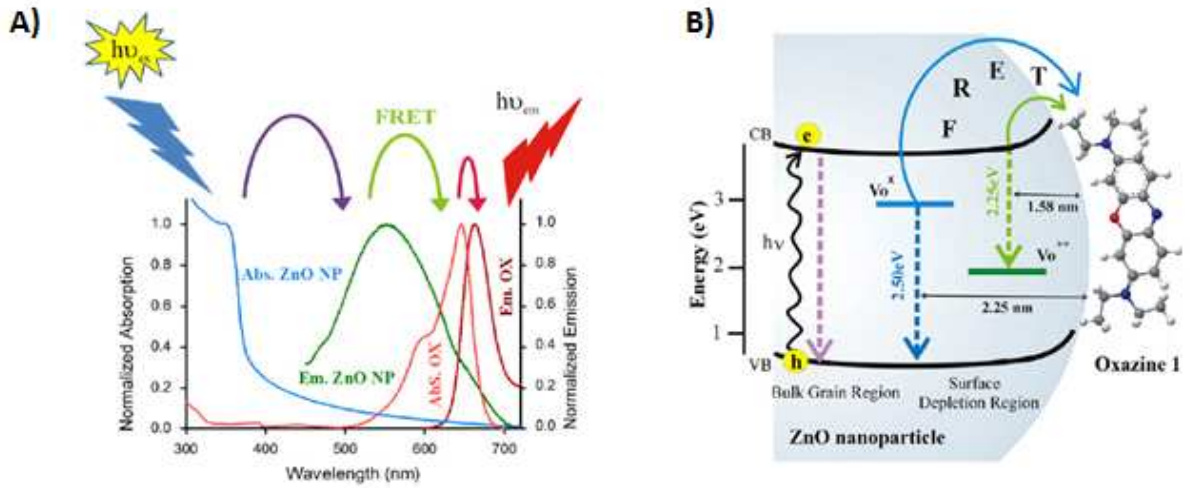

Figure (IV.2) : A) spectres normalisés d'absorption (bleu) et d'émission (vert) des NPs de ZnO ayant un $rayon \sim 3nm$. B) schéma du nano-hybride ZnO-OX1 représentant la dynamique du FRET des lacunes d'oxygène, V_O^{++} et $V_O^{\times}$, des NPs de ZnO vers les molécules OX1.

L'efficacité du transfert d'énergie à partir des NPs de ZnO vers l'OX1 ainsi que la distance (r_{DA}) séparant le donneur de l'accepteur dans la paire ZnO - OX1 ont été déterminées[136] après avoir calculé la distance de Forster (R_0) et l'intégrale de recouvrement *J*:

La distance de Forster (R_0) est donnée par la relation suivante :

$$R_0 = 0.211 * [\kappa^2 n^{-4} Q_D J]^{1/6} \qquad \textbf{(1)}$$

κ^2 est un facteur décrivant l'orientation relative dans l'espace des dipôles de transition du donneur et de l'accepteur de valeur 2/3 pour une distribution isotrope, *n* est l'indice de réfraction du milieu et Q_D est le rendement quantique du donneur en l'absence d'accepteur.

J, l'intégrale de recouvrement, exprime le degré de recouvrement entre le spectre de l'émission du donneur et le spectre de l'absorption de l'accepteur:

$$J = \frac{\int_0^\infty F_D(\lambda)\varepsilon_A \lambda^4 \, d\lambda}{\int_0^\infty F_D(\lambda) d\lambda} \qquad \textbf{(2)}$$

$F_D(\lambda)$ est l'intensité de fluorescence sans unité. ε_A est le coefficient d'absorption molaire (en M^{-1} cm^{-1}) de l'accepteur à la longueur d'onde λ. Si λ est en nm, alors *J* est en M^{-1} cm^{-1} nm^4.

Quand la valeur de (R_0) est connue, la distance (r_{DA}) de la paire donneur-accepteur peut être facilement calculée en utilisant la formule suivante :

$$r_{DA}^6 = \frac{[R_0^6\,(1-E)]}{E} \qquad \textbf{(3)}$$

E est l'efficacité de l'énergie de transfert, elle est mesurée en utilisant le temps de vie de fluorescence du donneur, en absence (τ_D) et en présence (τ_{DA}) de l'accepteur:

$$E = 1 - \frac{\tau_{DA}}{\tau_D} \qquad \textbf{(4)}$$

Le modèle de Forster est habituellement utilisé pour des colorants moléculaires. Il a néanmoins été appliqué pour traiter le cas des nanoparticules. Ainsi Makhal *et al* pour calculer l'efficacité du RET dans la paire ZnO-OX1, ont considéré que l'émission des NPs de ZnO dans le visible provenait des lacunes d'oxygène neutres ou chargées positivement présentes dans la structure des NPs. Les états d'énergie correspondants à ces lacunes d'oxygène sont localisés à la surface et à l'intérieur, ils sont notés par : V_O^{++} et $V_O^{\times}$ respectivement. Dans la zone de déplétion de porteurs près de la surface, une lacune d'oxygène mono chargée V_O^{+} située **(figure (IV.2) : B)** peut se recombiner avec un trou pour générer des lacunes V_O^{++} conduisant ainsi à une émission à 550 nm (2.25 eV). Hors de la zone de déplétion, V_O^{+} devient neutre $V_O^{\times}$ **(figure (IV.2) : B)** en se recombinant avec un électron provenant de la bande de conduction menant ainsi à une émission à 495 nm (2.5 eV). En conséquence, la large bande d'émission de ZnO dans le visible peut être décomposée en deux composantes : une bande d'émission prédominante qui est centrée autour de $\lambda = 550\ nm$ et une autre bande centrée à la longueur d'onde $\lambda = 495\ nm$.

L'efficacité du RET peut être calculée pour ces deux transitions ($\lambda = 550\ nm$ et $= 495\ nm$) du spectre d'émission de ZnO. En appliquant le modèle de Forster, ils ont trouvé que les lacunes d'oxygène situées à proximité de la surface des nanoparticules (émission à $\lambda = 550\ nm$) conduit à une efficacité de FRET très élevée (> 90%) tandis que l'efficacité du FRET calculée pour la bande d'émission à $\lambda = 495\ nm$, provenant d'autres défauts situés profondément dans la structure des NPs de ZnO, est plus faible (63 %).

Apres avoir calculé le temps de vie moyen du complexe ZnO-OX1 suite à des mesures spectroscopiques d'émission transitoire picoseconde, ils ont obtenu la distance effective r_{DA} entre le donneur (ZnO) et l'accepteur (OX1) en utilisant les équations (3) et (4) :

Pour l'émission à $\lambda = 550\,nm$: le rayon $r_{DA} \approx 1.58\,nm$, **(figure (IV.2) : B)** entre le donneur et l'accepteur est plus petit que le rayon $r \approx 3nm$ de la nanoparticule et comparable à l'épaisseur t de la couche de surface de la nanoparticule alors $r > r_{DA} \approx t$

Pour l'émission à $\lambda = 495\,nm$: le rayon $r_{DA} \approx 2.25nm$, **(figure (IV.2) : B)** est beaucoup plus grand que celui obtenu à $\lambda = 550\,nm$. Alors, dans ce cas $r \approx r_{DA} > t$, ceci confirme que l'émission à $\lambda = 495\,nm$, provient des défauts situés profondément dans la structure de la nanoparticule.

Ce travail montre donc que le modèle de transfert d'énergie résonnant est applicable à des NPs de ZnO, mais ne s'interroge pas sur la répartition des colorants sur les nanoparticules, laquelle influence certainement la réponse du système. L'autre exemple sur le transfert d'énergie à partir des NPs de ZnO vers un colorant conjugué a été présenté par Beane *et al*[137]. Sans appliquer aucun modèle pour décrire le transfert d'énergie, ces auteurs ont montré l'importance de la description statistique des assemblages nanoparticules-colorants pour l'analyse du transfert d'énergie entre nanoparticules et colorant adsorbés. Le point de départ est l'étude de la paire nanoparticule de ZnO et cadavérine Alexa594 (cadavérine A594) par des mesures de photoluminescence (PL) stationnaire et résolue dans le temps. La cadavérine A594 contient une amine primaire, qui peut se lier à la surface des nanocristaux de ZnO. Pour ce faire, les échantillons ont été laissés s'équilibrer après mélange du ZnO et la cadavérine A594 pendant 5 minutes avant les mesures. Les mesures d'absorption UV-visible et de fluorescence stationnaire montrent que le spectre d'émission de ZnO est dominé par l'émission centrée à 510 nm provenant des défauts de surface du nanocristal **(figure (IV.3) : A)**. Le colorant cadavérine A594 présente un maximum d'absorption à 591 nm, tandis que le spectre d'émission est décalé de 19 nm (Stokes shift) avec un maximum à 610 nm **(figure (IV.3) : A)**. Un recouvrement spectral entre la bande d'émission de ZnO et la bande d'absorption de la cadavérine A594 est observé **(figure (IV.3) : A)** d'où la possibilité d'avoir un transfert d'énergie du ZnO vers la cadavérine A594 qui est adsorbée à sa surface.

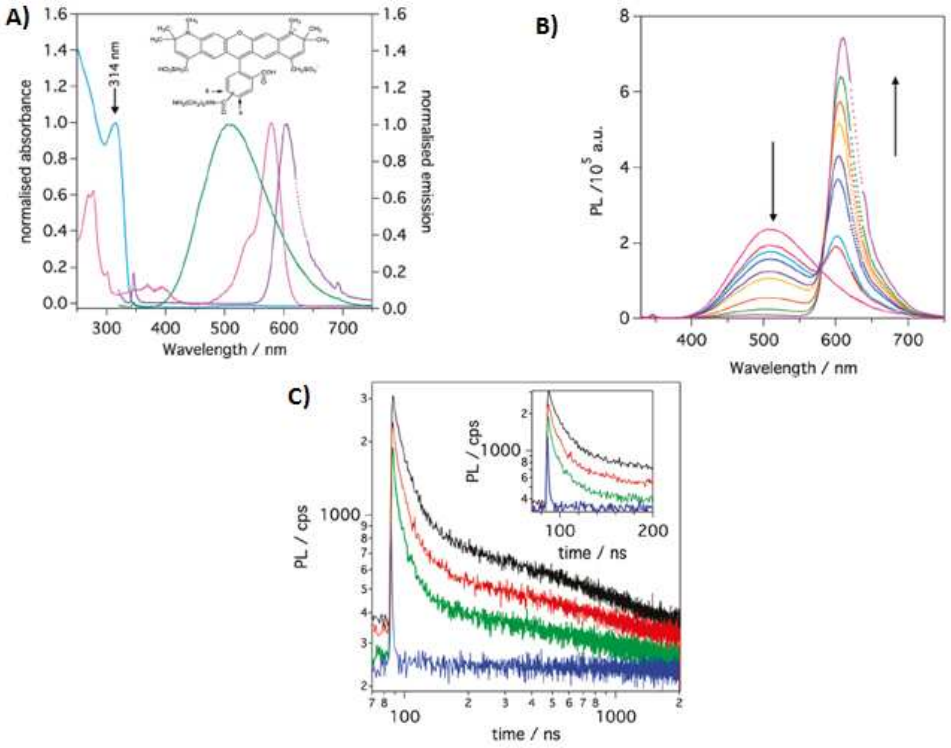

Figure (IV.3) : A) Spectres normalisés d'absorption de ZnO (bleu clair) et de la cadavérine A594 (violet clair) ainsi que les spectres normalisés d'émission de ZnO (vert) et de la cadavérine (violet fonce) dans l'éthanol. B) Les spectres d'émission de solutions éthanoliques contenant 212 nM de ZnO avec des concentrations croissantes de la cadavérine A594, de haut en bas à gauche de la figure, 0-1060 nM. L'excitation est faite à $\lambda = 314\ nm$. C) les déclins de photoluminescence d'une solution de ZnO à 212 nM avec 0.5 (rouge), 1 (vert) et 5 (bleu équivalents de la cadavérine A594 dans l'éthanol. L'excitation est faite à $\lambda = 300\ nm$ et l'émission est mesurée à $\lambda = 500\ nm$.

Les spectres d'émission de solutions de ZnO contenant des concentrations croissantes de la cadavérine A594 montrent que l'intensité de l'émission de ZnO dans le visible (provenant des défauts de surface) diminue et l'intensité de l'émission de colorant augmente de façon concomitante **(figure (IV.3) : B)**. Les mesures spectroscopiques résolues dans le temps démontrent que le transfert d'énergie dans ce système ZnO-cadavérine A594 provient de l'émission due aux défauts de surface. Ces mesures ont montré aussi une diminution de temps de vie apparent pour les deux composants, avec une décroissance des déclins de fluorescence de ZnO en augmentant le nombre d'équivalents du colorant **(figure (IV.3) : C)**, bien que les molécules soientt adsorbées. Ce changement du temps de vie apparent les a conduits à adapter aux nanoparticules le modèle cinétique de Sadhu[138] qui est à l'origine développé pour des fluorophores en milieu micellaire.

Ainsi, si l'on représente par $[NC\colon \Delta_n]$: le nanocristal (NC) d'oxyde de zinc portant les n molécules de colorants Δ adsorbées, $[NC^*\colon \Delta_n]$: le nanocristal d'oxyde de zinc à l'état excité (NC^*) avec n molécules de colorants adsorbées et $[NC\colon \Delta_n^*]$: le système après transfert d'énergie à l'une des n molécules adsorbées, les processus photochimiques en compétition sont alors :

1- la désactivation radiative du nanocristal, processus indépendant de la présence de colorant :

$[NC^*\colon \Delta_n] \rightarrow [NC\colon \Delta_n] + h\nu \qquad constante\ de\ vitesse\ de\ desactivation\colon (k_0)$

2- le transfert d'énergie vers un colorant adsorbé :

$[NC^*\colon \Delta_n] \rightarrow [NC\colon \Delta_n^*] \qquad constante\ de\ vitesse\ de\ desactivation\colon (n\,.\,k_q)$

L'originalité du modèle est de supposer que même si des molécules Δ sont adsorbées, le nanocristal peut se désexciter de manière radiative. La constante de vitesse globale de désactivation de l'état excité est donnée par : $k_0 + n\,.\,k_q$ et le temps de vie du nanocristal avec n colorant est donc exprimé par : $\tau = \frac{1}{(k_0 + n.k_q)}$

Les colorants sont supposées adsorbés aléatoirement suivant une isotherme de Langmuir et on considère que le nombre n des molécules Δ adsorbées sur chaque nanocristal (NC) suit une distribution de Poisson dont le paramètre λ_s est le nombre moyen des molecules de colorant par nanoparticule. Ce paramètre est aussi égal au rapport des concentrations du colorant et des NPs de ZnO $\left(\lambda_s = \frac{[A594]}{[ZnO]}\right)$. Le déclin de luminescence revient à sommer les contributions (exp-(k_0+nk_q)t) de chaque type de cluster [NC :Δ_n] pondérées par le nombre de ces clusters:

$$\frac{I}{I_0} = \sum_{n=O}^{n\rightarrow\infty} \frac{\lambda_s^n e^{-\lambda_s}}{n!}\ e^{-(k_0+nk_q)t} \qquad \textbf{(5)}$$

I est l'intensité de fluorescence en présence du fluorophore (A594), I_0 est l'intensité de fluorescence en absence du fluorophore (A594) .

L'équation **(5)** peut être simplifiée pour donner la forme suivante:

$$\frac{I}{I_0} = e^{-k_0 t - \lambda_s} \sum_{n=O}^{n\to\infty} \frac{\left(\lambda_s e^{-k_q t}\right)^n}{n!} = \exp -k_0 t - \lambda_s\left(1 - \exp(-k_q t)\right) \quad \textbf{(6)}$$

L'ajustement des déclins de fluorescence avec cette équation **(6)** permet donc de déterminer les constantes de vitesse k_0 et $k_q$ainsi que λ_s, le nombre moyen des molécules de colorants adsorbées à la surface du NC d'oxyde de zinc.

En utilisant ce modèle, ils ont calculé que même une seule molécule de colorant peut effectivement aboutir à l'extinction de la luminescence de ZnO, bien qu'un rapport molaire de 5 colorants par nanocristal soit nécessaire pour l'extinction de plus que 95% de l'ensemble de la photoluminescence, en raison de la distribution de Poisson de molécules de colorants parmi les nanocristaux de ZnO.

IV.3.2 Exemples d'assemblages NPs ZnO – photochrome

L'association entre les NPs de ZnO et une entité photochromique n'a pas beaucoup été étudiée. Après avoir consulté la littérature, on trouve juste deux rapports qui présentent l'étude de cet assemblage, soit avec l'azobenzène ou le dithiényléthène DTE.

Fages *et al.*[139] ont étudié une structure nanohybride contenant un azobenzène photochrome qui est greffé à la surface de nanobâtonnets ou de nanoparticules d'oxyde de zinc. L'azobenzène contient une longue chaîne aliphatique et un acide carboxylique qui servent respectivement en tant que groupement de solubilisation et unité de liaison avec le ZnO **(figure (IV.4) : A)**.

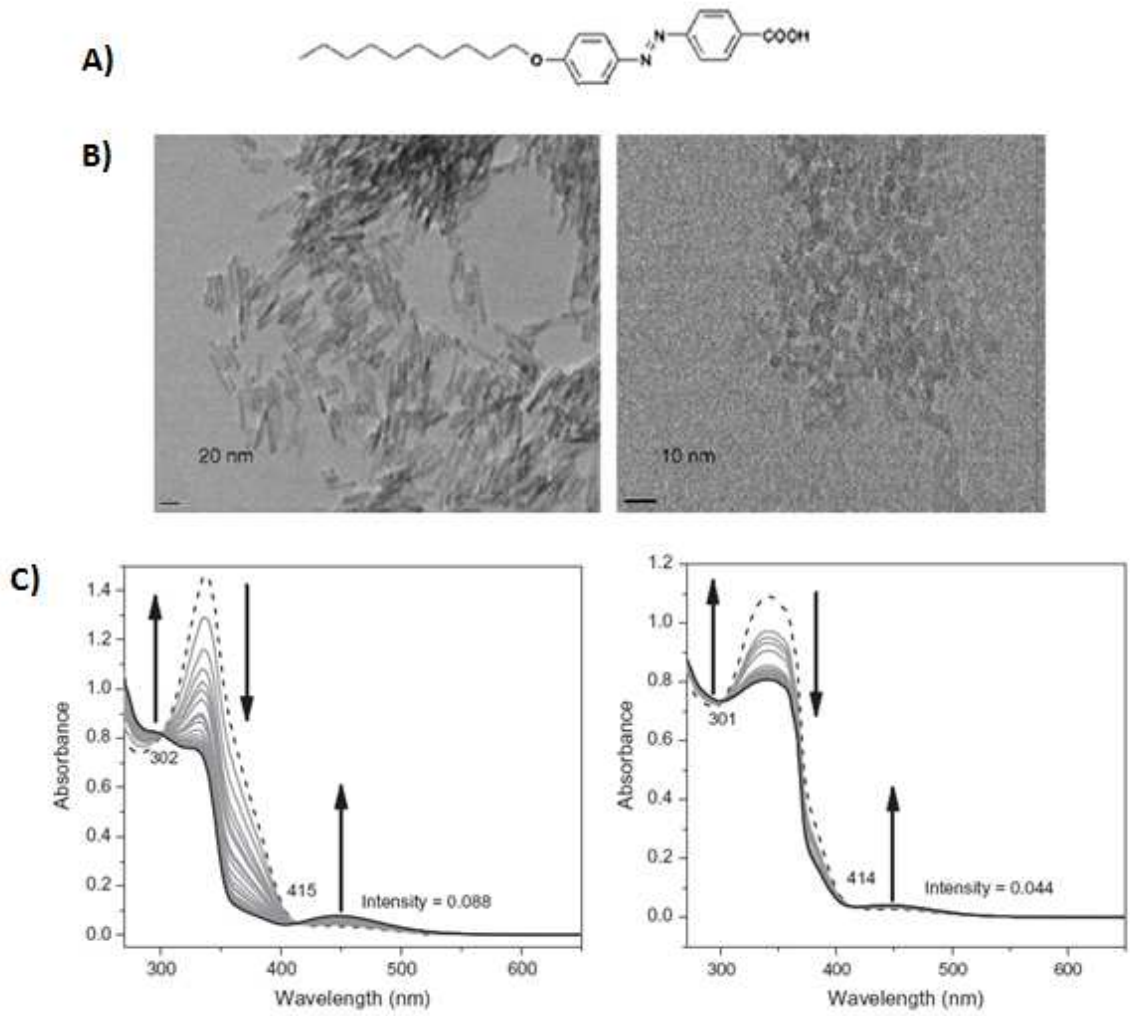

Figure (IV.4) : A) structure de l'azobenzène. B) clichés de TEM (*Transmission Electron Microscopy*) des nano bâtonnets (à gauche) et nano sphères (à droite) de ZnO avec l'azobenzène collé à leur surface. C) photoisomerisation de l'azobenzène greffé dans les couches auto assemblées sur les nano sphères (à gauche) et sur les nano bâtonnets (à droite) de ZnO durant une irradiation lumineuse à $\lambda = 378\ nm$ pendant 24 minutes. L'intervalle entre deux cycles consécutifs est égal à une minute. (temps d'irradiation totale: 24 min, [azobenzène] = 4 e-4 M pour les nano sphères et 2,5 e-4 M pour les nano bâtonnets dans le THF). Échantillon avant irradiation (ligne pointillée) et après 24 min d'irradiation (ligne noire solide), et aux différents temps d'irradiation (gris, traits pleins). Dans toutes les expériences: [ZnO] = 0,05 mg / mL

La structure de l'azobenzène étudié ressemble beaucoup à celle d'un composé oligothiophène que la même équipe avait précédemment utilisé pour former des monocouches bien organisées sur une surface de ZnO[140]. Le but de leur travail consiste donc à étudier la morphologie de surface des nanoobjets d'oxyde de zinc, **(figure (IV.4) : B)**, et surtout obtenir une meilleure connaissance des facteurs qui influent sur l'ordre local dans les monocouches organiques se trouvant sur ces colloïdes. Ils ont trouvé que les nano bâtonnets

de ZnO, ayant des facettes planes, permettent une organisation plus serrée des molécules dans la monocouche auto-assemblée que dans le cas des nano sphères qui ont une forme sphérique. Ils ont trouvé aussi que la photoisomerisation de l'azobenzene **(figure (IV.4) : C)** est fortement affectée par la forme des nanoparticules d'oxyde de zinc. Cependant, cette photoisomerisation s'est avérée moins efficace dans le cas des nano bâtonnets par rapport aux nanoparticules sphériques.

Dans le même groupe de recherche, une autre étude[141] sur un assemblage ZnO/photochrome a été réalisée. Cette étude concernait deux molécules de dithienylethene (1o) et (2o) **(schéma IV.1)**, fonctionnalisées avec une fonction acide carboxylique, qui ont été greffées à la surface des nanotubes d'oxyde de zinc.

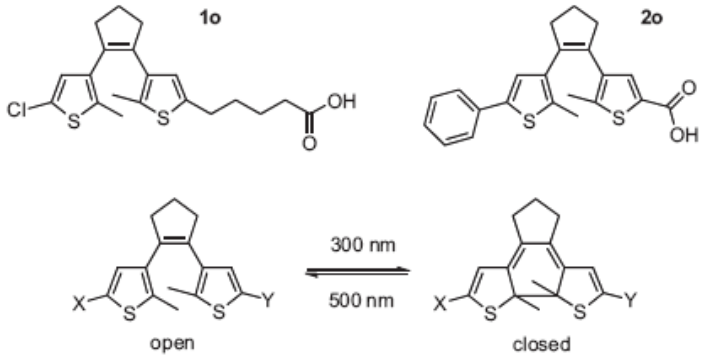

Schéma (IV.1) : Structures moléculaires utilisées dans cette étude et la réaction de photoisomérisation entre les formes de DTE, ouverte et fermée

Ils ont montré que le complexe résultant de l'association DTE-ZnO peut commuter dans un mode bidirectionnel, ce qui permet à la fois la fermeture et l'ouverture du cycle du DTE suite à des séquences d'irradiation successives de la forme ouverte à $\lambda = 300$ nm et de la forme cyclisée à $\lambda = 500$ nm. En fonction de la structure moléculaire du DTE utilisé, des pertes dans les processus photochimiques d'interconversion entre les deux photo-isomères, ouvert et fermé, ont été observées probablement en raison de la photodégradation. L'un des deux dérivés de DTE étudiés, contenait un groupement phényle terminal (2o) **(schéma IV.1)** fournissant ainsi une conjugaison plus longue du système π dans l'isomère cyclisé du DTE. A la suite de cette conjugaison, la bande d'absorption de la forme cyclisée dans le visible shift vers le rouge offrant ainsi une meilleure stabilité photochimique.

A partir des deux études précédentes, on peut conclure que les conversions photochimiques réversibles des produits photochromes peuvent être réalisées à la surface des NPs de ZnO sans altération de leurs propriétés optiques. Par contre, on n'a pas trouvé d'exemples qui étudient la photo-modulation de l'émission des nanoparticules de ZnO par l'intermédiaire de l'interconversion photo-induite d'un photochrome.

IV.4 Etude de l'assemblage NPs ZnO-DTE(COOH)$_2$

L'objectif de notre travail consiste à étudier la photomodulation de l'intensité d'émission de ZnO en présence du diacide DTE. **(Schéma IV.2)**

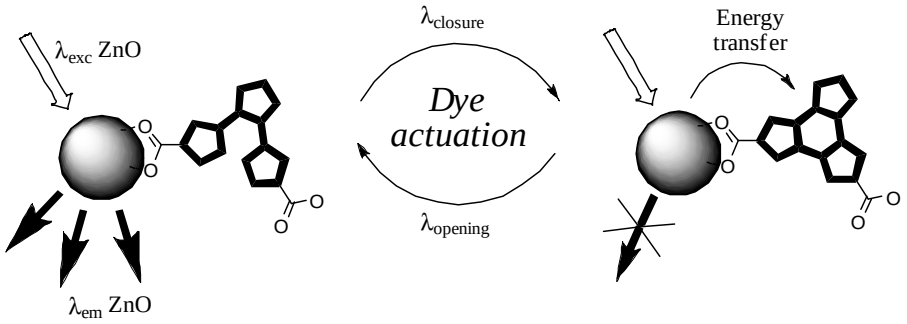

Schéma (IV.2) : les changements d'émission de fluorescence photo-induits dans le système impliquant le diacide DTE(COOH)$_2$ et les nanoparticules de ZnO.

Grâce à une collaboration avec M.L.Kahn (LCC Toulouse) nous avons pu avoir accès à des nanoparticules de ZnO fabriquées par voie organométallique. Ces particules sont toujours accompagnées de l'hexadécylamine (HDA) stabilisante : en conséquence (sans compter le solvant THF) le système est ternaire (ZnO, HDA, AH_2) ou quaternaire (ZnO, HDA, AH_2, BH_2). Nous avons donc choisi d'étudier en l'absence de photochimie l'impact mutuel que ces différents composants pouvaient avoir l'un sur l'autre, avant d'examiner effectivement la photomodulation de la luminescence de ZnO

IV.4.1 Les nanoparticules de ZnO stabilisées par HDA

Les NPs de ZnO utilisées dans notre étude, ont donc été synthétisées au LCC par voie organométallique[142] . Ainsi une solution de 0.32 M de dicyclohexylzinc [Zn (C_6H_{11})$_2$] dans le

THF anhydre a subi l'hydrolyse contrôlée à température ambiante[143,144] en présence d'un equivalent d'hexadecylamine. Le mélange réactionnel issu de cette synthèse se présente sous la forme d'un gel blanc plus ou moins solide et nous a servi comme stock pour toutes nos expériences. Avant chaque utilisation, la solution mère est homogénéisée par chauffage et, si besoin les solutions filles diluées sont centrifugées. Par la suite les dilutions sont effectuées de façon à toujours obtenir la même absorbance (*vide infra*)

IV.4.1.1 Détermination de la taille des NPs

La morphologie des NPs de ZnO a été étudiée par des mesures de microscopie électronique en transmission (TEM). Le traitement des images réalisé par le logiciel Image J® montre une distribution monomodale centrée à 6 nm. Cette valeur obtenue représente la taille moyenne des NPs. Ainsi, à partir des paramètres cristallographiques de la structure würtzite de ZnO et en prenant une forme sphérique en première approximation, on peut trouver la relation entre la concentration de nanoparticules ([NP_ZnO]) et la concentration initiale de zinc:

$$[NP\_ZnO] = \frac{[Zn(Cy)_2]}{5000}$$

Comme ces NPs de ZnO sont accompagnées par des ligands de HDA, lesquels peuvent être adsorbés à la surface de la NP via la fonction amine ou libres dans la solution. Un équilibre de coordination-décoordination rapide avec la surface peut être observé. Or la quantité de HDA liées à la NP dépend du nombre d'atomes de zinc disponibles à la surface de la NP ZnO. En supposant que la NP a la forme d'un prisme à section hexagonale, on a trouvé qu'elle peut comporter 800 à 1000 atomes de zinc qui peuvent se lier à l'amine. Alors les atomes de zinc situés à la surface de la NP constituent environ (800 à 1000)/5000 = 16 à 20% de la quantité de zinc initial. Ainsi, si chaque amine se lie avec un seul atome de zinc (soit par une liaison Zn-N ou Zn-OH ... N), dans une stœchiométrie de 1/1, alors les amines liées aux atomes de zinc comptent pour 16 à 20% de la concentration initiale en amine. Cette fourchette est certainement surévaluée : en considérant l'aire transversale d'une molécule d'amine (environ 18Å^2) on peut calculer une densité de 630 molécules HDA qui pouvant se lier sur une particule supposée sphérique ayant une surface S= $4\pi r^2$ = 11309 Å^2 .

IV.4.1.2 Mesures spectroscopiques stationnaires

La **figure (IV.5)** montre le spectre d'absorption ainsi que les spectres d'émission dans le visible des NPs. Le spectre d'absorption est caractéristique de NPs et se présente sous la forme d'une marche abrupte : en dessous d'un seuil défini par la taille (quand les objets sont très petits) et/ou la nature du matériau, le ZnO ayant un gap de 365 nm (3.40 eV), l'absorption est nulle tandis qu'au dessus elle se présente sous la forme d'un plateau croissant vers les hautes énergies. Pour les mesures de photoluminescence, on a dilué la solution de façon à avoir une absorbance de 0.2 à 340 nm correspondant à une solution de concentration [ZnO]=0.52 mM. La concentration en NPs de ZnO sera $[NP\_ZnO] = \frac{0.52\ e{-}3}{5000} = 1.04e - 7\ M$

On a utilisé deux longueurs d'onde d'excitation (340 et 365 nm) car il a été montré que les NPs de ZnO synthétisées par voie organométallique peuvent avoir deux émissions[145] dans le visible, bleue et jaune. L'émission jaune qui se situe entre 500 nm et 600 nm peut être obtenue après une excitation entre 280 et 360 nm alors que l'émission dans le bleu à 440 nm peut être obtenue suite à une excitation entre 360 et 420 nm.

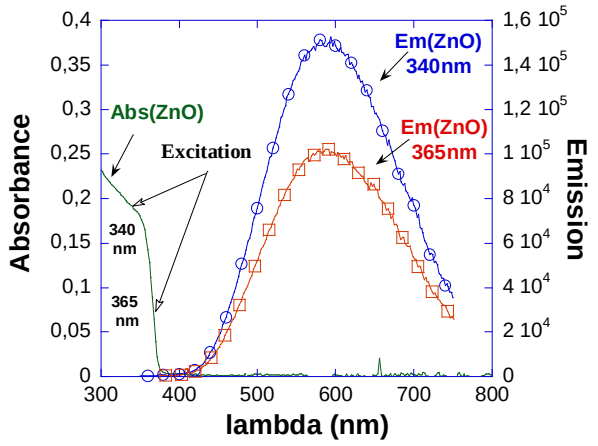

Figure (IV.5): spectres d'absorption UV-vis (vert) et d'émission d'une solution des NPs de ZnO stabilisées par des ligands HDA dans le THF ([ZnO]=0.52 mM), après excitation à $\lambda = 340\ nm$ (bleu) and $\lambda = 365\ nm$ (rouge).

Or pour chacune des deux excitations à 340 et 365 nm, on a obtenu deux émissions jaunes d'intensités différentes centrées à 586 nm. Après avoir calculé le rapport des absorbances et

des maxima d'intensités de fluorescence obtenues après ces 2 excitations, on a trouvé la même valeur.

$$\frac{Abs_{365\ nm}}{Abs_{340\ nm}} = \frac{I_{365\ nm}}{I_{365\ nm}} \approx 0.5$$

On peut conclure que c'est le même site émetteur qui est excité par ces deux longueurs d'onde. Alors il suffit d'exciter les NPs de ZnO avec l'une des deux.

IV.4.1.3 Détermination des temps de vie des NPs

Afin de déterminer les temps de vie des NPs de ZnO, des mesures de photoluminescence transitoires en régime nanoseconde ont été réalisées pour une excitation à 365 nm et des émissions mesurées à deux longueurs d'onde : 500 nm et 600 nm. La simulation des déclins de luminescence par une fonction bi exponentielle montre des temps de vie long et court pour chacune des deux longueurs d'ondes d'émission **Tableau (IV.1)**.

Lambda (nm)	τ_1 (µs)	τ_2 (µs)
500	2.4±0.008	0.04±0.001
600	2.9±0.013	0.06±0.002

Tableau (IV.1) : les temps de vie des NPs de ZnO à deux longueurs d'ondes 500 et 600 nm

Ces valeurs de temps de vie sont proches de celles précédemment observées (1.85 µs et 9 ns) par M. Kahn *et al*[144] avec des NPs de ZnO synthétisées par voie organométallique en présence de l'octylamine comme ligand stabilisant.

IV.4.2 Le photochrome diacide DTE(COOH)$_2$

IV.4.2.1 Etude de la photoisomérisation du DTE(COOH)$_2$ dans le THF

La photo-isomérisation du diacide DTE(COOH)$_2$ dans le THF a été réalisée afin de déterminer les propriétés spectrales des deux photoisomères du DTE et de les comparer avec celles trouvées dans l'acétonitrile (chapitre II).

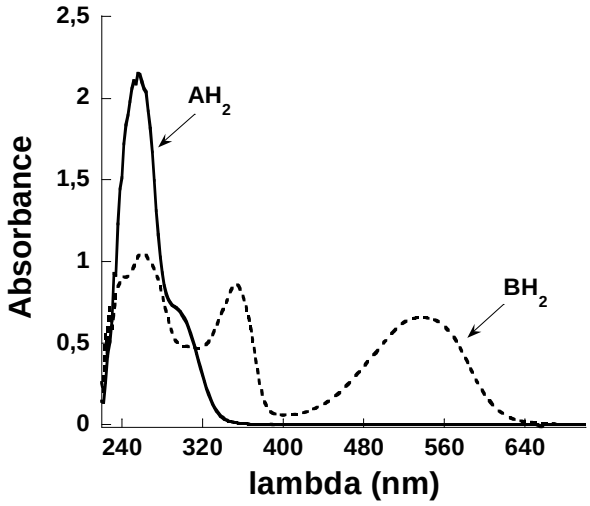

Figure (IV.6) : spectres d'absorption UV-visible des deux photo isomères, ouvert (AH_2) et fermé (BH_2) dans le THF. ([AH_2]= 0.1 mM et [BH_2]= 0.1 mM)

Sous irradiation à $\lambda = 313\, nm$, la forme ouverte (AH_2) absorbant dans l'UV avec un maximum d'absorption à 256 nm, se transforme en forme fermée (BH_2) ayant une bande d'absorption à des longueurs d'onde plus grandes que celles de la forme ouverte (AH_2). Les maxima d'absorption de la forme fermée (BH_2) apparaissent à 536 et 354 nm (**Figure IV.6)**. En comparant ces maxima d'absorption avec ceux obtenus dans l'acétonitrile, on conclut qu'il n'y a pas de changement de propriétés spectrales du DTE alors pas d'effet de solvatochromisme observé.

IV.4.2.2 Interaction entre l'amine HDA et DTE(COOH)$_2$

Comme les nanoparticules sont stabilisées par des ligands d'hexadecylamine HDA, une éventuelle réaction acide-base peut se produire entre les fonctions amine NH_2 et acide COOH du ligand et du photochrome diacide DTE respectivement.

L'interaction entre AH_2 et les ligands HDA, a été étudiée par l'intermédiaire des mesures spectroscopiques de RMN-DOSY qui ont montré une diminution du coefficient de diffusion du AH_2 en présence de l'amine HDA **(Tableau (IV.2).**

Coefficient de diffusion ($m^2 \cdot s^{-1}$)	Dans le THF	Dans le mélange AH_2/HDA
D $_{AH2}$	8.1 (±0.1) x 10^{-10}	12 (± 1) x 10^{-10}
D $_{HDA}$	12 (± 1) x 10^{-10}	10 (±1) x 10^{-10}

Tableau (IV.2): coefficients de diffusion de AH_2 dans le THF et dans le mélange AH_2/HDA/THF. [HDA]=0.55 mM et [AH_2]=0.1 mM

Cette interaction peut être une liaison hydrogène entre les fonctions COOH et NH_2 ou bien une paire d'ions COO^-NH3^+ provenant d'une réaction acido-basique.

On a vu au chapitre II que les spectres d'absorption UV visible des deux photoisomères du diacide DTE dans l'acétonitrile peuvent être modifiés légèrement par des réactions acido-basiques. Afin d'identifier le type d'interaction qui peut avoir lieu entre le ligand et le diacide DTE dans le THF, on a effectué des mesures d'absorption d'UV-visible du diacide DTE en présence de 0.2 équivalent d'amine HDA (**Figure IV.7)**

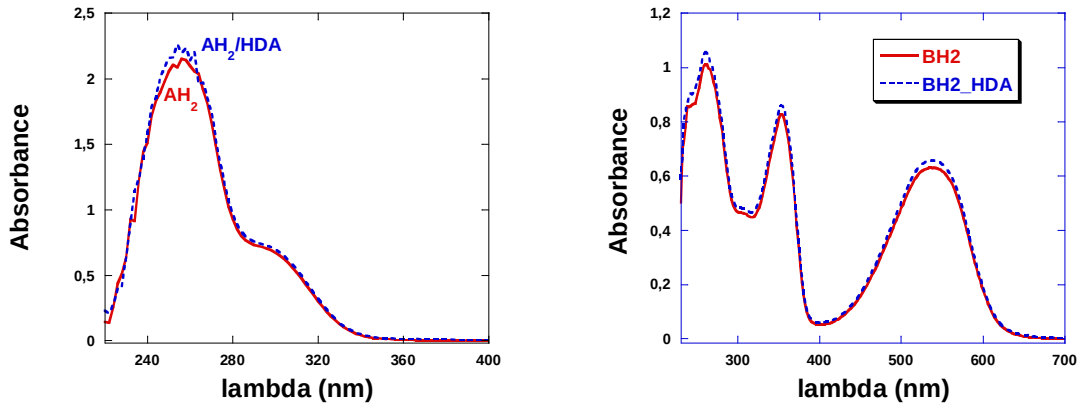

Figure (IV.7): spectre d'absorption des deux photoisomères AH_2 et BH_2 en absence et présence de 0.2 équivalents d'amine HDA. ([AH_2]= 0.1 mM, [BH_2]= 0.1 mM, [HDA]= 0.55 mM)

Les spectres d'absorption montrent qu'il n'y a pas de variation spectrale pour les deux photoisomères en présence d'amine, ce qui semble exclure un transfert de proton entre la fonction amine NH_2 du ligand et la fonction acide COOH du diacide DTE. Tout au plus pouvons nous affirmer qu'il se forme un complexe DTE_HDA

IV.4.3 Etude du système AH_2-NPs ZnO

L'interaction entre AH_2 et les NPs de ZnO a été étudiée tout d'abord par microscopie électronique en transmission et par RMN. Dans une seconde étape, les propriétés photophysiques de mélanges DTE/ZnO ont été étudiées soit de manière stationnaire soit résolues dans le temps. Des mélanges de AH_2 (0.2 équivalent) et de NPs de ZnO ont été préparés une nuit avant la prise des mesures. Le solvant de l'échantillon dédié pour la microscopie électronique a été évaporé sous vide alors que celui pour les analyses de RMN a été évaporé puis remplacé par du THF deutéré. On s'est limité à 0.2 équivalent de AH_2 par rapport aux NPs de ZnO pour ne pas dissoudre les NPs avec un excès de diacide et ne pas favoriser leur précipitation.

IV.4.3.1 Mesures de TEM

La morphologie des NPs de ZnO en présence de AH_2, a été étudiée par microscopie électronique en transmission **figure (IV.8)**.

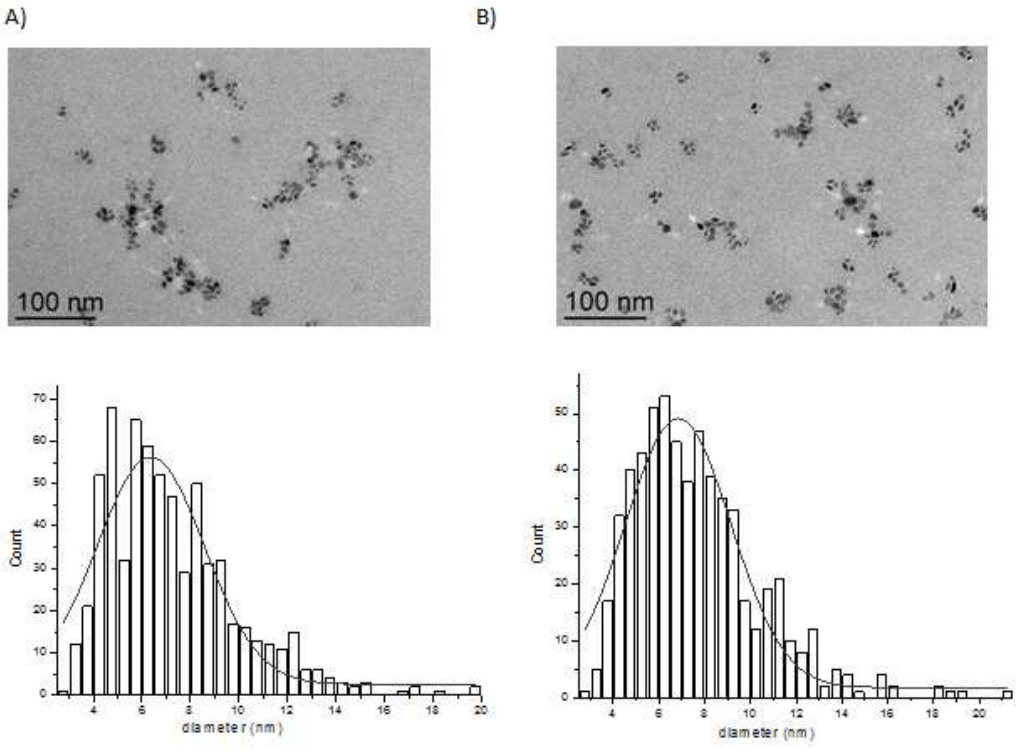

Figure (IV.8) : Images de microscopie électronique en transmission et diagrammes de taille des NPs: A) NPs de ZnO et B) ZnO- AH_2

Le traitement des images obtenues montre qu'il n'y a pas de changement de la taille moyenne des NPs de ZnO en présence de AH_2 **(tableau (IV.3).**

Echantillon	Taille moyenne (nm)
ZnO	6.4 ± 0.19
ZnO/ AH_2	6.8 ± 0.13

Tableau (IV.3): la taille moyenne des NPs de ZnO et du système ZnO- AH_2

Ces résultats montrent qu'il y a pas de modification notable de la taille des nanobjets, en particulier qu'il n'y a pas eu de dissolution des NPs de ZnO par les fonctions acides du DTE.

IV.4.3.2 Mesures de RMN

Les expériences de RMN-NOE transféré ont montré que la solution de ZnO / HDA / AH_2 présente des effets de NOE qui sont négatifs et faibles pour HDA et AH_2, indiquant ainsi l'existence d'une interaction avec les nanoparticules, mais aussi un échange rapide avec les espèces libres dans la solution. Or une molécule peut interagir de différentes façons avec une nanoparticule [ZnO-HDA]. En effet on peut envisager qu'elle soit fixée à la surface de la NP, associée à la couche de ligands HDA qui entoure la NP, ou qu'elle reste en solution **Schéma (IV.3)**.

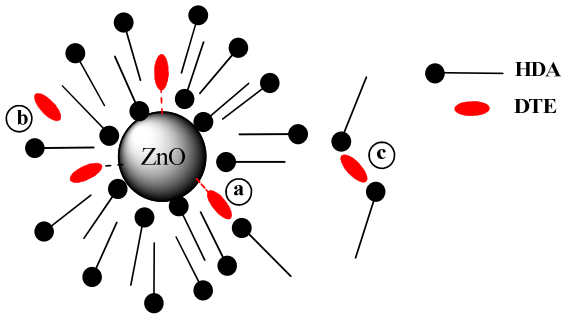

Schéma (IV.3): possibilités de coordination du DTE: a) ***lié à la surface de la NP,*** **b)** ***associé aux ligands de la bicouche couvrant la NP,*** **c)** ***libre en solution***

Stériquement, pour qu'une molécule DTE soit liée à la surface, il faut qu'elle se substitue à une molécule de ligand. Pour que cela soit envisageable il faut que la taille de la molécule de DTE soit comparable à celle de l'amine HDA. A partir de modèles moléculaires on peut estimer l'aire d'une molécule de DTE (réduite à sa section transversale triangulaire), on

trouve ainsi que pour AH_2 et BH_2, les surfaces valent 22.5 $Å^2$ et 16.5$Å^2$ respectivement et sont du même ordre de grandeur que l'aire occupée par une molécule de HDA. Cependant une telle interaction devrait être une chimisorption forte, ce qui semble incompatible avec les résultats de la RMN. Par cette dernière technique, s'il y a interaction, elle doit être labile, ce qui semble plus compatible avec une adsorption sur l'extérieur organique de la couche de ligand.

IV.4.3.3 Mesures d'émission stationnaire

Nous avons utilisé une analyse de type Stern-Volmer pour étudier l'interaction entre les NPs et la forme ouverte AH_2. Pour cela on a préparé des mélanges de ZnO-AH_2 avec des concentrations différentes en AH_2 dans le THF anhydre. Tous les échantillons ont été laissés à l'équilibre après mélange du ZnO et DTE pendant une nuit avant les mesures. La solution des NPs de ZnO utilisée avait une concentration de 0.52 mM en zinc ce qui correspond à 1.04*10^{-7} M en NP-ZnO.

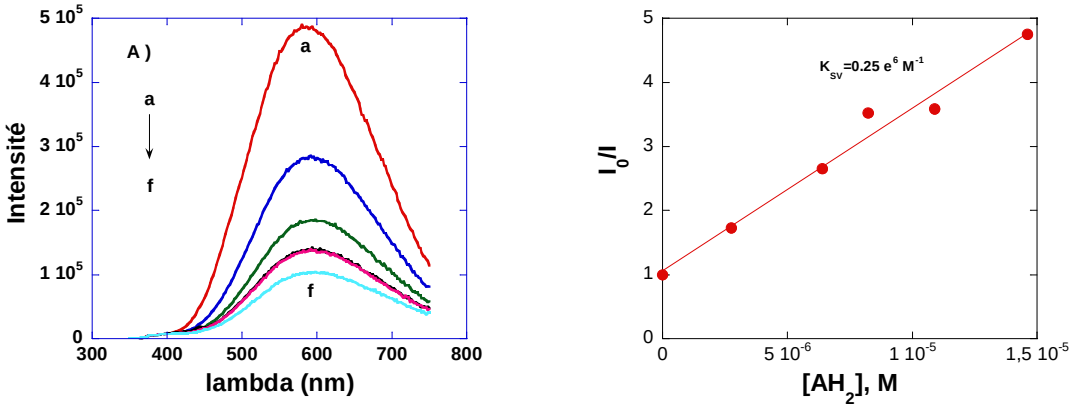

Fig (IV.9): quenching de l'émission des NPs de ZnO par AH_2 après excitation à 340 nm. A) L'émission avec des concentrations de AH_2: (a) 0, (b) 2.75*10^{-6} M, (c) 6.39 e^{-6} M, (d) 8.22*10^{-6} M, (e) 1.09*10^{-5} M, (f) 1.46*10^{-5} M. les concentrations initiales de $[ZnO]_0$=0.5 mM et $[AH_2]_0$=2.2*10^{-3} M. B) Analyse de type stern-Volmer pour le quenching des NPs ZnO par le AH_2

L'équation de Stern-Volmer est donnée par la relation suivante:

$$\frac{I_0}{I} = 1 + K_{SV}[Q] = 1 + k_q\tau_0[Q]$$

I_0 et I sont les intensités de fluorescence observées en absence et en présence du quencheur respectivement, [Q] est la concentration du quencheur. Pour un quenching dynamique, la constante de Stern-Volmer K_{SV} est le produit de k_q, constante de vitesse expérimentale du quenching bimoléculaire, et de τ_0, le temps de vie de l'état excité en absence du quencheur.

On a observé que l'intensité de l'émission de ZnO à 580 nm diminue avec l'augmentation de la quantité de AH_2 dans le milieu (**Figure (IV.9) A))** et que la variation de I_0/I *vs* [AH_2] est linéaire (**Figure (IV.9) B).** Suite à ces résultats obtenus avec AH_2, on s'est posé la question si l'origine du quenching de la luminescence des NPs de ZnO est due à l'adsorption de la fonction acide de AH_2 à la surface de la NP. Pour répondre à cette question on a choisi l'acide thiophène carboxylique (TC) comme une molécule modèle afin d'étudier l'effet d'un groupe acide d'une molécule similaire au DTE, sur l'intensité d'émission de ZnO. Pour cela, on a mesuré la variation de l'intensité d'émission des NPs de ZnO en présence de différentes quantités de TC **(figure IV.10)**

Acide thiophène carboxylique (TC) :

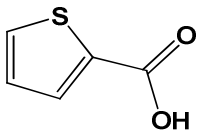

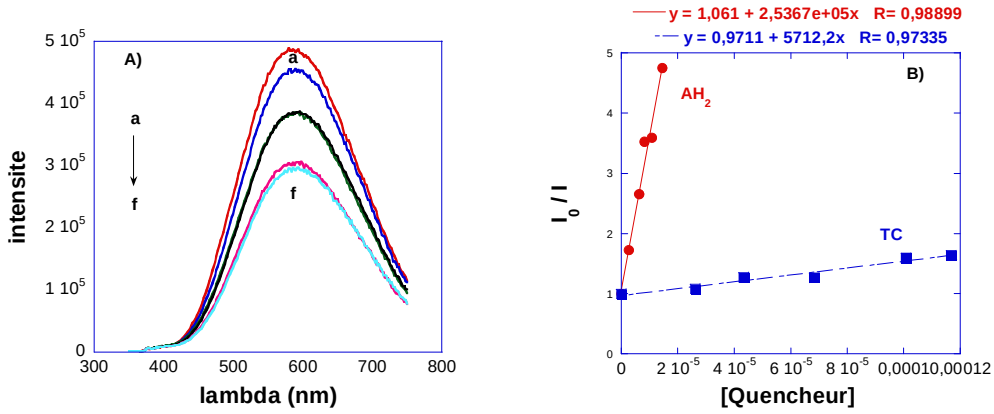

Fig (IV.10) : L'émission du système ZnO-TC avec des concentrations de TC: A) (a) 0.0, (b) 2.62*10^{-5} M, (c) 4.33*10^{-5} M, (d) 6.84*10^{-3} M, (e) 1.009*10^{-4} M, (f) 1.168*10^{-4} M. les concentrations initiales de [ZnO]$_0$=0.5 mM et [TC]$_0$=2.12*10^{-3} M. B) Analyse de stern Volmer pour AH_2 et TC

La **figure (I.10) B)** montre l'analyse de Stern-Volmer pour l'acide thiophènecarboxylique. La variation de I_0/I *vs* [Q] dans le cas de (TC) est une droite faiblement croissante. Cela signifie

cette molécule est un mauvais piégeur de l'état excité de la nanoparticule or elle représente grossièrement « la moitié » du photochrome étudié, en particulier la fonction acide et le soufre hétérocyclique. L'absence de piégeage permet donc de conclure que ces deux groupes fonctionnels n'ont pas d'impact sur la luminescence de NP-ZnO et le quenching observé avec AH_2 doit donc être lié au squelette entier de la molécule.

IV.4.3.4 Mesures d'émission résolues dans le temps

Les données de Stern Volmer sont souvent analysées en termes de quenching statique ou de quenching dynamique. Dans le cas d'un quenching dynamique déjà décrit plus haut, l'extinction de la luminescence provient d'un processus biomoléculaire avec l'émetteur et le quencheur. Le quenching statique résulte de la complexation de l'émetteur avec le quencheur donnant un complexe non émissif. Dans les deux cas, on aura une variation linéaire de I_0/I vs [Q]. Cependant dans le cas de quenching dynamique, le temps de vie apparent change en fonction de la concentration du quencheur, tandis que dans le cas d'un quenching statique le temps de vie de l'émetteur reste constant quelle que soit la concentration du quencheur car seules les molécules émettrices non liées peuvent relaxer d'une façon radiative.

Des expériences d'émission résolues dans le temps ont été réalisées pour des solutions de nanoparticules de ZnO en présence de différentes concentrations de quencheur AH_2. L'excitation a été réalisée à 365 nm et les émissions ont été mesurées à deux longueurs d'onde : 500 nm et 600 nm. Nous avons trouvé que le temps de vie des nanoparticules de ZnO diminue en augmentant la concentration de AH_2, ce qui exclut le modèle usuel du quenching statique.

La **Figure (IV.11)** montre les déclins de fluorescence de ZnO en absence et présence de 0.2 équivalent de AH_2 ou BH_2. Le déclin en présence de AH_2 est légèrement ralenti par rapport à celui de ZnO tout seul. Par contre, le déclin en présence de la forme fermée est nettement plus rapide.

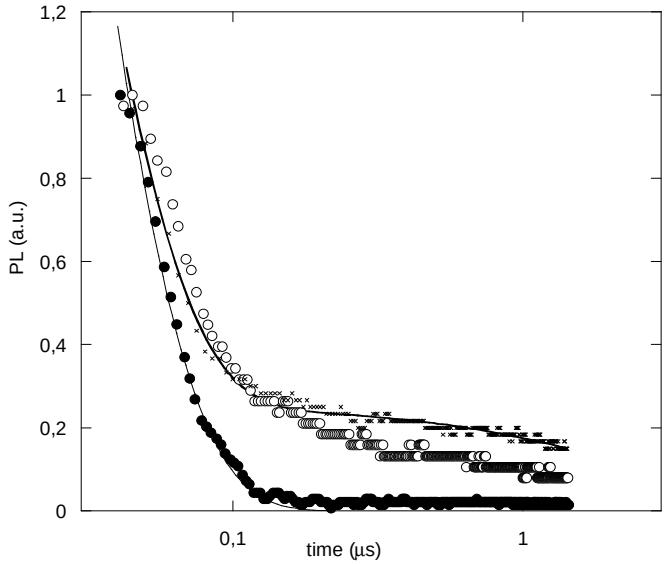

Figure (IV.11): les déclins de luminescence des solutions de ZnO (×) sans DTE; avec AH_2 (0.02eq) ouvert (o) et fermée BH_2 (●)(0.02eq). Excitation : 365 nm; Emission: 600 nm. L'ajustement des déclins de luminescence de ZnO tout seul et de ZnO+ AH_2 ont été réalisées par des fonctions bi exponentielles alors que pour le mélange ZnO+ BH_2, l'ajustement du déclin a été fait par une fonction mono exponentielle

IV.4.3.5 Détermination du type de quenching

Dans le cas des NPs émettrices, le processus de quenching est rendu plus complexe car une NP peut fixer à sa surface plusieurs molécules du quencheur tels que les colorants. On a vu dans l'exemple de Beane *et al* [137] un modèle basé sur la combinaison de l'adsorption de Langmuir et la quantité de colorants adsorbés sur la NP ([colorant]/ [NPs]) pour analyser les assemblages NPs-colorant. Ce modèle est bien adapté pour les NPs de ZnO dont la photoluminescence est liée à des défauts bien localisés. L'application de ce modèle à une expérience stationnaire est très simple et conduit, si le colorant a peu d'affinité avec la nanoparticule, à une variation linéaire de I_0/I dont la pente contiendra, le temps de vie de la NP, la constante de vitesse du quenching et la constante d'équilibre de l'adsorption. Ainsi un modèle fondé sur la même hypothèse que le quenching statique (chimisorption du colorant sur la nanoparticule) peut conduire à une représentation de Stern-Volmer linéaire tout en conservant un temps de vie apparent dépendant de la stœchiométrie de l'expérience.

IV.4.3.6 Mécanisme du piégeage

L'absence de recouvrement spectral entre les bandes d'absorption de AH_2 et d'émission de ZnO exclut la possibilité d'avoir un transfert d'énergie résonnant expliquant l'extinction de la luminescence des NPs de ZnO. De l'autre coté le ZnO est bien connu comme un photo oxydant très fort. Le couple redox de (ZnO^*/ZnO^-) peut être estimé relativement par rapport au couple redox E°(ZnO/ZnO^-) en utilisant la formule de Rehm Weller[146] simplifiée :

$E°(ZnO^*/ZnO^-) = E°(ZnO/ZnO^-) + E$

E est l'énergie du photon luminescent, et dans cette étude, *E*= 2.13 eV.

Hoyer *et al*[147] ont étudié les propriétés redox des films de ZnO dans l'eau par électrochimie et ils ont trouvé un potentiel de réduction apparent $E°(ZnO/ZnO^-) \approx -0,5$ V *vs* AgCl. Par conséquent, le potentiel d'oxydation $E°(ZnO^*/ZnO^-)$ est environ 1,7 V *vs* AgCl ou 1,6 V *vs* SCE. D'un autre côté, le couple redox de la première oxydation du diacide a été déterminé pour la forme ouverte ($E°(AH_2^+/AH_2)$ = 1.4V *vs* SCE) et la forme fermée ($E°(BH_2^+/BH_2)$ = 0.8V *vs* SCE) dans le chapitre II. Un quenching de l'état excité des NPs de ZnO est thermodynamiquement favorisé pour les deux formes. Ce genre de quenching nécessite un contact entre la NP et le colorant, ceci veut dire que seuls les colorants adsorbés à la surface peuvent être des quencheurs efficaces.

IV.4.4 Etude du système BH_2-NPs ZnO

Le photochrome est photolysé en solution dans le THF avant d'être mélangé au système ZnO-HDA : sa concentration correspond à l'état photostationnaire dans ce solvant seul.

IV.4.4.1 Possibilité d'un transfert d'énergie résonnant.

Le recouvrement spectral entre les bandes d'absorption de BH_2 et d'émission de ZnO **(figure (IV.12))** conduit au transfert d'énergie, FRET, qui peut avoir lieu du donneur (NPs ZnO) vers l'accepteur (BH_2).

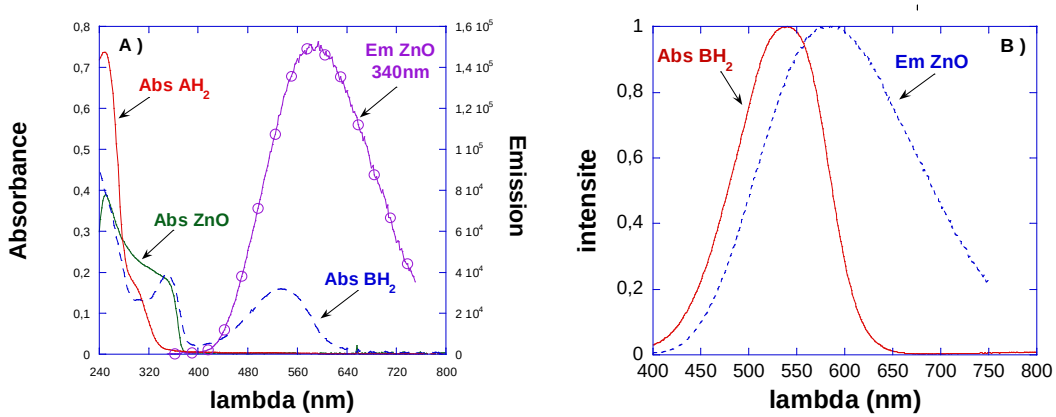

Figure (IV.12) : A) spectres d'absorption UV-vis des solutions dans le THF de AH_2 ($2*10^{-5}$ M) (rouge), de BH_2 (bleu), des NPs de ZnO stabilisées par des ligands HDA (0.52 mM) (vert), et spectre d'émission des NPs de ZnO après excitation à $\lambda = 340\ nm$ (mauve). B) le recouvrement spectral entre le spectre d'absorption de BH_2 et le spectre d'emission de ZnO

On a calculé le rayon r_{DA} séparant le donneur de l'accepteur en suivant la méthode de calcul utilisée par Makhal *et al* [134] (décrite plus haut). Les paramètres calculés sont regroupés dans le tableau suivant : (le temps de vie τ_{DA}est obtenu avec 0.0074 mM de BH_2 par rapport au [ZnO]=0.37 mM)

R_0	τ_{DA}	E	r_{DA}
30Å	$0.73\mu s$	70%	26Å

Ainsi le BH_2 est situé à 2.6 nm du centre émetteur localisé dans la NP de ZnO. Le rayon de la NP, supposée sphérique, vaut 3nm alors plusieurs possibilités peuvent être suggérées pour l'emplacement de BH_2, soit : adsorbé sur la NP ou adsorbé sur la couche de ligands HDA (longueur d'une molécule HDA vaut 2 nm).

IV.4.4.2 Analyses de Stern Volmer

Des analyses de Stern Volmer ont été réalisées pour étudier le quenching de la luminescence des NPs de ZnO par le BH_2. Pour cela on a préparé des mélanges de ZnO avec des quantités différentes de BH_2 et on a mesuré la variation de l'intensité d'émission des différents mélanges en fonction du rapport [BH_2] / [NP_ZnO], à 580 nm après une excitation à 340 nm.

Comme le BH_2 et le ZnO absorbent tous les deux à 340 nm **(figure (IV.12)A)**, il a fallu corriger les intensités d'émission des différents mélanges en utilisant la relation suivante:

$$\frac{I_{ZnO}}{I_{(ZnO+\mathrm{BH2})}} = \frac{quantité\ de\ lumière\ absorbée\ par\ ZnO\ \text{à}\ 340\ nm * I_{(ZnO+\mathrm{BH2})}}{I_{ZnO}}$$

$I_{(ZnO+\ BH2)}$ et $I_{(ZnO)}$ sont les intensités de fluorescence de ZnO observées en présence et en absence et du quencheur BH_2 respectivement

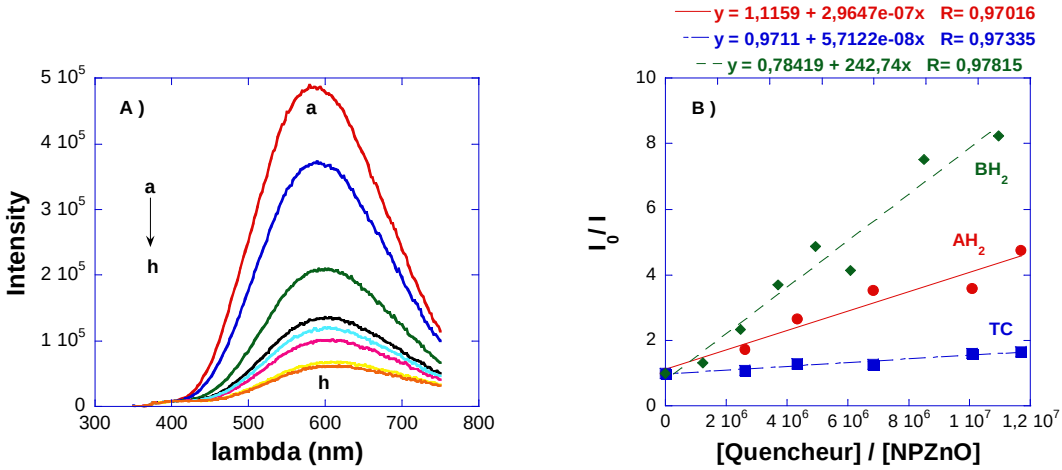

Figure (IV.13) : A) spectres d'émission des mélanges ZnO- BH_2 avec des concentrations de BH_2:(a) 0.0, (b) 3.54*10^{-7} M, (c) 7.07*10^{-7} M, (d)1.06*10^{-6} M, (e) 1.41*10^{-6} M, (f) 1.77*10^{-6} M, (g) 2.47*10^{-6} M, (h) 3.18*10^{-6} M. B) analyses de Stern Volmer pour les molécules AH_2, BH_2 et TC

Les variations de I_0 / I en fonction du rapport [Q]/[NP-ZnO] (**Figure (IV.13)B)** montre que BH_2 quenche plus que AH_2. Ceci est dû à la présence des processus redox [E°(ZnO*/ZnO$^-$)≈ 1,6 V vs SCE et (E°(BH_2^+/ BH_2) = 0.8V *vs* SCE)] et de transfert d'énergie entre le BH_2 et les NPs de ZnO (recouvrement spectral des bandes)

IV.4.5 Photo-modulation de l'émission et de l'absorption UV-visible

La spectroscopie UV-visible est utilisée pour suivre la conversion photo-induite de ZnO / HDA / AH_2 contenant l'isomère forme ouverte, vers son isomère forme fermée ZnO / HDA / BH_2 **Figure (IV.14)**. Ces modifications spectrales conduisent à la coloration de la solution, une fois l'état photo-stationnaire est atteint.

L'irradiation d'une solution de ZnO / HDA / AH_2 dans le THF avec la lumière UV ($\lambda = 313$ nm) conduit à la diminution dans les bandes d'absorption de haute énergie correspondants à l'isomère forme ouverte, et à l'apparition d'une bande d'absorption dans le visible correspondant à l'isomère forme fermée BH_2 ($\lambda_{max} = 526\ nm$).

L'irradiation de la solution colorée ZnO / HDA / BH_2 contenant l'isomère forme fermée avec de la lumière visible ($\lambda = 546$ nm) régénère la solution initiale incolore et le spectre correspondant à la forme ouverte AH_2.

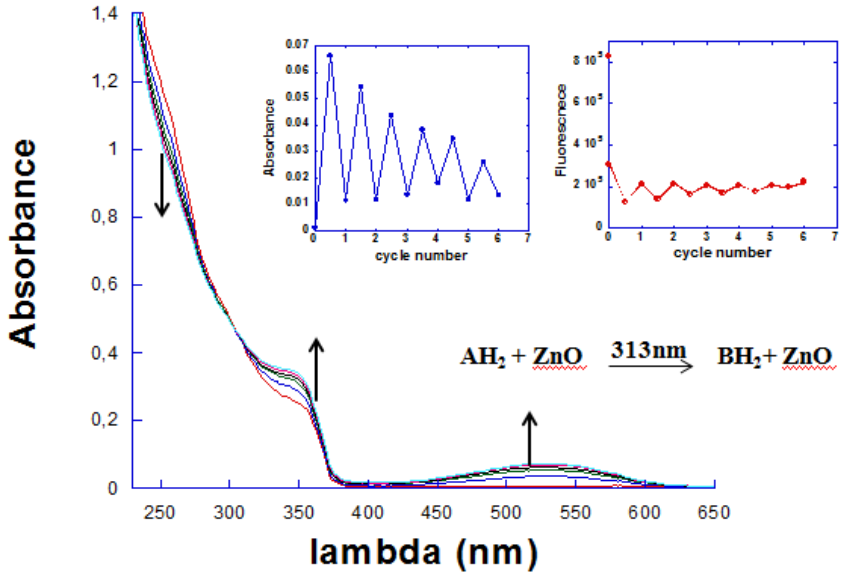

Figure (IV.13): changements dans les spectres UV-visible d'une solution de THF de ZnO + AH_2 ([ZnO]=0.80mM, [AH_2]=2.11 e-5 M (0.026eq de AH_2 par rapport au ZnO)) quand elle est irradiée à 313nm durant 0, 120, 240, 360, 480 and 600 s. encarts à gauche montre la modulation de l'absorption à 524 nm, correspondant à l'absorbance de la forme fermée (BH_2) durant des irradiations alternatives à 313 nm et à 546 nm (1200s). Encarts à droite montre la modulation de l'émission à 580 nm durant les irradiations alternatives à 313 nm (600s) et à 546 nm (1200s)

L'addition de l'isomère forme ouverte AH_2 à une solution de ZnO / HDA conduit à une diminution de l'intensité de fluorescence à 580 nm (encarts à droite **Figure (IV.13)** après une excitation à 340 nm. La conversion de la forme ouverte AH_2 présente dans cette solution en sa forme fermée par une irradiation lumineuse à 313 nm conduit une diminution beaucoup plus grande dans l'intensité de fluorescence de ZnO. Nous avons découvert que la fluorescence d'origine ne peut pas être régénérée lorsque la solution de ZnO / HDA / BH_2 est irradiée avec de la lumière visible à $\lambda = 546$ nm. L'interconversion du composé DTE entre

ses isomères ouvert et fermé, par une alternance de la lumière UV et visible, conduit à l'extinction totale de la luminescence du ZnO.

IV.5 Conclusion

Le diacide DTE(COOH)$_2$ affecte donc l'émission des nanoparticules de ZnO obtenues par voie organométallique. Cependant les deux isomères se révèlent très efficaces dans ce processus. L'utilisation d'une molécule modèle a permis de montrer que le quenching ne provient ni des fonctions COOH ni de la présence du soufre hétérocyclique, enfin des deux isomères, le cyclisé BH_2 est le plus efficace. Les études de RMN ont montré que le colorant sous sa forme ouverte semble fortement associé à l'hexadécylamine en excès dans la solution et qu'il interagit faiblement avec la nanoparticule. Les études photophysiques stationnaires permettent de comparer quantitativement les efficacités des deux photoisomères mais sont insuffisantes pour trancher entre un modèle statique, où le colorant est fixé à la nanoparticule, ou un modèle dynamique, par collision. Les études dynamiques montrent par ailleurs que le temps de vie apparent est affecté par la présence du DTE(COOH)$_2$ ouvert mais un modèle statistique simple permet de montrer que ceci n'est pas incompatible avec un colorant faiblement adsorbé. Deux hypothèses ont été proposées pour le mécanisme de piégeage. Un transfert résonant d'énergie : les propriétés spectroscopiques de la forme colorée du DTE(COOH)$_2$ permettent d'envisager un mécanisme de RET efficace dans une approche de type Forster. Cependant ce type de piégeage n'explique pas l'efficacité remarquable du DTE ouvert. L'autre hypothèse est un processus redox : une comparaison des couples redox des deux photoisomères avec ceux du ZnO* montre que, quel que soit l'état AH_2 ou BH_2 du photochrome, une photo-oxydation du produit organique est possible (et peut se superposer au RET dans le cas de l'isomère BH_2). Enfin, le diacide DTE(COOH)$_2$ a été utilisé comme un photo-modulateur de luminescence des nanoparticules de ZnO, l'état « ON » luminescent correspondant à la forme AH_2. Malheureusement la luminescence disparaît rapidement au cours des cycles successifs de coloration/décoloration. Là encore les propriétés redox de l'oxyde de zinc peuvent interpréter cette évolution : une photo dégradation du DTE en accord avec les propriétés photo-dépolluantes de ce matériau est en effet tout à fait envisageable.

General conclusion

General conclusion

Photochromism is the reversible light-induced transformation of a chemical species between two isomers forms X and Y that have different absorption spectra. It is simply described as a reversible change of color upon exposure to light. This difference in optical properties is always accompanied by an alteration in other physical and chemical properties in the concerned photochromic compound.

The combination of photochromism and chemical reactivity gives rise to a system where light controls reactivity and chemical reactivity controls photochromism. In this case chemical events can be used to regulate the photochromic behavior of the dye, and on the other side the photochromic dye can be used to reversibly turn chemical reactions on or off. Therefore the photochromic dye can act as a sensor or an actuator and its interaction with defined chemical systems leads to two applications: *photomodulation* and *gated photochromism.*

Photomodulation refers to the light-induced difference in the physico-chemical properties between the two photochromic isomers while *gated photochromism* corresponds to a special form of photochromism in which one or both forms of a photochromic system are chemically and reversibly transformed into a non-photochromic form. Among the various photochromic compounds that have been submitted to *gated photochromism* and *photomodulation* studies, dithienylethenes (DTE) exhibit some advantageous photochromic properties, such as thermal irreversibility and fatigue resistance.

The aim of this thesis was the study of photo-modulations and gated photochromism behaviors of a mini-sized diacid dithienylethene derivative, DTE $(COOH)_2$, in different guest systems. In chapter II, a quantitative study of the acidity photo-modulation and gated photochromism of DTE$(COOH)_2$ was carried out in presence of various amount of a base, tetrabutylammonium hydroxide, in acetonitrile/water mixtures. Photoisomerisation between the open and closed isomers was investigated by UV/visible and ^{1}H NMR spectroscopy. Chemical dynamic modelling methodology was used to establish the main photochromic, spectral and thermodynamic parameters of the base sensitive diacid. It was found that the photocyclisation quantum yield of the diacid form was remarkably high, around 90%. Partial neutralisation of the open isomer revealed a gated photochromism as the photocyclisation quantum yield of the mono and dianion were 50% and 67% respectively. Photomodulation of

the acidity results to a more than one pK_a unit difference between the open and closed forms which appears more acidic.

In chapter III, the photomodulation of the redox properties of the diacid DTE $(COOH)_2$ was exploited in the thermal bleaching of the colored isomer by the chemical oxidizing agent $Cu(OTf)_2$ whose redox couple lies between those of the closed and opened form. The chemical ring opening reaction of the diacid closed isomer into its ring opened isomer was investigated by UV visible spectroscopy either at very fast time scale (stopped flow) and compared to electrochemical bleaching. The main feature is the presence of an intermediate absorbing at low energy that does not exists in the coulometric titration. The experiments was realized with different configuration: bleaching of a preformed PSS mixture upon addition of copper(II) salt or photocoloration delayed by the copper species. Kinetic traces analysis was started using the chemical dynamics methodology and is still under investigation. However the role of species not figuring in the reaction balance such as transient concentration of proton, complexation with copper via the carboxylate or dye reaction with the solvent has been pointed out: it was found out that the addition of little amounts of base or acid can alter the overall bleaching rate respectively by inhibiting or accelerating the processes.

In chapter IV, we studied the association between the diacid DTE$(COOH)_2$ and the fluorescent counter-ion free ZnO nanoparticles(NPs) which are stabilized by hexadecylamine (HDA) ligands. The interaction between NPs and the diacid was investigated by UV/visible and ^1H NMR spectroscopy. NMR studies have shown that the dye in its open form is strongly associated with hexadecylamine, and interacts weakly with the nanoparticle. From emission spectroscopy measurements, we found out that both diacid photoisomers reduce the emission of ZnO nanoparticles. The closed isomer was the most efficient quencher of the two photo isomers. The use of a model molecule showed that the quenching does not originate from COOH functions or the presence of heterocyclic sulfur in the dye moiety. Two processes have been proposed for the quenching mechanism: Resonant Energy Transfer (RET) and Electron Transfer (ET) processes. Finally, the diacid was used to switch ON and OFF the luminescence of ZnO nanoparticles. Unfortunately, the luminescence disappears rapidly during successive cycles of coloration / discoloration.

Experimental section

I. Materials

All synthetic grade commercial reagents were used as received. Tetrahydrofuran (THF) was dried with Na/benzophenone ketyl. CH_2Cl_2 was dried with H_2Ca. All reactions were carried out under argon using the Schlenk tube technique, and the handling of the compounds sensitive to UV light was carried out in the dark.

II. Experimental procedures and instrumentation

II.1 Nuclear magnetic resonance spectroscopy:

^1H NMR spectra at various temperatures were recorded on a Bruker 500 spectrometer (^1H, 500 MHz) equipped with TXI probe and variable temperature unit at university "*Lille Nord de France*" and data sets were processed using Bruker Topspin 2.1 software and chemical shifts were reported in ppm relative to TMS or referenced to the residual non deuterated solvent.

II.2 UV-VIS spectrophotometry:

Absorption spectra were recorded on a HP 8451 diode array spectrophotometer. HPLC or spectroscopy quality solvents were used. All solutions were prepared by weighting to avoid error of volumetric devices so the protocol consist to weight cuvette with solution during time to control changes (evaporation..)

II.3 Photoisomerization experiments:

The photochromic solution (2.5 mL) was stirred with a magnetic bar in a 1cm×1cm quartz cell closed with a Teflon stopper fitted with the tip of an optical irradiation fibre. The optical path of the vertical irradiation was 2.5cm. The irradiation UV light was derived from a 200W high-pressure mercury lamp equipped with interference filters. To avoid unwanted photodegradation, irradiation was discontinued when a photo-steady-state was reached. The monochromatic light intensity was determined directly in the reactor using an acidified aqueous solution of potassium ferrioxalate. Before and after each experiment, the stability of the photon flux was checked by a home-made semiconductor photosensor: $I_0^{313} = 1.2x10^{-6}$ $mol.L^{-1}.s^{-1}$; $I_0^{365} = 3.2x10^{-6}$ $mol.L^{-1}.s^{-1}$.

II.4 Modeling :

The data from neutralisation and photochromism measurements were stored and processed on a desk PC computer using homemade software (Sa3) in order to obtain experimental $Abs_{exp}(\lambda)$

vs base added for neutralisation or $Abs_{exp}(\lambda)$ *vs* time for photochromic quantum yields determinations The minimization algorithm is of the Powell type. The required parameters are determined by minimizing the quadratic residual error RE ($RE = \frac{\sum p \sum j \left[Abs_{calc_{(j)}} - Abs_{exp_{(j)}}\right]^2}{pj}$)

, where *p* is the number of fitted plots simultaneously and *j* is the number of points in each plot. The set of optimized parameters was checked to be unique.

II.5 Fluorometry:

photoluminescent measurements were performed using a spectrofluorometer PTI (Photon Technology International) equipped with a 175 watts Xenon lamp EIMAC. All the spectra are automatically corrected from the apparatus response. Quartz cells (1 cm opticalpathlength). The spectral resolution of the slits is 2 nm

II.6 Stopped flow:

the Stopped-flow kinetics runs were carried out at "*Laboratoire de Chimie de Coordination, Toulouse"* at 5°C with a Bio-Logic SF20 apparatus coupled to a BioLogic PMS-250 photomultiplier detector, using a cuvette with 0.15 cm pathlength. The data were collected within the first 10 s, yielding reproductible results. Data analyses were carried out by using the home made software Sa3.

II.7 Cyclic voltammetry:

Cyclic voltammetry experiments were performed at "*Universitat Autònoma de Barcelona" at* scan rates ranging from 0.1 to 1000 V/s. The derived standard and peak potentials were electronically corrected (positive feedback) for ohmic drop. A computer controlled VersatileModular potentiostat was used for scan rates up to20 V/s. A homemade, solid-state amplifier potentiostat with positive feedback iR drop compensation and a Tacussel GSTP 4 function generator were used for the high scan rate measurements. Voltammograms were recorded on a digital oscilloscope. All experiments were conducted with a standard three-electrode setup in a conical electrochemical cell encased in a jacket that allowed the temperature to becontrolled at 20ºC by means of a thermostated circulating bath. The working electrode was a glassy carbon disk (0.5 mm diameter) that waspolished using a 1 μm diamond paste. The counter electrode was a glassy carbon disk (0.3 cm diameter). All potentials are recorded vs a SCE electrode that was isolated from the working electrode compartment by a

salt bridge with a ceramic frit that allowed ionic conduction between the two solutions while avoiding appreciable contamination.

II.8 Nanosecond time resolved luminescence experiments:

These were carried out using a laser flash photolysis apparatus. Excitation pulses (365 nm, fwhm 7 ns, 1 mJ, 0.5 Hz) were provided by a 10-Hz Nd:YAG laser (Continuum Surelite II) coupled to an OPO (Continuum Panther EX OPO) and shutter controlled by an NInstrument card. Samples were contained in a quartz cell (10×10 mm^2 section) at an adjusted concentration ($\sim 10^{-4}$ $mol.dm^{-3}$) to get an absorption value of about 1 at the pump excitation wavelength. The emitted light was dispersed by a monochromator (Horiba Jobin-Yvon, iHR320, 5 nm resolution) and analyzed with a photomultiplier (R1477-06, Hamamatsu) coupled to a digital oscilloscope (LeCroy 454, 500 MHz). The experiment was average for different pulses and repeated for different wavelengths of the monochromator (controlled by labview home built software). The deconvolution of the individual decays with experimentally measured instrument response function (IRF) lead to 4 ns time resolution. Single wavelengths as well as global analyses of the luminescent data were performed using IgorPro6.2.

III. SYNTHETIC PROCEDURES FOR COMPOUNDS

III.1 Synthesis of 2-Chloro-5-methylthiophene (1)

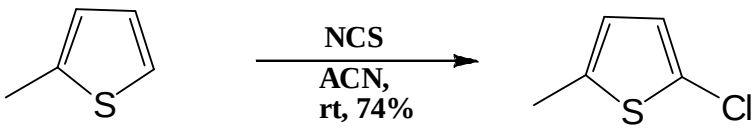

N-chlorosuccinimide (6.81g, 51mmol) was added slowly to a stirred solution of 2-Methylthiophene (5 mL, 51 mmol) in acetonitrile. The suspension was stirred for 60 min at room temperature. Then 100mL water was added to the reaction mixture and the water layer was extracted with pentane (3*50mL). The combined organic phases were washed with water (100 mL), dried ($MgSO_4$), filtered and the solvent evaporated in vacuo to yield a slightly yellow liquid (6.76 g, 74%) enough pure to use in further reactions.

^{1}HNMR (300 MHz, $CDCl_3$): δ=2.30 (s, 3 H), 6.40-6.42 (m, 1 H), 6.58 (d, J= 2.2 Hz, 1 H) ppm.

III.2 Synthesis of 1,5-Bis(5-chloro-2-methylthien-3-yl)pentane-1,5-dione (2)

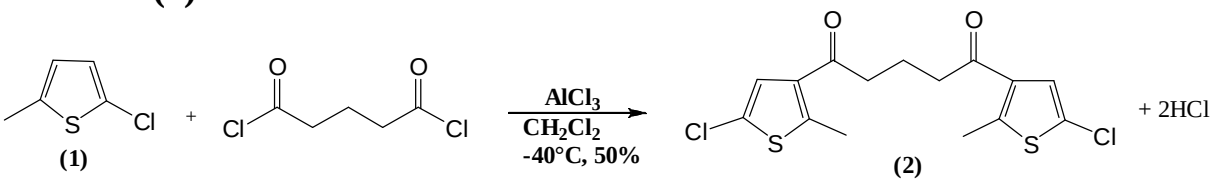

Under N2 and with vigorous stirring, glutaryl dichloride (3.5 g, 21 mmol) was added dropwise to a cooled solution at -40 °C of **1** (5.66 mL, 43 mmol) and $AlCl_3$ (5.4 g, 41 mmol) in dry CH_2Cl_2 (25 mL). After addition of glutaryl dichloride, the reaction mixture was stirred for 2 h at -40 °C. Then ice-cold water (100 mL) was carefully added to the reaction mixture and the water layer was extracted with diethyl ether (3*50mL).The combined organic phases were washed with water (100 mL), dried ($MgSO_4$), filtered and the solvent was evaporated in vacuo to yield a blue green solid which was suspended in ethanol. Filtration and washing with ethanol yielded **2** (3.8g, 50%)

^{1}H NMR (300 MHz, $CDCl_3$): δ = 1.98-2.12 (m, 2 H), 2.66 (s, 6 H), 2.86 (t, *J* = 6.8 Hz, 2 H), 7.19 (s, 2 H) ppm.

III.3 Synthesis of 1,2-Bis(5-chloro-2-methylthien-3-yl) cyclopentene (3)

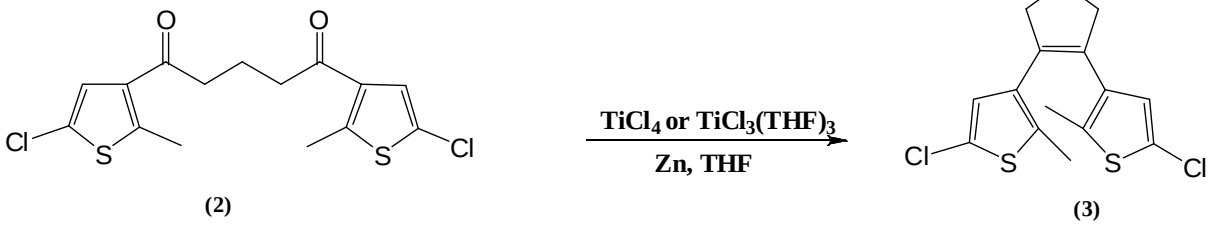

III.3.1 Method I "Instant method":

A mixture of **2** (5.35 g, 0.0153 mol), $TiCl_3(THF)_3$ (10.5 g, 0.028 mol), Zn dust (2.37 g, 0.036 mol) and THF (45 mL) was stirred under nitrogen at reflux40 °C for 1 h. The mixture was cooled to room temperature and poured through a glass filter containing silica gel that was pretreated with petroleum ether. The silica was rinsed with petroleum ether. After evaporation of the solvent, a yellow solid (4.73 g, 96%) remained. Pure **3** was obtained as a white solid (2.37 g, 48%) after purification by chromatography on silica gel (petroleum ether).

III.3.2 Method II

$TiCl_4$ (3mL, 0.027mol) was carefully added with a syringe to an ice-cooled solution of Zinc dust (4g, 0.061mol) in dry THF (100mL). The suspension was stirred at reflux for 30 min. The mixture was allowed to cool at room temperature and a solution of **3** (10g, 0.027mol) in THF (30 mL) was added dropwise over 2h, followed by stirring at reflux overnight. The mixture was cooled to room temperature and poured through a glass filter containing silica gel that was pretreated with petroleum ether. The silica was rinsed with petroleum ether. After evaporation of the solvent, a yellow solid remained. Pure **3** was obtained as a white solid (5.6 g, 63%) after purification by chromatography on silica gel (petroleum ether).

^{1}H NMR (300 MHz, $CDCl_3$) δ : 1.98 (s, 6 H),1.94-2.09 (m, 2 H), 2.71 (t, *J* = 7.5 Hz, 4 H), 6.58 (s, 2 H) ppm

III.4 Synthesis of 1,2-Bis(5'-carboxy-2'-methylthien-3'-yl)-cyclopentene (4)

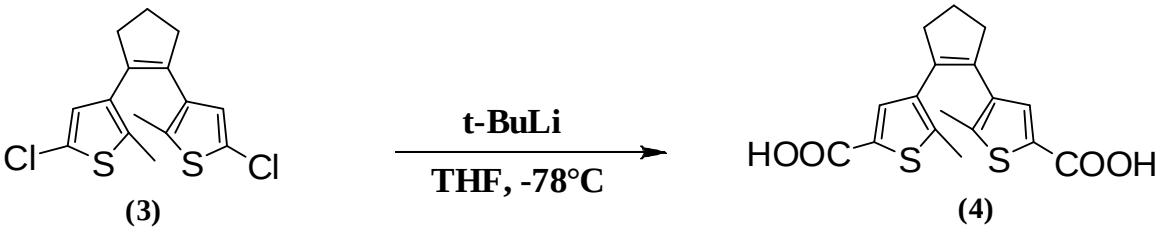

(3) **(4)**

To a solution of **3** (410 mg, 1.25 mmol) in dry THF (20 mL) cooled to -78°C was added tert-butyllithium (3 mL of a 1.7 M solution in pentane) slowly under argon with syringe. After 1 h few portions of carboglace were added to the reaction mixture then the reaction was allowed to warm to room temperature and stirred for a further 30 min. The THF was removed under vacuum, and the residue was partitioned in 100 mL of diethyl ether and washed twice with 125 mL of Na_2CO_3 solution. The combined aqueous layers were acidified by dropwise addition of concentrated HCl until pH=1. The resulting white precipitate was collected by vacuum filtration, triturated with cold CH_2Cl_2 (3 * 5 mL) to remove the monoacid, then dried in vacuo affording the pure diacid as a white solid (0.388 g, 90%).

^{1}H NMR (300 MHz, CD_3OD) δ: 7.57 (s, 2H), 2.92 (t, *J*=7.50 Hz, 4H), 2.19 (m, 2H), 2.05 (s, 6H)

Supporting information

Chapter II

I. Photochemical Kinetics

The simplest reaction that one can meet in photochemistry:

$$\mathbf{A} \xrightarrow{h\nu} \mathbf{B}$$

This writing means that a photosensitive reactant A under irradiation is transformed into a product B by the absorption of a photon. However, any photochemical reaction involves an excited state A^*, due to the absorption of a photon. The state A^* can either return to its original shape or react to form B. It is assumed that product B also absorbs the light but it doesn't give rise to any transformation. Under these conditions, the overall reaction can be decomposed at least three elementary steps:

$\mathbf{A} \xrightarrow{h\nu} \mathbf{A^*}$	(I_a^A)	activation
$\mathbf{A^*} \longrightarrow \mathbf{A}$	(k_d)	deactivation
$\mathbf{A^*} \longrightarrow \mathbf{B}$	(k_r)	reaction

The state A^* includes all possible excited states of A (singlet state, triplet state, etc…). The first process is an activation step i.e. all the photons absorbed by A to give the excited state A^*. The rate of this step is equal to the intensity I_a^A of the absorbed light by A (formula2). The excited state A^* then undergoes two competitive processes of extinction: a radiative or nonradiative deactivation and a reaction leading to the formation of product B

The equation of evolution of the excited state A^* is given by:

$$\frac{d[A^*]}{dt} = I_a^A - (k_d + k_r)[A^*] \qquad \textbf{(1)}$$

In photochemical dynamic, I_a^A has the dimension of a chemical rate $(molL^{-1}.s^{-1})$

1) A steady state*

Under low power continuous irradiation, the concentration $[A^*]$ of the excited species $[A^*]$ which has a short lifetime (10^{-10} of a 10^{-8}s) remains very low with negligible variation. So, we can write:

$$\frac{d[A^*]}{dt} = 0 \text{ (It is not an approximation order as PSS) } \textbf{(2)}$$

Thus:

$$[A^*] = \frac{I_a^A}{(k_d + k_r)} \quad \textbf{(3)}$$

2) Formation rate of B

Knowing the expression of the concentration $[A^*]$ of the excited species A^*, we can write the formation rate B as the following:

$$\frac{d[B]}{dt} = k_r[A^*] = k_r \frac{I_a^A}{(k_d + k_r)} \quad \textbf{(4)}$$

The quantum yield Φ_{AB} can be defined as the ratio between the rate of the considered process and the intensity of absorbed light. For this reaction, we have:

$$\Phi_{AB} = I_a^A(\frac{d[B]}{dt}) \quad \textbf{(5)}$$

Where $\frac{d[B]}{dt}$ is the formation rate of B.

Taking into account formula (4), the quantum yield Φ_{AB} of the overall process can also be written as:

$$\Phi_{AB} = \frac{k_r}{(k_d + k_r)} \quad \textbf{(6)}$$

Thus, the quantum yield Φ_{AB} represents the ratio between the rate constant for the formation of B and the sum of the rate constants of all processes of deactivation of A^*

3) Conservation of matter

Envisaged for the reaction, we can write the equation of mass balance:

$$[A^*]+[A]+[B]=[A]_0 \quad \textbf{(7)}$$

where $[A]_0$ is the initial concentration of $[A]$. So, the relation between the derivatives is written as:

$$\frac{d[A^*]}{dt}+\frac{d[A]}{dt}+\frac{d[B]}{dt}=0 \quad \textbf{(8)}$$

Using formula (3) and that $\frac{d[A^*]}{dt}=0$, another relationship is extracted between $\frac{d[A]}{dt}$ and $\frac{d[B]}{dt}$

$$\frac{d[A]}{dt}=-\frac{d[B]}{dt} \quad \textbf{(9)}$$

4) The photochemical rate equation

The above relations allow writing the equation of the photochemical rate reaction:

$$\frac{d[A]}{dt}=-\frac{d[B]}{dt}=-\Phi_{AB}I_a^A \qquad \textbf{(10)}$$

Using the expression given previously for I_a^A , we can write:

$$\frac{d[A]}{dt}=-\Phi_{AB}I_a^A=-\Phi_{AB}\frac{I_0(1-10^{Abs_T})\varepsilon_A[A]l}{Abs_T} \qquad \textbf{(11)}$$

Thus, the general expression or the photochemical rate law for the consumption of the photoactive species A in a photochemical reaction under monochromatic irradiation in well stirred fluid solution is given by:

$$\frac{d[A]}{dt}=-\Phi_{AB}I_0\varepsilon_A[A]lF \qquad \textbf{(12)}$$

Where F is the photokinetic factor (F=(1- 10^{-Abs_T})/Abs_T). In this expression, the term $k'=\Phi_{AB}I_0\varepsilon_A l$ represents an apparent rate constant in s^{-1} and combines only parameters related to the reaction (it is time independent). it is a function only of the total absorbance at the wavelength of radiation: it varies over time if the total absorbance varies i.e. if the absorption of A is different from the absorption of B. It appears that:

$$\frac{d[A]}{dt}=-k'[A]F \quad \textbf{(13)}$$

Given the time-dependence of the photokinetic factor F, the differential equation (12) cannot be analytically integrated[148], due to the presence of the dependent variable $[A]$ as an

exponent in the photokinetic factor F. In such a situation, it is impossible to separate the variables and thus, equation (12) must be handled numerically.

II. Spectrokinetic study of DTE compounds

Dithienylethenes are among the most well-known photochromic compounds that are transformed in both directions by absorption of electromagnetic radiation.The absence of back-thermal reaction is the main advantage of such compounds for their potential use in optical data storage applications[149].

For the purpose of kinetic analysis, these systems can be modeled by two reversible photochemical reactions:

$$\mathbf{A} \underset{h\nu}{\overset{h\nu}{\rightleftharpoons}} \mathbf{B}$$

If the two isomers can be isolated, the determination is easy, because the conversion rate at the photo steady state can be reached from absorbance measurements. But if only one or none isomers can be isolated the situation is much more complicated.

Two classical approaches have been described in the literature:

1) Fisher[150] method applies when one isomer has been isolated and needs the recording of two PSS after irradiation at two different wavelengths.
2) Wyman[151] method works even, if none of the two isomers can be isolated, but needs three irradiation wavelengths.

Pimienta and al have shown[152] that kinetic analysis of Abs Vs. time curves recorded under continuous monochromatic irradiation at two selected wavelengths (λ' and λ'') is able to determine the required photochromic parameters, namely Φ_{AB} , Φ_{BA}, ε'_A, ε'_B , ε''_A, ε''_B even if neither A nor B have been isolated and if the ratio $[A]/[B]$ is not known accurately.

Under monochromatic continuous irradiation and assuming that the reacting solution is homogenous, the evolution equation of the overall system can be written from a single variable such as A:

$$\frac{d[A]}{dt} = -(\Phi_{AB}\varepsilon_A[A] - \Phi_{BA}\varepsilon_B[B])FI_0 l \qquad \textbf{(14)}$$

If the photochromism is monitored by UV/visible spectroscopy, Beer's law is also applied at any wavelength including the irradiation wavelengths:

$$Abs=AbsA+AbsB=[A]+\varepsilon\ Abs\ =\ Abs_{A}\ +\ Abs_{B}\ =(\varepsilon_{A}[A]+\varepsilon_{B}[B])l \qquad \textbf{(15)}$$

In these systems, the two species A and B obey to the mass balance equation:

$$[A]+[B]=[A]_0 \ \textbf{(16)}$$

Using equations (14) and (15), the photochromic parameters can be extracted from the kinetic analysis of the plots of absorbance *vs* time under continuous irradiation. For the calculation of the parameters, starting values are estimated, the differential equation (14) is numerically integrated and the Beer-lambert law is applied to obtain simulated curves of Abs *vs* t.
The comparison of the simulated curves with the experimental ones gives a residual error which is the sum of squares of the differences between the calculated and experimental values. Then the numerical values of the parameters are optimized in an iterative procedure designed to minimize this residual error.

From a single kinetic run monitored at λ' experimental data are obtained by measuring:

1) ***The initial absorbance:***

$$Abs^{\lambda'}(0)=(\varepsilon_{A}^{\lambda'}-\varepsilon_{B}^{\lambda'})[A]+\varepsilon_{B}^{\lambda'}[A]_0 \qquad \textbf{(17)}$$

2) ***The photosteady state PSS absorbance:***

$$\frac{Abs_{PSS}^{\lambda'}}{[A]_0}=\frac{\varepsilon_{A}^{\lambda'}\varepsilon_{B}^{\lambda'}(\Phi_{AB}+\Phi_{BA})}{\varepsilon_{A}^{\lambda'}\Phi_{AB}+\varepsilon_{B}^{\lambda'}\Phi_{BA}} \qquad \textbf{(18)}$$

3) ***The photokinetic slope (current slope):***

$$\frac{d_{Abs^{\lambda'}(t)}/dt}{[Abs_{PSS}^{\lambda'}-Abs^{\lambda'}(t)]F^{\lambda'}I_{t=0}^{\lambda'}}=\varepsilon_{A}^{\lambda'}\Phi_{AB}+\varepsilon_{B}^{\lambda'}\Phi_{BA} \qquad \textbf{(19)}$$

Equation (14) shows that the estimated evolution rate of absorbance $d_{Abs^{\lambda'}(t)}/dt$ and the photosteady absorbance $Abs_{PSS}^{\lambda'}$ can be used to calculate "apparent rate coefficient":

$$[\varepsilon_{A}^{\lambda'}\Phi_{AB}+\varepsilon_{B}^{\lambda'}\Phi_{BA}]F^{\lambda'}I_{t=0}^{\lambda'} \qquad \textbf{(20)}$$

In this expression:

$\varepsilon_A^{\lambda'}$ is measured from the spectrum of the starting compound A

$I_{t=0}^{\lambda'}$ is obtained by actinometry

F depends on the absorbance at the irradiation wavelength and on $\varepsilon_B^{\lambda'}$: the change in $Abs^{\lambda'}$ gives a value for F at any instant

To obtain enough information to extract all the parameters, we should have the change in absorbance under continuous irradiation at the irradiation wavelength which enable the calculation of F and at $\lambda_{\max}$ of B. Also we have to record the initial spectrum of A and the complete spectrum of the reaction mixture at time t near the final irradiation time to calculate later the spectrum of B (ε_B vs λ) by using Beer-Lambert law.

Actually the "apparent rate coefficient" has three parameters: $\varepsilon_B^{\lambda'}, \Phi_{AB}, \Phi_{BA}$ to determine and in this case, two sets of measurements are required at two irradiation wavelengths (λ' and λ'') which must be chosen such that the molar absorption coefficient ratios would be different: , ($\varepsilon_A^{'}/\varepsilon_B^{'}$ different f $\varepsilon_A^{''}/\varepsilon_B^{''}$) in the direct and reverse photochemical process. The best conditions are if the two wavelengths are located on the both side of an isosbestic point. The simultaneous application of the simulation and adjustment method on these evolution curves allow determining the values of the photochromism parameters.

UV/Vis spectrum of B

Once the values of ε_B are determined at the two irradiation wavelengths, the absorption spectrum of pure B can be found from the mixture spectra using Beer-Lambert law:

$$Abs_T = Abs_A + Abs_B = (\varepsilon_A.[A] + \varepsilon_B.[B])l \qquad \textbf{(21)} \text{ (with l=1cm)}$$

$$\varepsilon_B^{\lambda'} = \frac{Abs_T^{\lambda'} - \varepsilon_A^{\lambda'}.[A]}{[B]} \qquad \textbf{(21)}$$

By using the mass balance equation, $[A]+[B]=[A]_0$, equation (21) will be written: :

$$\varepsilon_B^{\lambda'} = \frac{Abs_T^{\lambda'} - \varepsilon_A^{\lambda'}.([A]_0 - [B])}{[B]} \qquad \textbf{(22)}$$

In this expression:

$[A]_0$: the initial concentration is known

$[B]$: is calculated from the PSS absorption which is measured at λ_{obsB} (the observation wavelength of B : it is a wavelength where A cannot absorb) and by using the value of ε_B at λ_{obsB} whose value is obtained after adjustment

$$[B] = \frac{Abs_{PSS}}{\varepsilon_B} \qquad \textbf{(23)}$$

Once $[B]$ is calculated, it is possible to calculate ε_B^{λ} at all the wavelengths using formula (22)

III. NMR and thermodynamic parameters determinations from T variable spectral shifts

Fitting of equation $\delta = \frac{\delta_1 - \delta_2}{K+1} + \delta_2 = \frac{\delta_1 - \delta_2}{1 + \exp(\frac{-\Delta G^0}{RT})} + \delta_2$ has been performed on data from **Figure (2.1)** with three adjustable parameters (2 chemical shifts (δ_1 and δ_2) and ΔG^0)

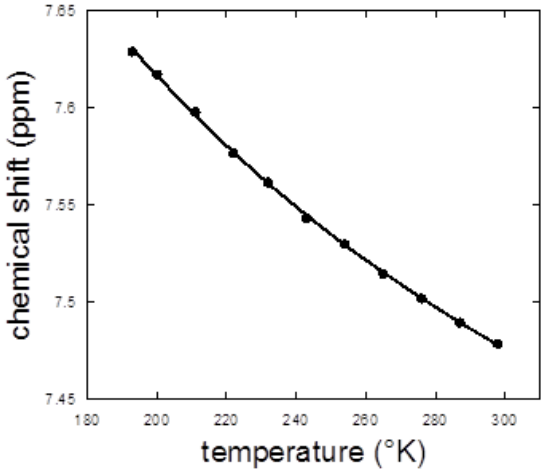

Figure (2.1): decrease of the chemical shifts the thiophenic proton Ht on the diacid DTE 1 with temperature. Fitting of the variation of the chemical shift of the thiophenic proton Ht allows the estimation of the $\Delta G^0 / R$ parameter at about 280 ± 80 °K^{-1} with δ_1 = 7.8 and δ_2 = 6.3 ppm. Note the increase of the shielded parallel conformation with temperature. K ≈ 0.4 ± 0.1 at 300°K *i.e.* α ≈ 80 ± 5 % of the anti-parallel conformer. Such a value is not incompatible with our quantum yield results.

The principle of this equation is the presence of an A ← → B like equilibrium with two distinct NMR spectra 1 and 2. The observed spectrum is a weighted average between 1 and 2. Their relative ratio is related to the equilibrium constant K.

The relationship between K and T is given by the Gibbs law: $\Delta G^0 = -RT\ln(K)$

Then,

$$\delta = \frac{\delta_1}{K+1} + \frac{\delta_2 k}{k+1} = \frac{\delta_1 - \delta_2}{k+1} + \delta_2 \qquad \textbf{(24)}$$

$$`\delta = \frac{\delta_1 - \delta_2}{1 + \exp(\frac{-\Delta G^0}{RT})} + \delta_2 \qquad \textbf{(25)}$$

This is a 3 parameters equation. Therefore it can only be applied if the experimental data display a significant curvature. A straight line being defined by only two parameters, if the data points are too “linear” some co-variance between the three parameters will be witnessed. It is then necessary to vary sufficiently the constraints (here the temperature range) and to select carefully the proton probes in order they give rise to the most pronounced curvature.

III.1 The fitting model:

```
// -----NMR_temp_var.cpp
//
#include        "global.h"
//---------------------------------------------------------------------------
void Identification(Modele& modele)
{
modele.Fichier = String(__FILE__);
modele.Version = String(__DATE__) + String("  ") + String(__TIME__);
modele.Auteur = "DL";
nom_syst = "NMR_temp_var";
n_diff = 0;
first_var = 0;
```

```
nv_mod = 1;                // nombre de variables du modèle
nexp = 1;                  // nombre d'expériences
}
//---------------------------------------------------------------------------
void eqdiff (Sa_data x, Sa_data* y, Sa_data* dy)
{
}
//---------------------------------------------------------------------------
void fappel()
{
for (int i = 0; i < npt; ++i)        // boucle sur le nombre de points (npt)
{
ca[0][i] = (p[0] - p[1])/(1 + exp(-p[2]/ind[i])) + p[1];          // T = ind[i]

}
}
//---------------------------------------------------------------------------
```

Experimental data:

Temprature (°K)	δ (ppm)
193	7,6287
200	7,6169
211	7,5978
222	7,5766
232	7,5615
243	7,5431
254	7,5298
265	7,5146
276	7,5019
287	7,4894
298	7,4785

III.2 Analysis of the various fitting tests.

Two approaches have been carried-out: a) the three parameters are adjustable; b) $\Delta G^0/R$ is fixed at a given value and the deltas are floating. After each optimization, the residual error is plotted versus the $\Delta G^0/R$ value.

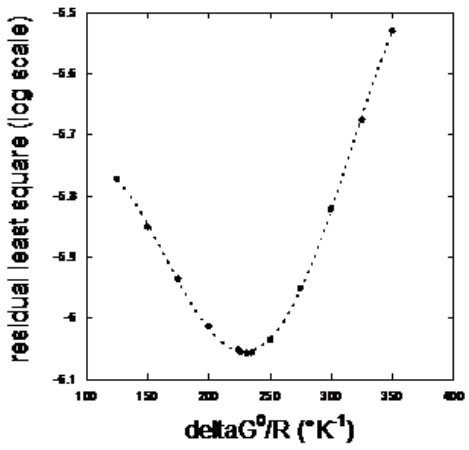

Figure (2.2): Diagram showing the best fit values of the thermodynamic parameter $\Delta G^0/R$; 192 < $\Delta G^0/R$ < 262 (°K^{-1}) insures a residual least square error less than 1 e-6

The least square minima are not "sharp" if the curvature is too low and the data noisy.

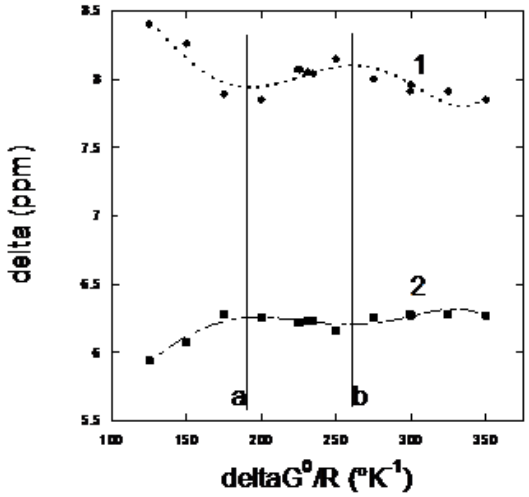

Figure (2.3): Best fit values of delta 1 and delta 2 according to the value of $\Delta G^0/R$. Optimized values lie within the a-b interval; 7.93 < δ_1 < 8.13 ; 6.20 < δ_2 < 6.25 ppm.

A tutorial with numerical simulation of reacting systems and experimental kinetic curve fitting can be found in the modern kinetic and chemical dynamics website: http://cinet.chim.pagesperso-orange.fr.

Chapter III

I. Open form

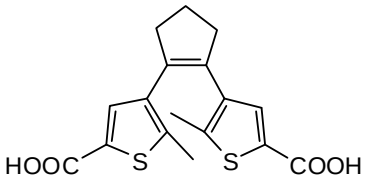

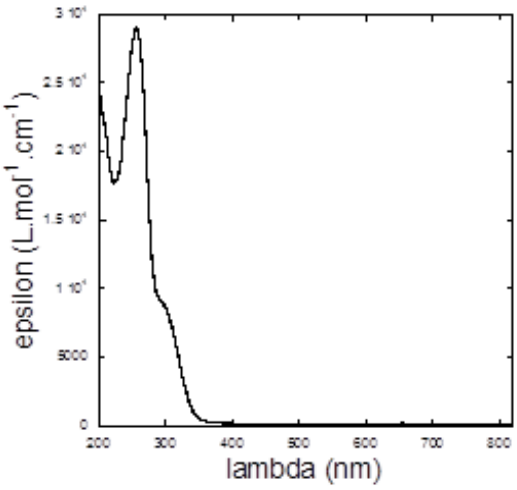

Figure (3.1): UV spectrum of the AH_2 open form in CH_3CN (epsilon $_{(258nm)}$ = 29000L.mol^{-1}.cm^{1}).MW = 348 g/mol

II. Closed form

Closed form is obtained from UV irradiation of a CH_3CN solution of the **AH_2** open form until a PSS was reached.

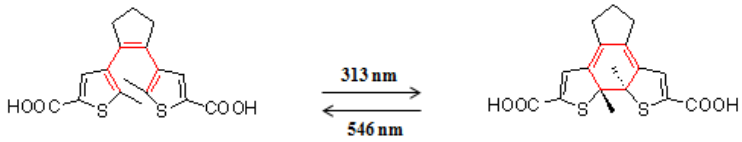

Scheme (3.1) :Photochemical ring closure reaction of DTE $(COOH)_2$

III. Photocoloration

Irradiation with UV light (313nm) of an acetonitrile solution of the open form **AH_2** of the diacid DTE$(COOH)_2$ triggers the photocyclisation reaction and generates the ring-closed isomer **BH_2**. During UV irradiation, absorption maximum of the open form **AH_2** at high energy decreases while absorption maximum of **BH_2** increases in the visible domain. The change in color of the solution from colorless to blue is due to the formation of the extended pi-conjugated backbone created in the ring-closed isomer. The corresponding UV/ Vis absorption spectra of the closed form B**H_2** shows two absorption maximum at 536 and 354nm with a clear-cut isosbestic point at 315nm.

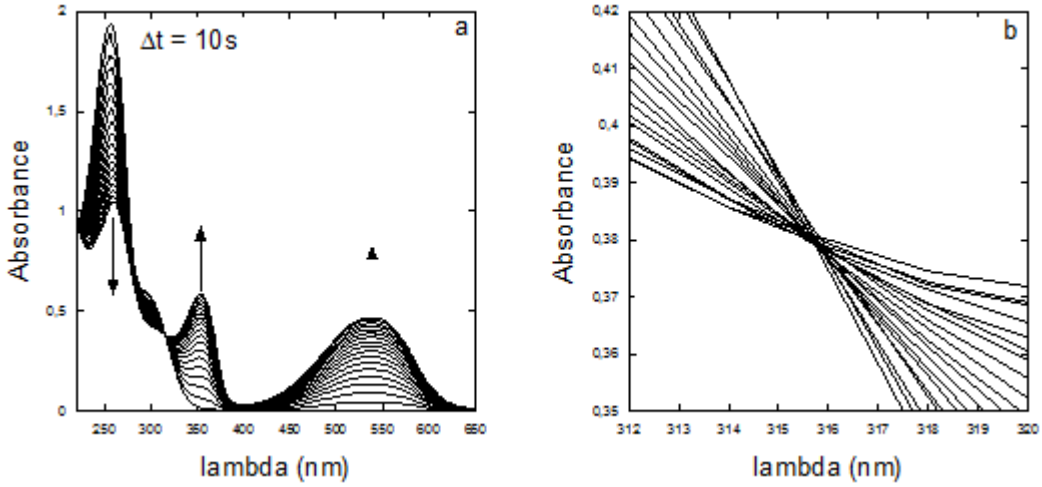

Figure (3.2): Photocoloration of the DTE in CH3CN under 313nm UV irradiation.a: overlay spectra showing that the last spectrum (t = 180s) contains more than 80% of the photochromic compound is under its closed form. b: detail of the isosbestic point.

From previous studies, epsilon $_{\text{closed (538nm)}}$ = 9100L.mol^{-1}.cm^{-1}; epsilon$_{\text{(isosbestic point at 316nm)}}$ = 5900 L.mol^{-1}.cm^{-1}.

The percentage of non-cyclised open form from any mixture of open + closed (**AH_2** + **BH_2**), is given by the following formula:

$$\%_{open\ form} = 100 - 64{,}8r \quad \text{with} \quad r = \frac{Abs_{538}}{Abs_{316}}$$

IV. Cu(II) triflate:

$C_2CuF_6O_6S_2$, MW : 361.68 g mol^{-1}

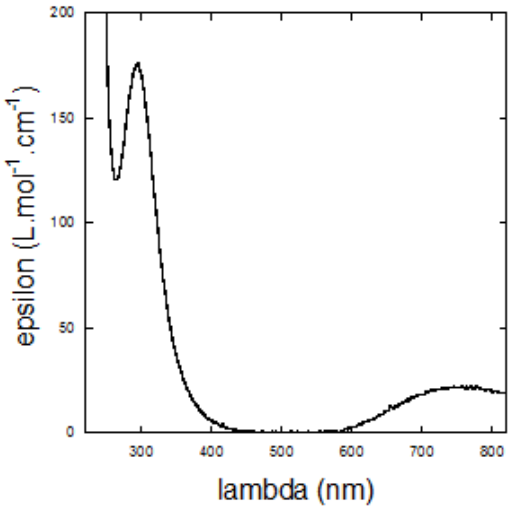

Figure (3.3): Calibrated Cu(II) triflate spectrum in CH_3CN as used to determine $[Cu(II)]_0$ concentrations.

IV.1 Cu(II) addition experiment:

A stirred solution of the open isomer **AH_2** in a quartz cell is irradiated at 313 nm with an optical irradiation fiber leading to the formation of the colored PSS solution. The obtained PSS solution is weighted then degassed before adding a defined amount of Cu(II) which is weighted also. During the addition of Cu(II) in the quartz cell which is removed from the spectrophotometer, spectrokinetic measurements were triggered in the spectrophotometer. Once the Cu(II) is added , the resulted solution in the quartz cell is quickly mixed. Then the cell is replaced in the spectrophotometer to monitor kinetics reaction.

IV.2 Stopped flow experiment:

We used Stopped flow technique to study the rapid kinetic reaction between PSS solution and Cu(II). Acetonitrile solutions of Cu(II) and PSS are placed into two syringes. Small volumes of solutions are rapidly driven from syringes, mixed and then stopped in an observation cell. The sample cell is irradiated with monochromatic light and as the reaction between PSS and Cu(II) proceeds the change in the recorded signal, the absorbance at a specific wavelength (536 nm or 780 nm) is recorded as a function of time. Analysis of the kinetic transient provides the determination of reaction rate and the reaction mechanism.

References

References

[1] Gilbert A. , Baggott J., *Essentials of molecular photochemistry*, CRC Press, Boca Raton, **1991**, p.538

[2] Woodward R.B., Hoffmann R. *Journal of the American Chemical Society* **1965**, 87, 39

[3] Fodor S. P.A.; Read J.L.; Pirrung M.C., Stryer L.; Lu A.T.;Solas D.; *Science*, **1991**, *251*, 767-773

[4] Zhang Y.; Erdmann F.; Baumgrass R.; Schutkowski M.; Fisher G.; *J. Biol. Chem.* **2005**, *280*, 4842-4850

[5] Castano A.P.; Mroz P.; Hamblin M.R.; *Nature Reviews Cancer*, **2006**, *6*, 535-545

[6] Callan J.F., de Sliva A.P., McClenaghan N.D.*Chem.Commun***. 2004**, 2048

[7] Yoshida T., Arishima K., Ebisawa F., Hoshino M., Sukegawa K., Ishikawa A., Kobayashi T., Hanazawa M., Horikawa M. *J.Photochem.Photobiol. A : Chem* **1996**, *95*, 265

[8] Gutierrez R., Grossmann F., Schmidt R., *Chem.Phys.Chem.* **2003**, *4*, 1252

[9] Sato M., Kinoshita T., Takizawa A.,Tsujita Y. *Macromolecules* **1988**, *21*, 1612

[10] Lewis F.D., Bedell A.M., Dykstra R.E., Elbert J.E., Could I.R., Farid S. *J.Am.Chem.Soc.* **1990**, *112*, 8055

[11] Malatesta V., J. C. Crano and R. J. Guglielmetti (Eds.), Vol. 2, Ch. 2, Plenum, New York (**1999**)

[12] Cohen, M.D.; Schmidt, G.M.T.; Flavian, S. *J. Chem. Soc*. **1964**, 2041

[13] RauH. *Photochemistry and Photophysics*; rabek J.F. ed.; CRC Press: Boca Raton, **1990;** vol2

[14] Krongauz, V.; Weiss, V. *Chem. Rev*. **2000**, *100*, 1741

[15] Zhang, X.Y.; Jin, S.; Ming, Y.F.; Liang, Y.C.; Yu, L.H.; Fan, M.G.; Luo, J.; Zuo, Z.H.; Yao, S.D. *J. Photochem. Photobiol. A.: Chem*. **1994**, *80*, 221

[16] Baillet, G.; Giusti, G.; Gugliemetti, R. *Bull. Chem. Soc. Jpn*. **1995**, *68*, 1220

[17] Yokoyama,Y. *Chem. rev*. **2000**, *100*, 1717

[18] Darcy, P.J.; Heller, H.G.; Strydom, P.J.; Whittall, J. *J. Chem. Soc. Perkin Trans.*, **1981**, 1, 202

References

[19] Irie M. *Chem. Rev*., **2000**, *100*, 1685

[20] Irie M.; Mohri M. *J. Org. Chem.* **1988**, *53*, 803 – 808

[21] Kellogg R. M.; Groen M. B.; Wijnberg H. *J. Org. Chem.* **1967**, *32*, 3093 – 3100

[22] Huang Z.-N.; Xu B.A.; Jin S.; Fan M.-G. *Synthesis* **1998**, 1092

[23] Hanazawa M.; Sumiya R.; Horikawa Y.; Irie M. *J. Chem. Soc. Chem. Commun.* **1992**, 206.

[24] Tamai N.; Miyasaka H. *Chem. Rev*. **2000**, *100*, 1875-1890

[25] Spangenberg A.;Metivier R.; Gonzalez J.; Nakatani K.; Yu P.; Giraud M.; Leaustic A.; Guillot R.; Uwada T.; Asahi T. *Advanced Materials* **2009**, *21*, 309-313

[26] Kobatake S., Terakawa Y. *Chem. Commun*., **2007**, 1698–1700

[27] Stellacci F.; Bertarelli C.; Toscano F.; Gallazi M. C.; Zotti G.; Zerbi G. *Advanced Materials* **1999**, *11*, 292-295

[28] Takeshita M.; Choi C. N.; Irie M. *Chemical Communications* **1997**, 2265-2266

[29] Takeshita M.; Irie M. *Tetrahedron Letters* **1999**, *40*, 1345-1348

[30] Miyasaka H; Arai S.; Tabata A.; Nobuto T.; Irie *M. Chem. Phys. Lett.* **1994**, *230*, 249

[31] Irie M.; Sakemura K.; Okinaka, M.; Uchida, K. *J. Org. Chem.* **1995**, *60*, 8305-8309

[32] Uchida K.; Nakayama Y.; Irie M. *Bull. Chem. Soc. Jpn.* **1990**, *63*, 1311-1315

[33] Moriyama Y.; Matsuda K.; Tanifuji N.; Irie S.; Irie M. *Org. Lett.* **2005**, *7*, 3315-3318

[34] Peters A. ; Branda N.R. *J.Am.Chem.Soc.* **2003**, *125*, 3404

[35] Koshido T., Kawai T., Yoshino K. *J. Phys. Chem.*, **1995,** *99*, 6110–6114

[36] Browne W. R.; de Jong J. J. D.; Kudernac T.; Walko M.; Lucas L. N.; Uchida K.; van Esch, J. H.; Feringa B. L. *Chem. Eur. J.* **2005**, *11*, 6430-6441

[37] Guirado G., Coudret C., Hliwa M., Launay J.-P. , *J. Phys. Chem.*, **2005**, *109*, 17445-59

[38] Kawai S.H., Gilat S.L., Ponsinet R. , Lehn J.-M. *Chem. Eur. J.*, **1995**, *1*, 285–293

[39] Odo Y.; Matsuda K.; Irie M. *Chem.dEur. J*. **2006**, *12*, 4283–4288

[40] Kutsunugia Y., Coudret C., Micheau J.C., Kawai T.; *Dyes and Pigments;* **2012**, *92*, 838-846

[41] Ohsumi M, Fukaminato T, Irie M. *Chem. Commun.*, **2005**, 3921–3923

References

[42] Takeshita M.; Irie M. *J. Org. Chem*. **1998**, *63*, 6643–6649

[43] Mulder A.; Jukovic, A.; van Leeuwen F. W. B.; Kooijman H.; Spek A. L.; Huskens J.; Reinhoudt D. N. *Chem.Eur. J.* **2004**, *10*, 1114–1123

[44] Shiqiang Cui, Shouzhi Pu, Weijun Liu, Gang Liu, *Dyes and Pigments*, **2011**, *91*, 435-441

[45] Sud D.; Norsten T. B.; Branda N. R. *Angew. Chem., Int. Ed.* **2005**, *44*, 2019–2021

[46] Hecht S., Stoll R. S., *Angew. Chem. Int. Ed.* **2010**, *49*, 5054 – 5075

[47] Irie, M., Fukaminato, T., Sasaki, T., Tamai, N. and Kawai, T. *Nature*, **2002**, *420*, 759–760

[48] Takeshita M., Uchida K., Irie M. *Chem. Commun.*, **1996**, *15*, 1807–1808

[49] Samachetty H. D., Lemieux V., Branda N. R. *Tetrahedron* **2008**, *64*, 8292–8300

[50] Jeong, Y. C.; Park, D. G.; Lee, I.S.;Yang, S.Y.; Ahn, K.H., *J. Mater. Chem.* **2009**, *19*, 97

[51] Cusido, J.; Deniz, E.; Raymo, F.M. *Eur. J. Org. Chem.* **2009**, 2031

[52] Takeda J.; Tayu T.; Kurita S.; Yokoyama Y.; Kurita Y.; Kuga T.; Matsuoka M. *Chem.. Phys. Lett.* **1994**, *220*, 443

[53] Raymo F. M., Tomasulo M., *J. Phys. Chem. A*, **2005**, *109*, 7343–7352

[54] Folling J., Polyakova S., Belov V., Van Blaaderen A., Bossi M. L., Hell S. W., *small*, **2008**, *4*, , 134 – 142

[55] Irie M, Miyatake O, Uchida K. *J Am Chem Soc* **1992**;*114*, 8715-8716

[56] Irie M, Miyatake O, Uchida K, Eriguchi T. , *J Am Chem Soc* **1994**;*116*, 9894-900

[57] Qin B., Yao R., Zhao X. and Tian H., *Org. Biomol. Chem*. **2003** , *1* ,2187- 2191

[58] Kawai, S. H.; Gilat S. L. ; Lehn J.M. *Eur. J. Org. Chem.* **1999**, 2359 – 22366

[59] Kobatake, S.; Matsumoto, Y.; Irie, M. *Angewandte Chemie-International Edition* **2005**, *44*, 2148-2151

[60] Stauffer M.T., Weber S.G., *Anal. Chem.*, **1999**, *71*, 1146-1151.

[61] a)- Andersson J., Li S., Lincoln P., Andreasson J., *J. Am. Chem. Soc.* **2008**, *130*, 11836–11837; b)- Irie M., Miyatake O., Uchida K., *J. Am. Chem. Soc.* **1992**, *1 14*, 8715-8716.

[62] IUPAC Compendium of Chemical Terminology, PAC, 2007, *79*, 293 *(Glossary of terms used in photochemistry, 3rd edition (IUPAC Recommendations 2006))* on page 347 doi:10.1351/goldbook.GT07386.

References

[63] a)- Samachetty H. D., Branda N. R. , *Pure Appl. Chem.*, **2006**, *78*, 2351–2359; b)- Stoll, S. Hecht R.S., *Angew. Chem. Int. Ed.* **2010**, *49*, 5054 – 5075.

[64] a) Li Z., Zhang C., Ren Y., Yin J., Liu S. H. *Org. Lett.*, **2011**, *13* , 6022–6025; b)- Yumoto, M. Irie K., Matsuda K., *Org. Lett*., **2010**, *10*, 2051 – 2054; c)- Nakashima T., Miyamura K., Sakai T., Kawai T., *Chem. Eur. J.* **2009**, *15*, 1977 – 1984**;**

[65] Chen Z.H., Zhao S.M., Li Z.Y., Zhang Z., Zhang F.S., *Sci China Ser B-Chem.* **2007**, *50*, 581-586.

[66] a)- Lemieux V., Spantulescu M.D., Baldridge K.K., Branda N.R., *Angew. Chem. Int. Ed.* **2008**, *47*, 5034 –5037 ; b)- Samachetty H. D., Branda N. R. *Chem. Commun.,* **2005**, 2840-2842.

[67] a)- Cui S., Pu S., Liu W., Liu G., *Dyes and Pigments* **2011**, *91*, 435-441 ; b)- Zhang J., Tan W., Meng X., Tian H., *J. Mater. Chem.* **2009**, *19*, 5726–5729 ; c)- Xiao S., Yi T., Zhou Y., Zhao Q., Li F., Huang C., *Tetrahedron,* **2006**, *62*, 10072–10078 ; d)- Yokoyama Y., Yamane T., Kurita Y., *J. Chem. Soc., Chem. Commun.,* **1991**, 1722-1724.

[68] a)- Hurenkamp J. H., de Jong J. J. D., Browne W. R., van Esch J. H., Feringa B. L., *Org. Biomol. Chem.,* 2008, *6*, 1268–1277; b)- Akazawa M., Uchida K., de Jong J.J., Areephong J., Stuart M., Caroli G., Browne W. R., Feringa B. *Org. Biomol. Chem.* 2008, *6*, 1544-7; c)- Mulder A., Jukovic J., Van Leeuwen F. W. B., Kooijman H., Spek A.L., Huskens J., Reinhoudt D., N. *Chem. Eur. J.*, 2004, 10, 1114-1123; d)- Lucas L.N., de Jong J.J.D., van Esch J.H., Kellogg R.M., Feringa B.L., *Eur. J. Org. Chem.* 2003, 155-166 ; e)- Norsten T.B., Branda N.R., *J. Am. Chem. Soc.* 2001, *123*, 1784-1785.

[69] Delbaere S., Vermeersch G., Micheau J.C., *J. Photochem. Photobiol. C: Photochem. Rev.* **2011**, *12*, 74–105.

[70] Boggio-Pasqua M., Ravaglia M., Bearpark M.J., Garavelli M., Robb M.A. *J. Phys. Chem. A* **2003**, *107*, 11139-11152.

[71] a)- Pu S., Fan C., Miao W., Liu G., *Dyes and Pigments* **2010**, *84*, 25–35; b)- Pu S., Liu W., Liu G., *Dyes and Pigments*, **2010,** *87*, 1-9; c)- Kobatake S., Terakawa Y., Imagawa H., *Tetrahedron,* **2009**, *65*, 6104–6108; d)- Liu W., Pu S. , Liu G., *J. Mol. Structure* **2009**, *936*, 29–36; e)- Ribeiro-Santos A., Ballardini R., Belser P., Gandolfi M.T., Iyer V.M., Moggi L., *Photochem. Photobiol. Sci.*, **2009**, *8*, 1734–1742; f)- Fan C., Pu S., Liu G., Yang T., *J. Photochem. Photobiol. A: Chem.* **2008**, *197*, 415–425; g)- Pu S., Yan L., Wen Z., Liu G., Shen L., *J. Photochem. Photobiol. A: Chem.* **2008**, *196*, 84–93; h)- Fan C., Pu S., Liu G., Yang T., *J. Photochem. Photobiol. A: Chem.* **2008**, *194*, 333–343; i)- Morimitsu K., Kobatake S., Irie M., *Tetrahedron Letters,* **2004**, *45*, 1155–1158; j)- Kobatake S., Irie M., *Chem. Lett. 32*(11), **2003**, 1078 – 1079; k)- Matsuda K., Shinkai Y., Yamaguchi T., Nomiyama K., Isayama M., Irie M., *Chem. Lett.* **2003**, *32*, 1178 -1179; l)- Shibata K., Muto K., Kobatake S., Irie M., *J. Phys. Chem. A* **2002**, *106*, 209-214;

[72] Fukumoto S., Nakashima T., Kawai T., *Angew. Chem. Int. Ed.* **2011**, *50*, 1565 –1568

References

[73] Goldberg A., Murakami A., Kanda K., Kobayashi T., Nakamura S., Uchida K., Sekiya H., Fukaminato T., Kawai T., Kobatake S., Irie M., *J. Phys. Chem. A,* **2003,** *107,* 4982-4988.

[74] Levitt M., Perutz M. F. , *J. Mol. Biol.* **1988**, *201*, 751-754

[75] a)- Yang T., Pu S., Chen B., Xu J., *Can. J. Chem*, **2007**, *85*, 12 – 20; b)- Uchida K., Matsuoka T., Kobatake S., Yamaguchi T., Irie M., *Tetrahedron*, **2001**, *57*, 4559-4565.

[76] a)- Kilic E., Aslan N., *Microchim Acta*, **2005**, *151*, 89–92; b)- Barcza L., Buvári-Barcza A., *J. Chem. Educ.*, **2003**, *80(7)*, 823-828.

[77] Peters M.V., Stoll R.S., Kühn A., Hecht S., *Angew. Chem. Int. Ed.* **2008**, *47*, 5968 –5972.

[78] Kobatake S., Terakawa Y., *Chem. Commun.* **2007**, 1698–1700

[79] Zhou Z., Xiao S., Xu J., Liu Z., Shi M., Li F., Yi T., Huang C., *Org. Lett.*, **2006**, *8*, 3911 – 3914.

[80] a)- Zhang J., Tan W., Meng X., Tian H., *J. Mater. Chem.*, **2009**, *19*, 5726–5729; b)- Takeshita M., Choi C.N., Irie M., *Chem. Commun*., **1997**, 2265 – 2266.

[81] Irie M., Miyatake O., Uchida K., *J. Am. Chem. Soc.* **1992**, *1 14*, 8715-8716.

[82] Bren V A, *Russ. Chem. Rev.* **2001**, *70*, 1017 – 1036.

[83] Pina F., Melo M.J., Laia C.A.T., Parola A.J., Lima J.C., *Chem. Soc. Rev.* **2012**, DOI: 10.1039/c1cs15126f.

[84] Hoffmann R. W., Barth W., *J. Chem. Soc., Chem. Commun.*, **1983**, 345-346

[85] Connelly N. G., Geiger W. E., *Chem. Rev.* **1996**, *96*, 877-910

[86] Kirchgessner M., Sreenath K., Gopidas K. R., *J. Org. Chem.* **2006**, *71*, 9849-9852

[87] Ouali A., Taillefer M., Spindler J.F., Jutand A., *Organometallics* **2007,** *26*, 65-74

[88] Irangu J., Ferguson M. J., Jordan R. B., *Inorg. Chem.* **2005**, *44*, 1619-1625

[89] Inamo M., Kamiya N., Inada Y., Nomura M., Funahashi S., *Inorg. Chem.* **2001**, *40*, 5636-5644

[90]Bortolamei N., Isse A. A., Di Marco V. B., Gennaro A., Matyjaszewski K., *Macromolecules* **2010**, *43*, 9257–9267

[91] Sumalekshmy S., Gopidas K.R. , *Chem. Phys. Lett.* , **2005**, *413*, 294–299

[92] Sreenath K.,. Thomas T. G, Gopidas K. R., *Org. Lett*., **2011**, *13*, 1134-1137

References

[93] Rendler S., MacMillan D.W. C., *J. Am. Chem. Soc.* **2010**, *132*, 5027–5029

[94] Haase G., Dunkley W. L., *Journal of Lipid Research*, **1969**,*10*, 561-567

[95] Urbañski N.K., Berêsewicz A., *Acta Biochimica Polonica*, **2000**, *47*, 951-962

[96] Cui S., Pu S., Liu W., Liu G., *Dyes and Pigments*, **2011,** *91*, 435-441

[97] Giraud M., Leaustic A., Guillot R., Yu P., Dorlet P., Metivier R., Nakatani K., *New J. Chem*., **2009**, *33*, 1380–1385

[98] K. Takayama, K. Matsuda, M. Irie, *Chem. Eur. J.* **2003**, *9*, 5605 - 5609

[99] Shiga T., Miyasaka H., Yamashita M., Morimoto M., Irie M., *Dalton Trans*., **2011**, *40*, 2275-2282

[100] Zhang J., Tan W., Meng X., Tian H., *J. Mater. Chem.*, **2009**, *19*, 5726–5729

[101] Sud D., Norsten T. B., Branda N. R., *Angew. Chem. Int. Ed.* **2005**, *44*, 2019 –2021

[102] Delcourlt M. O., Rossi M. J., *The Journal of Physical Chemistry*, **1982,** *86*, 3233-3239

[103] Das O., Paria S., Zangrando E., Paine T. K., *Inorg. Chem.* **2011**, *50*, 11375–11383

[104] Bickley J., Bonar-Law R.P., Borrero Martinez M.A., Steiner A., *Inorganica Chimica Acta* , **2004**, *357*, 891–894

[105] Sreenath K., Suneesh C.V., Gopidas K. R., Flowers R. A., *J. Phys. Chem. A*, **2009**, *113*, 6477–6483

[106] Mohamadin M. I., Abdullah N., *Int. J. Phys. Sci.*, **2011**, *6*, 2526-2535

[107] Ulusoy H. I., Gurkan R., Akcay M., *Turk J Chem*, **2011**, *35*, 599 – 612

[108] Habermeyer B., Takai A., Gros C. P., El Ojaimi M., Barbe J. M., Fukuzumi S., *Chem. Eur. J.* **2011**, *17*, 10670 – 10681

[109] Naguib Y. M. A., Steel C., Cohen S. *G.*, Young M. A., *J. Phys. Chem.* **1987**, *91*, 3033-3036

[110] Warren J. J., Tronic T. A., Mayer J. M., *Chem. Rev.* **2010,** *110*, 6961–7001

[111] Kim E., Kim M., Kim K., *Bull. Korean Chem. Soc.* **2008**, *29*, 827- 832

[112] Politz J. C., *Trends Cell Biol.* **1999**, *9*, 284–287

[113] Yoffe A. D., *Adv. Phys.*, **2001**, *50*, 1

References

[114] Zhou Z., Hu H., Yang H., Yi T., Huang K., Yu M., Li F., Huang C., *Chem. Commun*., **2008**, 4786–4788

[115] Klajn R., Stoddartb J. F., Grzybowski B. A., *Chem. Soc. Rev.*, **2010**, *39*, 2203–2237

[116] Erno Z., Yildiz I., Gorodetsky B., Raymo F. M., Branda N. R.*; Photochem. Photobiol. Sci.*, **2010**, *9*, 249–253

[117] Li H., Han C., Zhang L., *J. Mater. Chem.*, **2008**, *18*, 4543–4548.

[118] Querner C., Reiss P., Sadki S., Zagorska M., Pron A., *Phys. Chem. Chem. Phys.*, **2005**, *7*, 3204–3209.

[119] Mihailovic M., Henneghien A.L. , Faure S., Disseix P., Leymarie J., Vasson A., Buell D.A., Semond F., Morhain C., Zuniga Perez J., *Optical Materials*, **2009**, *31*,532–536.

[120] Sanches L., Peral J., Domenech X. *Electro Chim.Acta*, **1996,** *41*, 1981.

[121] Huang W.J., Fang G.C., Wang C.C. *Colloid.Surfaces. A. Physicochem. Eng. Aspects*, **2005,** *260*, 45

[122] Annapoorani R., Dhanjeyan M.R., Renganathan R. J. *Photochem. Photo Boil. A. Chem.*, **1997.** *111*, 215.

[123] Matsubara K., Fons P., Iwata K., Yamada A., Sakurai K., Tampo H., Niki S. *Thin Solid Films*, **2003,***431*: 369.

[124] Zhang Q., Xie C., Zhang S., Wang A., Zhu B.,Wang L., Yang Z. *Sens. Actuators B.*, **2005,** *110*, 370.

[125] Zang J., Yu W., Zang L. *Phys. Lett. A.*, **2002,** *299*, 276.

[126] Brus L. E., *J. Phys. Chem.*, **1984**, *80*, 4403

[127] Li D., Leung Y. H., Djurisic A. B., Liu Z. T., Xie M. H., Shi S. L., Xu S. J., Chan W. K., *Appl. Phys. Lett.*, **2004**, *85*, 1601

[128] Son D. I., You C. H., Kim W. T., Kim T. W., *Nanotechnology*, **2009,** *20*, 365206,

[129] Oba F., Togo A., Tanaka I., Paier J., Kresse G., *Physical Review B,* **2008,** *77*(24), 245202–245206

[130] van Dijken A., Meulenkamp E. A., Vanmaekelbergh D., Meijerink A., *J. Phys. Chem. B*, **2000**, *104*, 1715

[131] Fang Z., Wang Y., Xu D., Tan Y., Liu X., *Opt. Mater*., **2004**, *26*, 239.

[132] Monticone S., Tufeu R., Kanaev A. V., *J. Phys. Chem. B*, **1998**, *102*, 2854

References

[133] Yu H.-h.; Wong M. K. F.; Ali E. M.; Ying J. Y. *Chem. Comm.* **2008**, 4912–4914

[134] Makhal A., Sarkar S., Bora T., Baruah S., Dutta J., Raychaudhuri A K, Pal S. K., *Nanotechnology*, **2010**, *21*, 265703. doi:10.1088/0957-4484/21/26/265703

[135] Pal S. K., Mandal D., Sukul D., Bhattacharyya K ., *Chem.Phys.*, **1999**, *249*, 63–71

[136] Baruah S. , Dutta J; *J. Cryst. Growth*, **2009**, *311*, 2549–54

[137] Beane G. A., Morfa A. J., Funston A. M., Mulvaney P., *J. Phys. Chem. C*, **2012**, *116* (5), 3305–3310

[138] Sadhu, S.; Tachiya, M. *J. Phys. Chem.*, **2009**, *113*, 19488–19492

[139] Shah S. M., Martini C., Ackermann J. , Fages F., *Journal of Colloid and Interface Science* **2012**, *367*, 109–114

[140] Martini C., Poize G., Ferry D., Kanehira D., Yoshimoto N., Ackermann J., Fages F., *Chem Phys Chem*, **2009,** *14*,2465

[141] Remy S.; Shah S.M. ; Martini C.; Poize G.; Margeat O.; Heynderickx A.; Ackermann J.; Fages F.; *Dyes and Pigments*, **2011**, *89*, 266-270

[142] Kahn M.L., Glaria A., Pages C., Monge M., Saint Macary L., Maisonnat A., Chaudret B., *J. Mater. Chem.*, **2009**, *19*, 4044–4060

[143] Monge M., Kahn M. L., Maisonnat A., Chaudret B., *Angewandte Chemie International Edition*, **2003**, *42*, 5321-5324

[144] Kahn M. L., Monge M., Snoeck E., Maisonnat A., Chaudret B., *Small*, **2005**, *1*, 221-224.

[145] Kahn M. L., Cardinal T., Bousquet B., Monge M., Jubera V., Chaudret B., *ChemPhysChem*, **2006**, *7*, 2392

[146] Rehm D., Weller A., *Isr. J. Chem.*, **1970**, *8*, 259–271.

[147] Hoyer P., Weller H., *J. Phys. Chem.* **1995**,*99*, 14096-14100

[148] Ottavi G., Ortica F., Favaro G., *Int. J. Chem. Kinet.* **1999,** 31, 303

[149] Kobatake S., Yamashita I., *Tetrahedron* **2008**, 64, 7611

[150] Fisher E., *J. Phys. Chem.* **1967,** 71, 3704

[151] Wyman G., *Mol. Photochem.* **1974,** 6, 81

[152] Pimienta V., Micheau J.C., *Mol. Cryst. Liq. Cryst.* **2000,** 344, 157

Photo-modulations *vs* gated photochromism in a dithienylethene dye

The aim of this thesis is the study of photo-modulations and gated photochromism behaviors of a mini-sized diacid dithienylethene derivative DTE$(COOH)_2$ in different guest systems. These two behaviors originate from the coupling between the photochemical isomerization and various associated chemical process involving one or both of the photo-isomers.

First, the study of the acidity photo-modulation and gated photochromism of DTE$(COOH)_2$ was carried out in presence of various amount of a base, tetrabutylammonium hydroxide, in acetonitrile/water mixtures. Chemical dynamic modelling methodology was used to establish the main photochromic (quantum yields), spectral (molar extinction coefficients) and thermodynamic (equilibria constants) parameters of the base sensitive diacid. Despite its very simple structure, results show that DTE$(COOH)_2$ can be exploitable for a reversible photo-acid generation.

Behaviors of photoisomers of diacid DTE$(COOH)_2$ were also studied in presence of copper (II). Copper (II) was used as an oxidizing reagent to promote the thermal ring opening reaction of the diacid dithienylethene closed isomer. The presence of little amounts of base, $nBu_4NOH.30H_2O$ or triflic acid, CF_3SO_3H can alter the ring opening reaction causing the inhibition or the acceleration of the process, respectively.

Finaly, the use of the diacid DTE$(COOH)_2$ as a luminescence photo-modulator was explored using fluorescent counter-ion free ZnO nanoparticles stabilized by hexadecylamine (HDA) ligands. Unexpectedly, both diacid photoisomers were found to reduce the emission of ZnO nanoparticles, the closed colored one being the most efficient quencher of the two. The extinction of the emission intensity by electron and energy transfer processes was suggested. Although little photodegradation was occuring, the possibility of switching ON and Off the ZnO luminescence was demonstrated.

Keywords: Diacid dithienylethene, gated photochromism, photomodulation, ZnO nanoparticles, copper (II)

Photo-modulations *vs* "gated phtochromism" d'un dérivé de dithienyléthène

L'objectif de cette thèse est l'étude de la photo-modulation et du « gated photochromism » d'un diacide dithienyléthène $DTE(COOH)_2$ ayant une structure minimale très simple, dans différents milieux. Ces deux comportements proviennent de la combinaison de l'isomérisation photochimique et d'une réaction chimique associée impliquant un ou les deux photo-isomères.

Tout d'abord, l'étude de la photo-modulation et du « gated photochromism » du diacide $DTE(COOH)_2$ a été réalisée en présence de différentes quantités d'une base, l'hydroxyde de tétrabutylammonium, dans un mélange acétonitrile / eau. La méthode de modélisation dynamique a été utilisée pour établir les principaux paramètres photochromiques (rendements quantiques), spectroscopiques (coefficients d'extinction molaire) et thermodynamiques (constantes d'équilibres) du diacide. Malgré sa structure très simple, les résultats montrent que $DTE(COOH)_2$ peut être exploitable comme un photo-générateur d'acide.

Les comportements des photo-isomères de diacide $DTE(COOH)_2$ ont également été étudiés en présence de cuivre (II). Dans ce système, le cuivre (II) est utilisé comme un réactif oxydant pour promouvoir la réaction d'ouverture thermique de l'isomère cyclisé du diacide dithienylethene. La présence de petites quantités de base ($nBu_4NOH.30H_2O$) ou d'acide (CF_3SO_3H) dans le milieu peut altérer la réaction d'ouverture de cycle provoquant l'inhibition ou l'accélération de la réaction d'ouverture, respectivement.

Finalement, l'utilisation du diacide $DTE(COOH)_2$ comme un photo-modulateur de luminescence a été étudiée en présence des nanoparticules de ZnO fluorescents qui sont stabilisées par des ligands d'hexadécylamine (HDA). De façon inattendue, les deux photoisomères du diacide ont réduit l'émission des nanoparticules de ZnO, l'isomére cyclisé était le plus efficace des deux. L'extinction de l'intensité de l'émission par le transfert des électrons et des processus de transfert d'énergie ont été suggérés comme mécanismes. Bien que la photodégradation se produise, la possibilité d'activer et de désactiver la luminescence de ZnO a été réalisée.

Mots clés : Dithienyléthène diacide, gated photochromism, photomodulation, nanoparticules de ZnO, cuivre (II)